

POLITECNICO DI TORINO

Master's degree in Mechatronic Engineering

A.y. 2024/2025

Graduating session April 2025



**Politecnico
di Torino**

Electro-mechanical characterization of a walking
beam transfer machine for flat glass applications

Focus on mechanical validation and PLC programming

Tutors

Prof. Luigi Mazza

Ing. Matteo Ramonda

Candidate

Alessandro Trasforini

Abstract

The main goal of this thesis project was to conduct an in-depth study of a walking beam transfer machine, adapted for custom flat glass applications. This peculiar typology of machine has been present for years in the catalogue of offers of Bottero s.p.a., a relevant player in the field, and it is often customised to satisfy and meet the specific and various criteria requested by different commissioners. Hence, the necessity of having a complete and general overview on the cinematic and dynamic behaviour of the machine and of its mechanics, as well as conscious knowledge about the dimensioning and verification of the components involved, with the purpose of unify and standardize them as much as possible to increase efficiency, simplicity and modularity.

This study can be divided into two main parts: a mechanical characterization of the principal structures involved and the PLC software development and programming of the machine.

In particular, the machine characterization focused on a precise analysis of the main mechanisms, as well as component evaluation and validation of the mechanical design, including dimensioning and stress analysis (Finite Element Method) of the most solicited parts, along with a cinematic and dynamic study of the lifting and translating mechanism of the walking beam. The main goals were to provide a precise estimate of the motor torques necessary to achieve the requested performance and check whether the actual motor and components choices were overestimated or not in terms of load capacity and internal stress reactions. Moreover, a formulation of a general model for cinematic and dynamic tracking of the lifting and conveying processes was developed on Excel, so that it could be adapted to any machine adopting both or one of the same mechanisms, just replacing the parameters values with the current ones and obtaining a complete overview of the machine as an output.

After having had a general overview of the PLC hardware and sensor system connected to the machine, the PLC software development consisted in an introduction to the program Studio 5000x by Rockwell Automation, together with a study of all motion control libraries available, followed by the motion programming in Ladder code through Motion Control techniques and Kinetix Motion.

The libraries consented to download a set of kinetic parameters on the PLC controller of the walking beam to program the desired behaviour, including velocity profiles and motion sequence, in a single cycle routine, on the basis of simple input data provided by position sensors and HMI interactions i.e. push buttons. This programming section also includes the implementation of subroutines for emergency and other basic features that will be incorporated in the general architecture of the plant, along with a 3D simulation of the behaviour of the machine in CodeSys

software environment through Factory I/O modelling app and on-field tests together with the automation department.

Table of contents

Summary	12
Chapter 1 A brief introduction to glass manufacturing.....	15
1.1 An economic overview of the flat glass industry	15
1.1.1 Low impact and smart housing.....	16
1.1.2 Automotive industry and solar energy demand	16
1.1.3 The regional markets	16
1.2 Flat glass.....	17
1.2.1 Invention of float glass and general process.....	17
Chapter 2 The mechanical analysis.....	20
2.1 Purpose of the machine	20
2.2 The lifting mechanism: analytical approach	22
2.2.1 The articulated quadrilateral or four bar planar linkage model	25
2.2.2 Grashof's law for a planar-four bar linkage.....	26
2.2.3 The Grashof's limit case for articulated parallelogram	27
2.3 The lifting mechanism: kinematic analysis	28
2.3.1 The angular position derivation	29
2.3.2 Angular velocities derivation.....	37
2.3.3 Angular acceleration derivation.....	38
2.4 The lifting mechanism: dynamic analysis	40
2.5 The lifting mechanism: dimensioning of critical elements	47
2.5.1 Connecting rods bearings.....	48
2.5.2 Connecting rods threads verification	50
2.5.3 Motor crank dimensioning.....	53
2.5.4 Lifting arm r22 dimensioning	58
2.5.5 Crank r21 dimensioning.....	61
2.5.6 Shaft S2 bearing verification	64
2.5.7 Lifting bearings dimensioning.....	68
2.5.8 Radial load on speed reducer shaft	69
2.6 The translating mechanism: analytical approach	70
2.7 The translating mechanism: kinematic approach	71
2.8 The translating mechanism: dynamic approach	73

2.9 The translating mechanism: component dimensioning	79
2.9.1 Toothed belt	79
2.9.2 V-shaped rollers	82
2.10 Results	83
Chapter 3 Rockwell Automation PLC	84
3.1 Studio 5000 intro	84
3.1.1 Programming modules	84
3.1.2 Connections	85
3.1.3 Kinetix Motion instructions	85
3.2 Software development in Studio 5000	89
3.2.1 Main architecture	89
3.2.2 Motion groups.....	90
3.3 Axis02_translating.....	94
3.4 Main routine	96
3.5 P00_error_detector	97
3.6 P01_emergency	98
3.7 Main routine	99
3.8 P02_initialize.....	100
3.9 Main routine (Step 0-20)	102
3.10 P05_startup.....	102
3.11 Main routine (Step 40-60)	102
3.12 Results	104
Chapter 4 Codesys translation and Factory I/O simulation	105
4.1 Codesys	105
4.2 Factory I/O	106
4.3 The chosen scenario	106
4.4 The I/O configuration.....	109
4.5 Modbus protocol.....	110
4.6 I/O communication protocol configuration	111
4.7 Software development in Codesys	114
4.7.1 The batch method.....	115
4.8 The program structure	116
4.9 Results	123

Appendix A	126
Appendix B	137

Table of figures

Figure 1: IMARC group projections for flat glass global market.....	15
Figure 2: float glass manufacturing process.....	18
Figure 3: the walking beam transfer machine	20
Figure 4: the walking beam steady state position below the main line	21
Figure 5: schematization from above of the walking beam	22
Figure 6: the walking beam lifting mechanism on the right-hand side.....	23
Figure 7: schematization of the external lifting mechanism on the right-hand side ..	23
Figure 8: schematization external-internal lifting mechanism.....	24
Figure 9: detailed view of coupling between cranks r21 and r22, with and without chassis	24
Figure 10: view from above of the couplings between external and internal lifting mechanisms; on the right, detail of r21-r22 coupling	25
Figure 11: four bar planar linkages possible configurations.....	26
Figure 12: Grashof's parallelogram in the lifting mechanism.....	27
Figure 13: idle position	29
Figure 14: lifting mechanism in extrastroke lift position.....	30
Figure 15: velocity profile for the lifting speed reducer	31
Figure 16: left four bar planar linkage	33
Figure 17: the right four bar planar linkage or Grashof's parallelogram in the lifting mechanism.....	36
Figure 18: force analysis on crank r1	41
Figure 19: dynamic force analysis on link rA.....	42
Figure 20: dynamic force analysis on link r21	43
Figure 21: dynamic force analysis on link rB	44
Figure 22: dynamic force analysis on links r31 & r32.....	45
Figure 23: datasheet parameters of lifting motor from manufacturer	46
Figure 24: motor couple C_m variations during half cycle	46
Figure 25: technical datasheet of the eyelets with bearings.....	48
Figure 26: Normal and shear forces distribution along rA	50
Figure 27: Normal and shear forces distribution along rB.....	51
Figure 28: force distribution on pin of motor crank r1	54
Figure 29: FEM analysis on crank r1	57
Figure 30: force distribution on pin of lifting crank r22	59
Figure 31: FEM analysis on lifting crank r22	61
Figure 32: force distribution on pin of crank r21	62
Figure 33: FEM analysis on crank r21	64
Figure 34: on the left, shafts s2 with cranks r21 and r22 installed; on the right, section view of bearings on shaft S2	65
Figure 35: force distribution along shaft S2.....	66
Figure 36: roller bearing datasheet.....	67

Figure 37: lifting bearing on crank r22	68
Figure 38: datasheet for front bearing on lifting crank r32	68
Figure 39: datasheet for rear bearing on crank r22	69
Figure 40: maximum radial load speed reducer on lifting mechanism	70
Figure 41: section view of the translating mechanism	70
Figure 42: scheme of the horizontal translation mechanism	71
Figure 43: velocity profile for the translating speed reducer	73
Figure 44: dynamic analysis pulley P1	74
Figure 45: dynamic analysis pulley P2	75
Figure 46: dynamic analysis cart	75
Figure 47: static friction case in v-roller dynamic analysis	77
Figure 48: dynamic friction case in v-roller dynamic analysis	77
Figure 49: datasheet parameters for translating motor from manufacturer	78
Figure 50: driving torque $C_m, P1$ of the translating mechanism	78
Figure 51: security factor for a conveyor belt subject to steady load	81
Figure 52: tooth resistance for AT20 open belt based on angular velocity	81
Figure 53: belt conveyor model provided by belt manufacturer	82
Figure 54: v-roller wheels datasheet compared to the obtained results	82
Figure 55 MSO function block	86
Figure 56 MASD function block	86
Figure 57: MASR function block	87
Figure 58: MSF function block	87
Figure 59: MAS function block	88
Figure 60: MAM function block	89
Figure 61: tree of devices in the network	90
Figure 62: general properties for both axis	91
Figure 63: Axis01 motor specifications	91
Figure 64: Axis01 scaling settings	92
Figure 65: homing settings	93
Figure 66: axis02 motor setup	94
Figure 67: axis02 scaling settings	95
Figure 68: axis02 motion planner settings	95
Figure 69: axis02 homing settings	96
Figure 70: first rungs of main routine	97
Figure 71: P00_error_detector	97
Figure 72: step 10-20 main routine	98
Figure 73: P01_emergency subroutine function block	98
Figure 74: P01_emergency structure	98
Figure 75: P02_initialize calling rung	100
Figure 76: P02_initialize structure	100
Figure 77: P02_initialize structure	101
Figure 78: step 10-20 structure	101
Figure 79: main routine step 50-60	103

Figure 80: P30_homing.....	103
Figure 81:P90_servo_off.....	104
Figure 82: resulting velocity profiles from studio 5000 simulation (lifting in red and translation in green).....	104
Figure 83: Codesys logo	105
Figure 84: Factory I/O logo.....	106
Figure 85: The setup in Factory I/O	108
Figure 86: I/O card in Factory I/O	109
Figure 87& 88: I/O communication setup in Factory I/O.....	111
Figure 89: communication device setup in Codesys.....	112
Figure 90: I/O card setup in Codesys	112
Figure 91: device communication setup in Codesys.....	113
Figure 92: I/O parameters in Codesys.....	114
Figure 93: I/O variables declaration in the main program	115
Figure 94: batch method example	115
Figure 95: start of cycle or step 9 effect.....	116
Figure 96: counter CTU_0	117
Figure 97: Counter effect	117
Figure 98: from step 1 to step 2	118
Figure 99: step 2 effect.....	118
Figure 100: from step 2 to step 3	118
Figure 101: step 3 effect.....	118
Figure 102: from step 3 to step 4	119
Figure 103: step 4 effect.....	119
Figure 104: conveyor motion set	119
Figure 105: from step 4 to step 5	119
Figure 106: step 5 effect.....	120
Figure 107: from step 5 to step 6	120
Figure 108: step 6 effect.....	120
Figure 109: from step 6 to step 7	121
Figure 110: step 7 effect.....	121
Figure 111: from step 7 to step 8	121
Figure 112: step 8 effect.....	121
Figure 113: from step 8 to step 9	122
Figure 114: step 9 effect.....	122
Figure 115: reset/emergency effect.....	122
Figure 116: position reset.....	123
Figure 117: STOP procedure rung	123

Tables

Table 1: main components lengths.....	28
Table 2: angular positions in relevant configurations.....	31
Table 3: kinematic parameters.....	32
Table 4: Load distribution and composition on lifting mechanism.....	40
Table 5: loads on the mobile chassis.....	47
Table 6: maximum resultant loads.....	49
Table 7: <i>maximum normal and shear forces acting on eyelets</i>	52
Table 8: maximum values of stress and safety factors.....	53
Table 9: motor crank pin force analysis results.....	55
Table 10: maximum forces, moments and stress components acting on pin of crank r1.....	56
Table 11: maximum ideal stresses and safety factors acting on pin of crank r1.....	56
Table 12: data related to the highest torque point in lifting mechanism.....	57
Table 13: comparison between a 30%-70% and a 70%-30% load distribution.....	58
Table 14: crank r22 pin force analysis results.....	60
Table 15: maximum forces, moments and stress components acting on pin of crank r22.....	60
Table 16: maximum ideal stresses and safety factors acting on pin of crank r22.....	60
Table 17: crank r21 pin force analysis results.....	63
Table 18: maximum forces, moments and stress components acting on pin of crank r1.....	63
Table 19: maximum ideal stresses and safety factors acting on pin of crank r21.....	63
Table 20: force analysis results on shaft S2.....	67
Table 21: equivalent shear forces acting on the shaft.....	67
Table 22: basic load rating and loads for lifting bearings.....	69
Table 23: comparison maximum admissible.....	70
Table 24: relevant parameters for pulleys P1 and P2.....	71
Table 25: kinematic parameters of the translating mechanism.....	71
Table 26: total load composition.....	76
Table 27: tags for bits.....	86

Summary

The global glass manufacturing market value was estimated at 262,30 billion euros in 2023 and is forecasted to increase at a compound annual growth rate of 7.5% from 2024 to 2032, because of the increasing adoption of smart and lightweight glass solutions, and growing trend of recyclable materials in the packaging sector.

These numbers wouldn't be possible without the efforts and investments in realization of cutting-edge and versatile machines to be implemented in the glass production lines around the world: among all the industry players, Bottero s.p.a. has had a significant role in providing to the biggest glass manufacturers efficient production lines including highly customizable equipment.

The company has offered me the opportunity to develop my master thesis project around their walking beam, a peculiar transfer machine included in a flat glass line to be delivered to one of their many customers abroad. This piece of equipment has been ideated with the aim of withdrawing glass sheets from the main line conveyor and deliver them to a secondary line: for this reason, it is equipped with a lifting comb, made of custom designed carbon fibre arms, in order to sustain the weight of glass without deforming, and fitting in between the rolls of the conveyors. Moreover, it includes two translating mechanisms to perform the requested movements, both supplied by custom independent SEW Eurodrive electric motors with speed reducers.

A single cycle could be outlined as follows: the carbon fibre waits for the glass slabs underneath the glass flow plane and in between the rollers of the main conveyor. When the command is executed, the conveyor stops and the slabs above the comb are ready to be lifted.

Through the action of its motor, the lifting mechanism is actuated: in a few seconds, the comb comes up and lifts the glass up to a specific height. Consequently, the second mechanism is actuated and the horizontal translation of the glass loaded comb takes place: this motion is performed by the second motor, which supplies, through a pulley, a belt conveyor connected to the wheeled cart that act as a basis for the lifting comb itself.

In order to deposit the glass slabs, the motion is simply reversed in position, velocity and acceleration direction: first, the lifting mechanism proceeds downwards to the initial position and, by doing so, leaves the glass slabs on the secondary conveyor line; secondly, the horizontal motion is reversed by the motor and the comb fits again in between the rolls of the main line conveyor.

The lifting mechanism consists in a motor actuated slider- crank mechanism that can be approximated to a combined two "four-bar planar linkages" model, repeated on

both sides of the fixed chassis, while the horizontal translation can be reconducted to a belt transmission model.

From a mechanical point of view, the aim of the thesis consisted in analysing the kinematics and dynamics of the two mechanisms, evaluating the motor torque requested by the performance needed and the forces exchanged, especially in crucial points of the machine, i.e. bearings, eyelets, motor shaft. Consequently, it was possible to check if the motors chosen by the designers were suitable or overestimated for the application and proceed with dimensioning and verifications of the aforementioned sensible components.

At last, a general model for the walking beam was produced: the created models and equations were imported on an Excel spreadsheet, so that it is possible to describe the expected torques, forces, velocities and accelerations in many points of the machine by just adjusting dimensions, inertia parameters and masses.

This step is fundamental in order to bring simplification, clarification and unification in a highly customized environment, where a lot of components are usually produced just to satisfy the needs of a single configuration amongst hundreds available and could be subject to dismissal or changes within the lifecycle of a single machine (approximately 10 years).

By means of this system, it is possible to extrapolate data from all the possible configurations and compare them to select and reduce the number of custom parts to be produced and that can be adapted to all the machines in the catalogue, strongly reducing costs in terms of time, manufacturing, human errors and, hence, money.

From the software point of view, it was necessary to program the motion of the machine during the single cycle, following the trapezoidal velocity profiles provided. For this purpose, Studio 5000x suite by Rockwell Automation was used, as it integrates better with the Rockwell inverter on board of the machine and unlocks specific libraries for motion control, in particular Kinetix Motion libraries by Allen-Bradley, allowing coordinated multi-axis motion control and offering a wide range of commands. The main routines and subroutines were written entirely in PLC ladder code and are expected to be integrated in the main architecture of the plant.

The main routine was developed as a main hub collecting some essential subroutines, providing emergency and error checks based on the parameter error and failure flags, as well as providing a step-to-step schedule of motion subroutines and commands based on the outputs of the position sensors and absence of execution errors from previous steps.

Among the developed subroutines we can mention:

- Emergency subroutine, blocking the machine in its current state and preventing further motion, until the emergency mode is disabled and restart button is pressed;
- Lifting subroutine, managing the lifting motion based on the selected option (nominal, extra-stroke);
- Translating subroutine, managing the horizontal translation;
- Error checking subroutine, providing error detection in process execution and sensor feedbacks;

Subsequently, a 3D simulation by means of Factory I/O application, integrated in Codesys, was performed, in order to visualize the work done, as an anticipation of the on-field tests that were conducted.

This thesis project represented an opportunity to challenge the acquired knowledge during these years at Politecnico di Torino in a stimulating and multisided project, providing an in-depth study of a real machine, underlining the critical, improvable aspects with the purpose of enhancing the existing performance, increasing the knowledge on the actual machine and simplifying the unnecessary variety options offered.

Moreover, it was an exciting first introduction to the professional world, attending a technical office on a daily basis and working side to side with experienced colleagues, always ready to provide guidance and help.

Chapter 1 A brief introduction to glass manufacturing

1.1 An economic overview of the flat glass industry

Flat glass refers to a type of glass that is produced in large, flat sheets with smooth surfaces, typically used in a wide range of application, such as windows, mirrors, and glass doors. Depending on the application requirements, it could be treated or coated to achieve better performances under several profiles, such as its insulation, strength or just for aesthetic finishes (like tinted or frosted glass). It is an essential component in fields such as architecture and design, automotive industry but also solar energy generation.

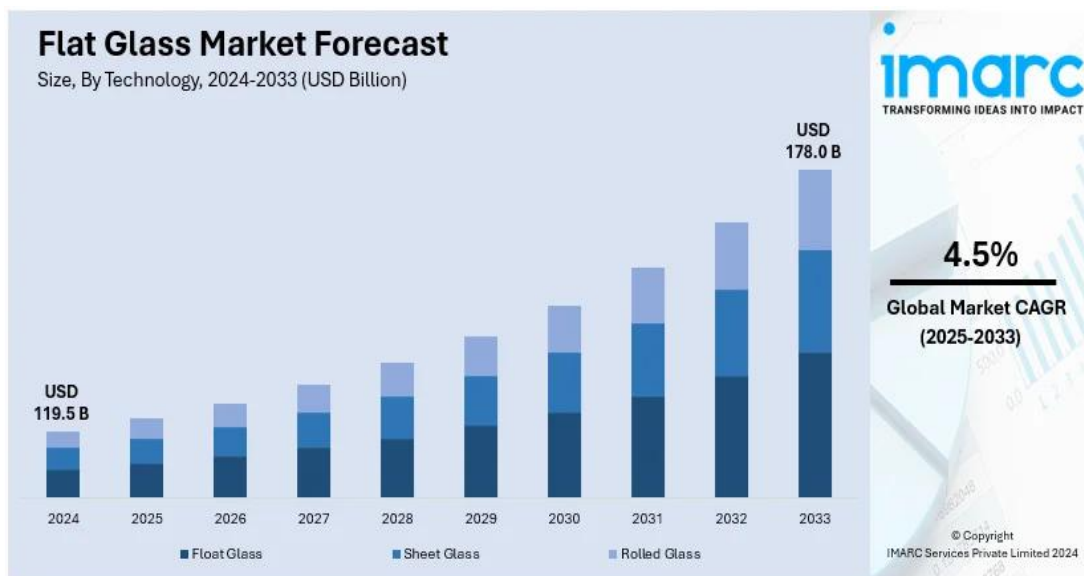


Figure 1: IMARC group projections for flat glass global market

According to a research by IMARC group, the flat glass market valued at about 119,5 billion USD and it is expect to reach 178 billion USD in 2035, with a compound annual growth rate (CAGR) of 4,5% (Figure 1). The compound annual growth rate expresses the annualized average of revenue growth between two years compared and, in this case, it is mainly due to the contribution of some key changes in the market industrial

drivers.

At the moment, three main factors are contributing to an increase in demand and offer of flat glass on a global scale: green and smart architecture, automotive and EV production, diffusion of solar energy technology

1.1.1 Low impact and smart housing

The impellent necessity of expanding the city environments, due to concentration of working opportunities and better living conditions and comforts, has led to a boom in sustainable construction and building, which demand low emission, good looking and highly performing materials such as flat glass itself. The material could be employed in a variety of solutions due to its light weight, such as windows, facades and curtain walls.

1.1.2 Automotive industry and solar energy demand

Despite always providing an essential contribution to the demand of this product, the automotive industry underwent to a significant change in materials and design since the advent of Electric Vehicles (EV), driving the demand for large windows and sunroofs.

Similarly, the growing requests for solar energy as a renewable source to be directly integrated in architecture and other solutions, is supposed to bring even more benefits to the flat glass market.

1.1.3 The regional markets

Currently, the Asia Pacific region represents the biggest portion of the global market, with China crowned as the largest consumer and producer of flat glass: this fact could be connected with the industrial ambition and nature of the country, together with the big boom in smart, sustainable and efficient urbanization of rural areas promoted by the Chinese government, due to the need of expanding the cities and providing housing to an increasing number of people. India and Japan are also worth a mention, with India's heavy adoption of solar energy infrastructures nationwide and Japan offering innovative solutions for lightweight yet resistant glass for EV.

Europe, instead, detains the title for fastest growing market, due to the sustainability and efficiency policies and regulations imposed by the EU in the context of the Green deal, which aims at reaching carbon neutrality by 2050. Hence the surge in requests of insulated and coated glass in architecture or the adoption laminated and tempered glass by car manufacturers to increase safety and efficiency.

Similarly, the North American region follows, not only with the adoption of glass as a sustainable material for efficient and low emission building but also in solar energy

production, with the installation of panels providing a total of 25 GigaWatt in 2024 alone.

Glass is “an amorphous material obtained by the supercooling of a melt, usually containing silicon dioxide, or silica, that is characterized by its disorderly atoms. While in crystalline quartz, atoms are pinned to regularly spaced positions in a repeating pattern, in glass, the same molecules of silicon and oxygen atoms (Si+O) are arranged in a more disordered pattern.”

In recent research, it has been stated that " glass is a non-equilibrium, non-crystalline condensed state of matter. The structure of glasses is similar to that of their parent supercooled liquids (SCL), and they spontaneously relax toward the SCL state. Their fate, in the limit of infinite time, is to crystallize". Since the Late Bronze Age, human beings surrounded themselves with glass. At first, in Ancient Egypt and Mesopotamia it was considered as a precious material, at parity with gold and silver; then, during the Middle Ages, it started to be used in buildings as a shield and protection with respect the outside world.

Today it is an essential element in various fields and applications, from architecture and design to scientific environment and packaging. Here a first distinction can be made, based on shape and, so in the manufacturing process: hollow glass and flat glass.

1.2 Flat glass

Until the 16th century, flat glass was obtained either from large discs of crown glass or by blowing large cylinders, which were cut open and flattened, then cut into panes. The latter technique became the most popular and diffused in manufacturing up to the early 19th century: those hollow glass cylinders were from 180 to 240 cm long and 25 to 36 cm in diameter, elements that impacted the overall dimensions of the panes of glass that could be cut, resulting in windows divided by transoms into rectangular panels, despite using a single glass panel. The first advances in automating glass manufacturing were patented in 1848 by Henry Bessemer, who ideated a system producing a continuous ribbon of flat glass between rollers: the process, however, was expensive, as the surfaces of the glass needed polishing.

1.2.1 Invention of float glass and general process

Between 1953 and 1957, at the Cowley Hill Works St Helens, Lancashire, United Kingdom, Sir Alastair Pilkington and Kenneth Bickerstaff of the Pilkington Brothers developed the first successful commercial application for forming a continuous ribbon of glass using a molten tin bath on which the molten glass flows unhindered under the

influence of gravity. The success of this process, called float glass or Pilkington process, lay in the careful balance of the volume of floating molten glass (typically consisting of sand, soda ash or sodium carbonate, dolomite, limestone, and sodium sulphate) on a bed of molten metal of a low melting point (typically tin, but sometimes lead also), where it was flattened by its own weight, providing uniform thickness and a very flat surface to the sheet.

The choice of molten tin as a vector for the float glass process because it has a higher density ($\sim 6.5 \text{ g/cm}^3$) than glass ($\sim 2.3 \text{ g/cm}^3$), so the molten glass floats on it; also, its boiling point is higher than the melting point of glass, and its vapour pressure at process temperature is low, causing the least amount of reactions and interference during molten glass forming and cooling. However, tin oxidises in natural atmosphere, forming tin dioxide (SnO_2), or “dross”, which adheres to the glass. To prevent oxidation, the tin bath is provided with a positive pressure protective atmosphere of nitrogen and hydrogen.

The raw materials are mixed in batches, then fed together with a controlled proportion of waste glass into the furnace, which usually is 9 m wide, 45 m long and with capacity of more than 1,200 tons of glass. Here the temperature is brought up to approximately $1,600^\circ\text{C}$ but, after the mixed materials are homogeneously molten, it is stabilised to approximately $1,200^\circ\text{C}$ in the forehearth to ensure a homogeneous density of the glass (*Figure 2*).

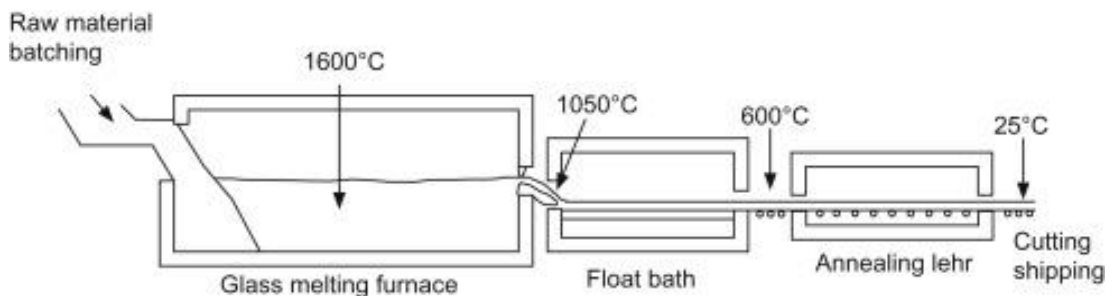


Figure 2: float glass manufacturing process

The molten glass is thereafter poured in a controlled way through a gate, the tweel, and by means of a ceramic lip, the spout lip, into a 6 cm deep bath of molten tin: in this way, the glass ribbon's width and thickness are controlled and perfectly smooth surfaces on both sides are obtained.

While flowing along the tin bath, the temperature is gradually reduced from $1,100^\circ\text{C}$ until at approximately 600°C and the glass ribbon is lifted from the bath by rollers at a controlled speed: by changing both flow and roller speed, sheets of varying thickness can be achieved. Top rollers positioned above the molten tin may be used to control both the thickness and the width of the glass ribbon.

Once off the bath, the glass sheet passes through a lehr kiln for approximately 100 m, where it is cooled gradually so that it anneals without strain and does not crack from

the temperature change. On exiting the "cold end" of the kiln, the glass is cut by machines.

At this point of the production, the glass slabs could undergo different processes, depending on the destination application:

- **Lamination:** where glass sheets are laminated, so are bonded to two or more layers of glass with an interlayer of plastic (such as PVB or EVA), increasing safety, sound insulation, and UV protection.
- **Coating:** additional coatings are sometimes applied to the glass to enhance such as **thermal insulation**, **UV resistance**, or **anti-reflectivity**. For example, in order to improve energy efficiency in windows, low-emissivity (Low-E) coatings are applied to glass.
- **Tempering:** for instance, in automotive or architecture, glass is tempered, so it is heated to a high temperature and then rapidly cooled, introducing compression on the surface, increasing strength and safety.
- **Polishing:** The edges of the glass sheets are smoothed to prevent sharp edges that could cause injury or damage during handling or installation.

The float process is considered the world standard for high quality glass manufacture and today there are around 500 glass float lines in the world. Some of them were designed, entirely or in part, in Bottero s.p.a, which for decades has been providing machinery and production solutions for some of the biggest glass producers from China to USA and South America.

Chapter 2 The mechanical analysis

2.1 Purpose of the machine

The name “walking-beam conveyor” generally defines a transportation system for heavy material and it comes from the peculiar structure of the machine, which includes a series of support or beams that move back and forth with a repeated and programmed motion in order to "walk" or move components. Usually, the walking beams are equipped with rollers and are moved by means of cams or other mechanisms supplied by hydraulic actuators or motors.

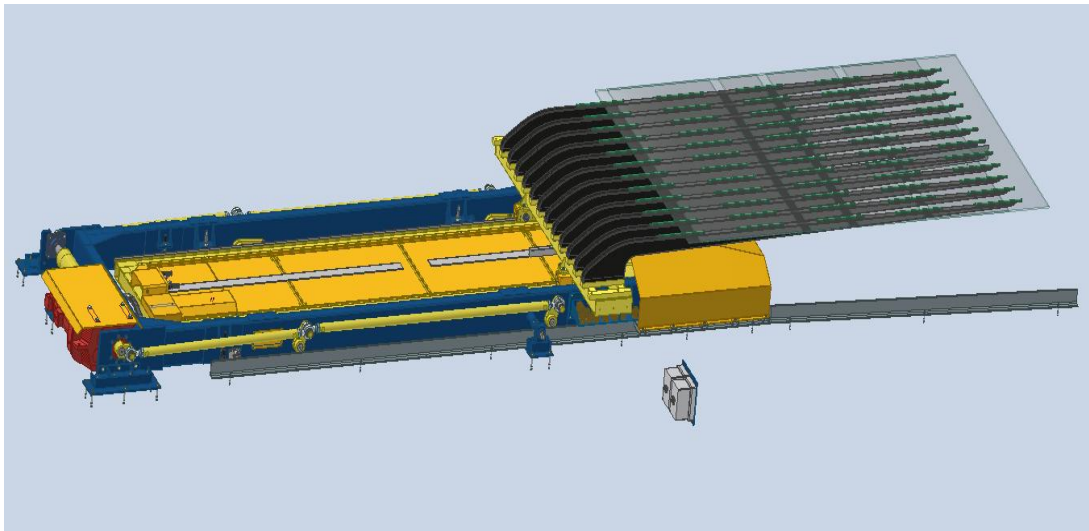


Figure 3: the walking beam transfer machine

The structure usually includes a pair of longitudinally extending, parallel, fixed support rails, including at least one walking beam in between: underneath it, there must be at least two lifters capable of raising the walking beam from a return position below the rails to a conveying position above the rails. In general, the machine is able to collect and move components from one section of the plant to another, usually conveyors, in many industries and different processes, maintaining the ability to provide precise, controlled movements, even for heavy components, without loss of safety or efficiency.

In the case taken under analysis (Figure 3), the walking beam machine has been developed as a transfer machine, with the specific aim of extracting glass slab units from the main line of glass flow and deposit them on a conveyor on a secondary line, where the glass sheets will undergo different treatments.

The transfer movement is composed by two decoupled, subsequent and repeated translations:

- the first one is a lifting operation performed by a slider-crank mechanism, which converts the rotational motion imposed by the motor into a linear one;
- The second one is the horizontal translation of the loading cart, actuated through a belt transmission system supplied by a second motor;

The walking beam has been equipped with a lifting comb, consisting in carbon fibre arms, installed and designed to perfectly fit in between the rolls of a roll conveyor and positioned slightly below the line of flow, so that it can't damage or interfere with the glass above (**Figure 4**).

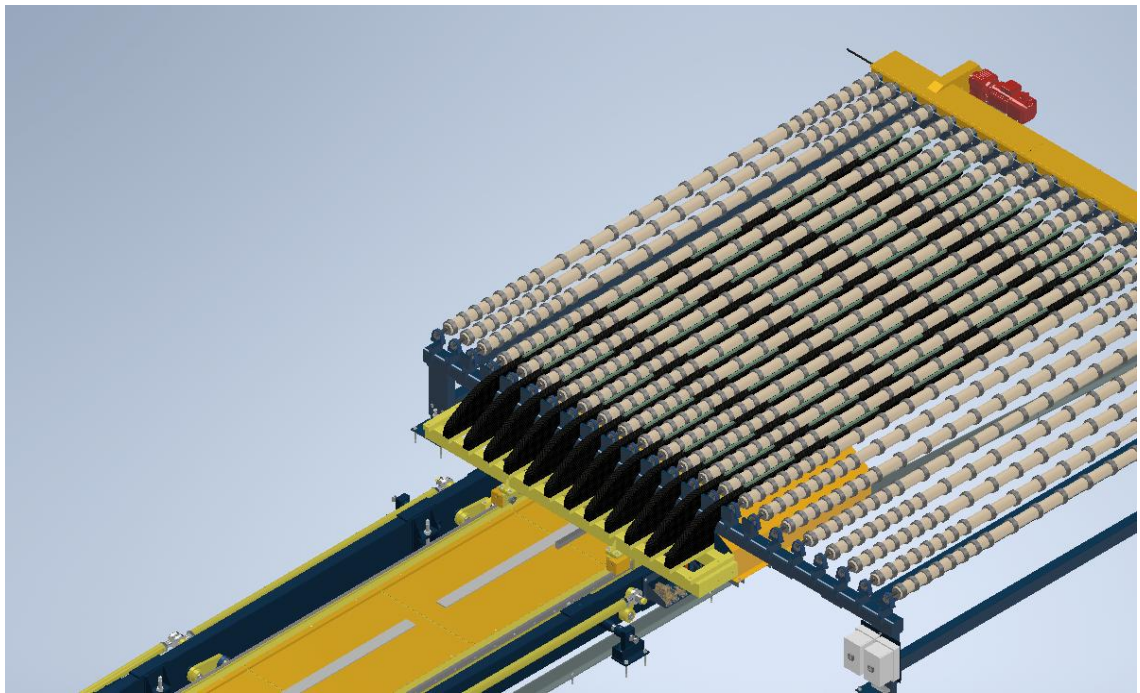


Figure 4: the walking beam steady state position below the main line

The choice of carbon fibre is mainly due to a mechanical need, as the weight and distribution of glass on the comb would cause severe deformations in a steel counterpart, eventually causing the fall of tons of glass, with all its hazardous safety-related consequences for the operators and the machinery nearby, not to mention the costs of the material loss.

The comb waits in its rest position underneath the main line until the conveyor starts decelerating and, ultimately, stops.

At this point, the walking beam receives the start signal and the motor supplies the lifting mechanism, which lifts the mobile chassis by means of four arms: therefore, the comb withdraws the glass sheet from the main line.

After that the lift outstroke is reached, the translation starts, as the motor installed underneath the mobile chassis supplies a belt conveyor connected to a wheeled cart that act as a basis for the carbon fibre comb.

At the end of the horizontal stroke, the two translations are reversed: first, the mobile chassis is lowered, so that the glass is deposited on the secondary conveyor; finally, the belt conveyor brings back the mobile cart and the comb in the origin position under the main conveyor.

Considering the masses involved and the application requirements, the cycle is fast: it takes approximately 15 seconds to complete a single cycle. The fastest contribution is given by the lifting process, which takes around 2 seconds, as it is important to promptly withdraw the glass from the main line without obstructing it and allowing to resume the glass sheets flow.

2.2 The lifting mechanism: analytical approach

As mentioned before, from a mechanical point of view, the lifting and translating motion are completely decoupled and independent, as they take place in two separated steps. Hence it is possible to study each subsystem separately, reducing the complexity.

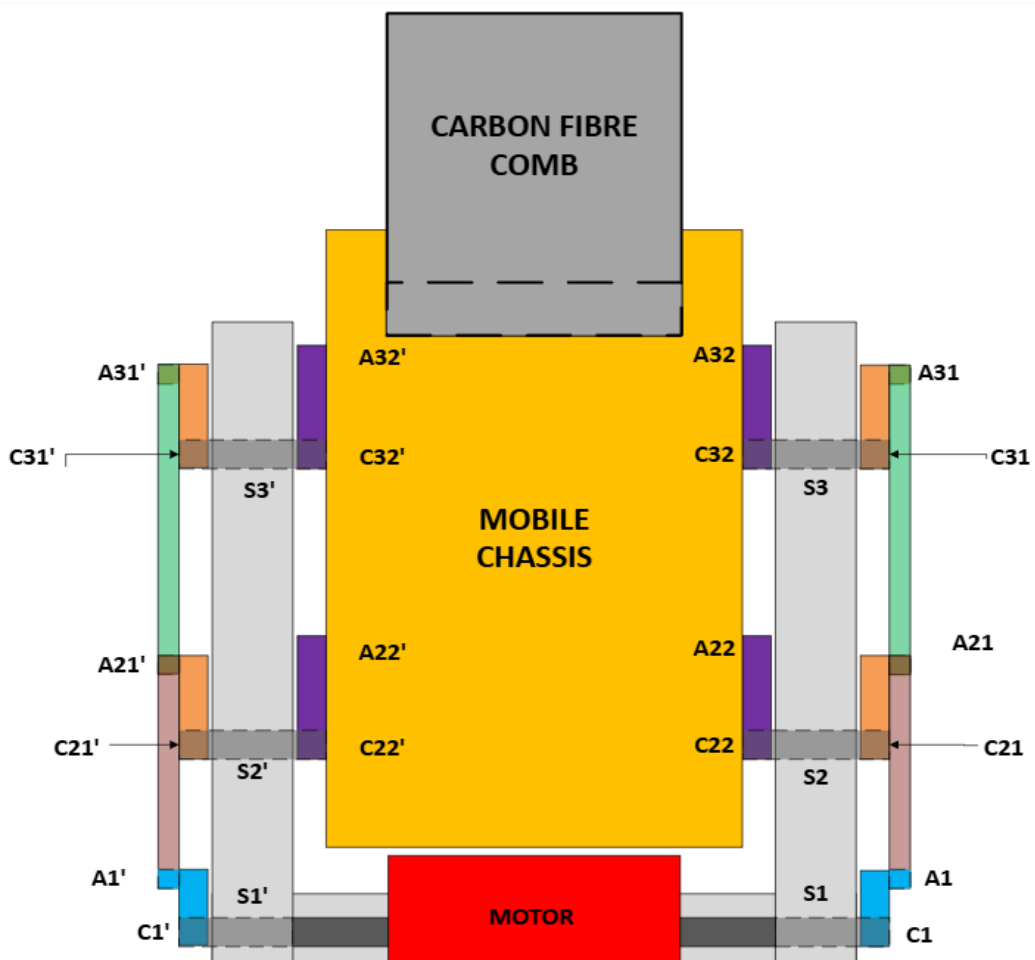


Figure 5: schematization from above of the walking beam

The lifting system is composed by:

- A fixed chassis;
- A motor with its speed reducer;
- A symmetric slider crank mechanism for lifting;

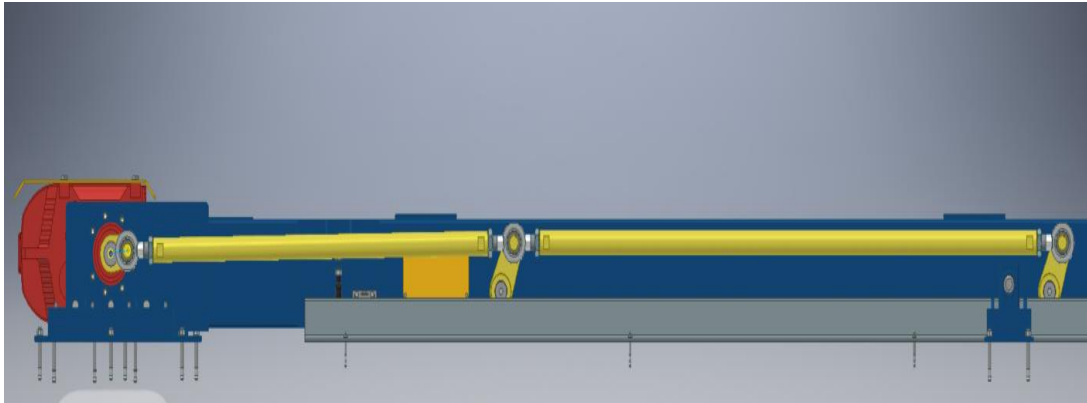


Figure 6: the walking beam lifting mechanism on the right-hand side

The slider crank mechanism (in *Figure 6*, in yellow) represents a simple solution to convert the rotary motion of the motor into the desired linear motion of the mobile frame.

The mechanism is symmetrical on the two sides of the machine, and, for this reason, it is possible to conduct our analysis by studying one of the two sides, just considering the distributed load of the lifting weight per side and half of the total motor torque provided.

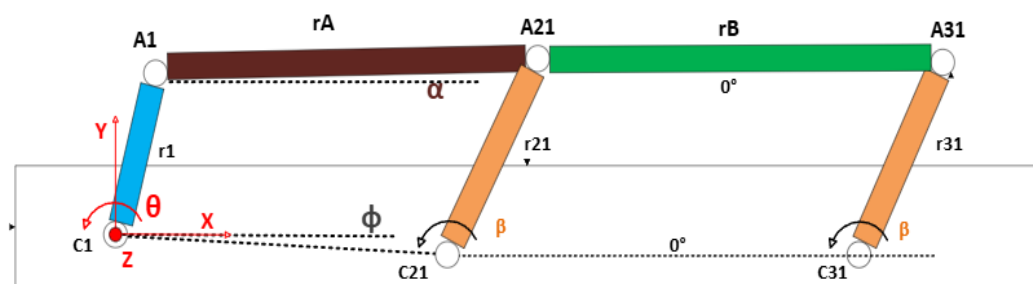


Figure 7: schematization of the external lifting mechanism on the right-hand side

Each side is comprehensive of three arms (r_1 , r_{21} , r_{31}), or cranks, joined by two connecting rods (r_A , r_B), or couplers, with eyelets. R_1 is mounted directly on the speed reducer shaft by means of a key slot and has centre of rotation C_1 ; coupler r_A connects crank r_1 and r_{21} in point A_1 and A_{21} respectively, while r_B connects r_{21} to r_{31} in points A_{21} and A_{31} (*Figure 7*). Moreover, r_{21} and r_{31} rotate around their centres, namely C_{21} and C_{31} , and are mounted with the same angle inclination β_0 on two equal and separated shafts, S_2 and S_3 , hosted in hubs

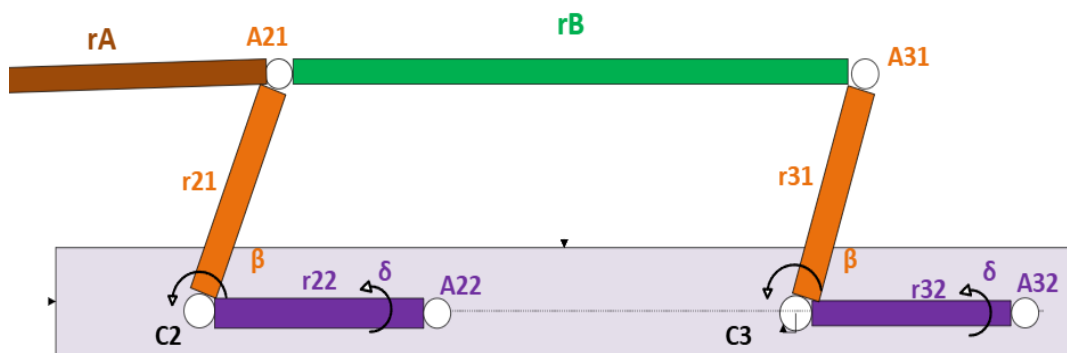


Figure 8: schematization external-internal lifting mechanism

in the fixed chassis: internally they are coupled with the lifting cranks, r_{22} and r_{32} respectively, maintaining a fixed relative angle δ_0 in angular position (*Figure 8*). In this way, it results that r_{21} and r_{22} are mounted on the same shaft S_2 (*Figure 9*) and so, r_{31} and r_{32} do on shaft S_3 .

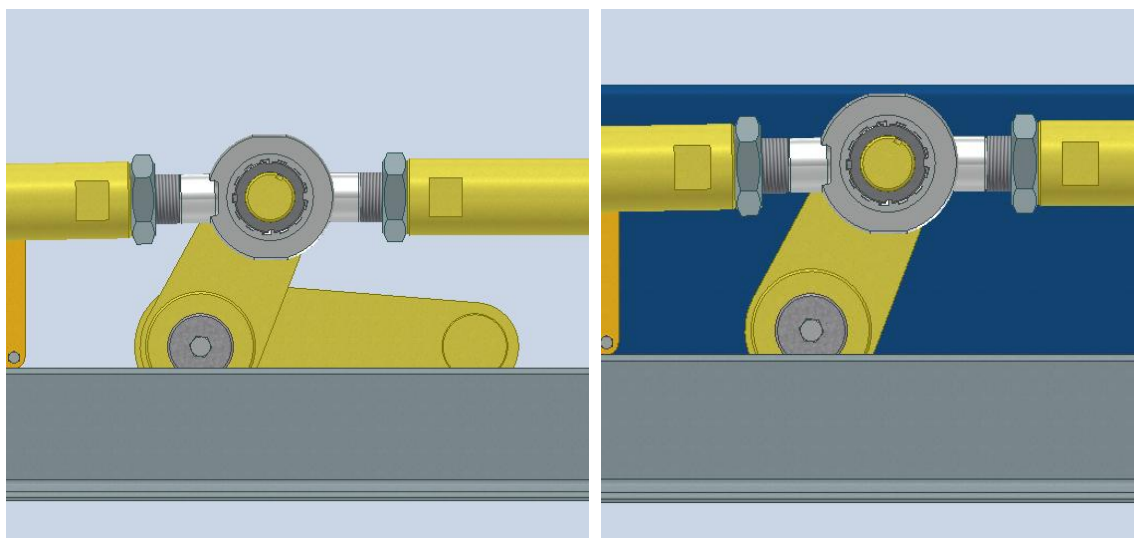


Figure 9: detailed view of coupling between cranks r_{21} and r_{22} , with and without chassis

The working principle is straightforward: on right hand side, crank r_1 receives half the total motor couple C_{M1} directly from the speed reducer shaft and rotates *counterclockwise* with angular displacement θ around C_1 . The motion is transmitted

by rA to the right-hand portion of the mechanism, so r21 and, via rB, r31. As the lifting arms are internally coupled on common shafts with the external cranks, the rotation of r21 and r31 causes also the rotation of r22 and r32, allowing the lifting of the mobile chassis to take place (**Figure 10**). The same mechanism is repeated symmetrically on the left-hand side of the machine.

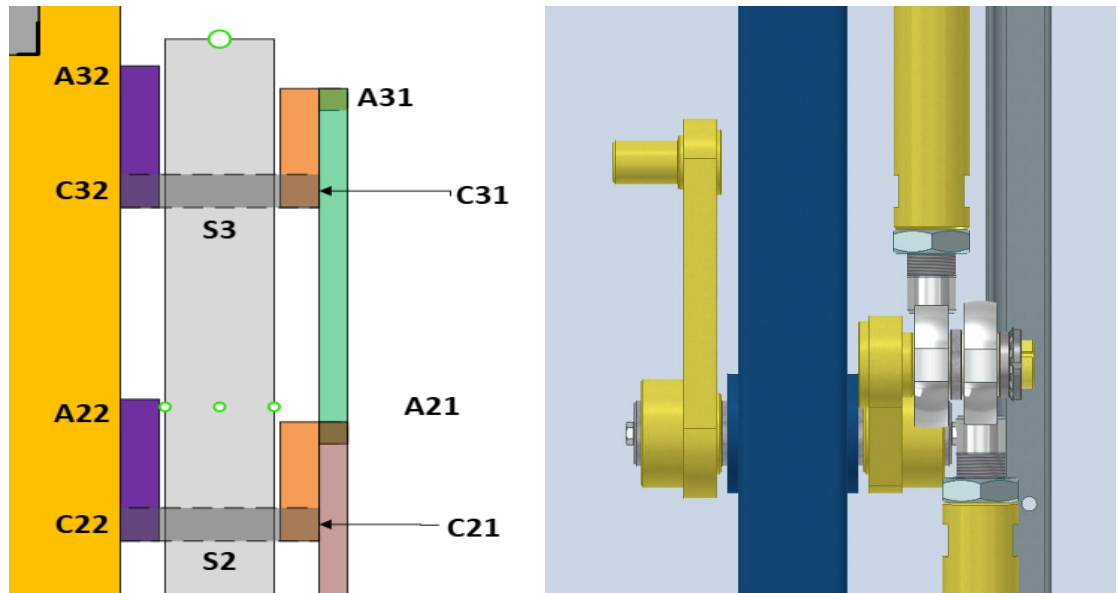


Figure 10: view from above of the couplings between external and internal lifting mechanisms; on the right, detail of r21-r22 coupling

Since the mechanical system provided is subject to motion and solicitations in a two-dimensional space and the components could be approximated as rod-shaped objects, the system can be considered as a combination of two “four bar linkage” planar mechanisms.

2.2.1 The articulated quadrilateral or four bar planar linkage model

The articulated quadrilateral belongs to the family of simple planar kinematics and consists in a set of four rigid bodies, usually rod shaped, joined together by means of hinges. The mechanism can be used to produce and exploit rotation, oscillation and/or reciprocation motions between links: by changing characteristics of the links (i.e. length), behaviour (i.e. replacing a crank with a rocker) or by combining more four link planar mechanism, a variety of different outcomes could be obtained.

For sake of the topic, some general nomenclature will be introduced. Considering a generic four bar planar link, we can always identify one link with has a fixed position

and known as frame while, in the opposite position, the connecting rod or coupler is found; the input link provides movement to the whole mechanism and it is transmitted to the output link: depending on the degree of mobility of the input and output link, a

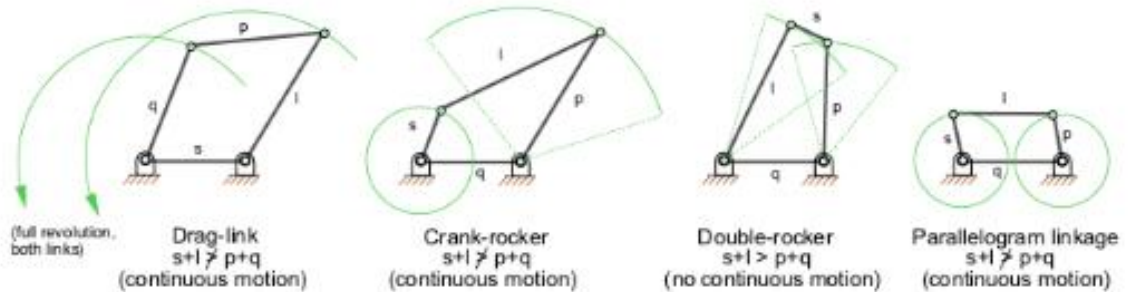


Figure 11: four bar planar linkages possible configurations

further distinction in four link planar mechanism could be done. The term *crank* identifies a link that can perform a complete revolution, the term *rocker* instead refers to a not revolving link; based on the presence of either both or just one typology of input-output link, we can specify more the case under analysis. For instance, if our mechanism includes both a crank and a rocker, it is a “*crank-rocker mechanism*”, if it includes only cranks, it is a “*double crank mechanism*”.

2.2.2 Grashof’s law for a planar-four bar linkage

The Grashof’s law states that in a four-bar mechanism, the sum of the lengths of the longest link (l) and the shortest one (s) cannot overcome the sum of the other two links lengths (q and p) if a continuous relative motion between two members is desired (Figure 11).

$$s + l \leq p + q$$

This relation is used to determine whether at least one element in a four-bar linkage is able to perform a 360° revolution; it appears evident that if the inequality is not satisfied, then no element is able to fully revolve.

In the case that any two links have the same length, the following relation holds:

$$s + l = p + q$$

Meaning that also the two links left will have the same length; depending on the configuration we could have:

- A parallelogram mechanism.
- A deltoid mechanism.

2.2.3 The Grashof's limit case for articulated parallelogram

The cranks R21 and R31, linked together by connecting rod RB, form a peculiar case of articulated quadrilateral known as the Grashof's parallelogram.

As mentioned before, the parallelogram case is one of the two possible configurations that could be obtained when the Grashof's law is in the form

$$s + l = p + q$$

where

$$s = R21 = R31 \text{ and } l = RB = \overline{C21C31} \text{ by construction}$$

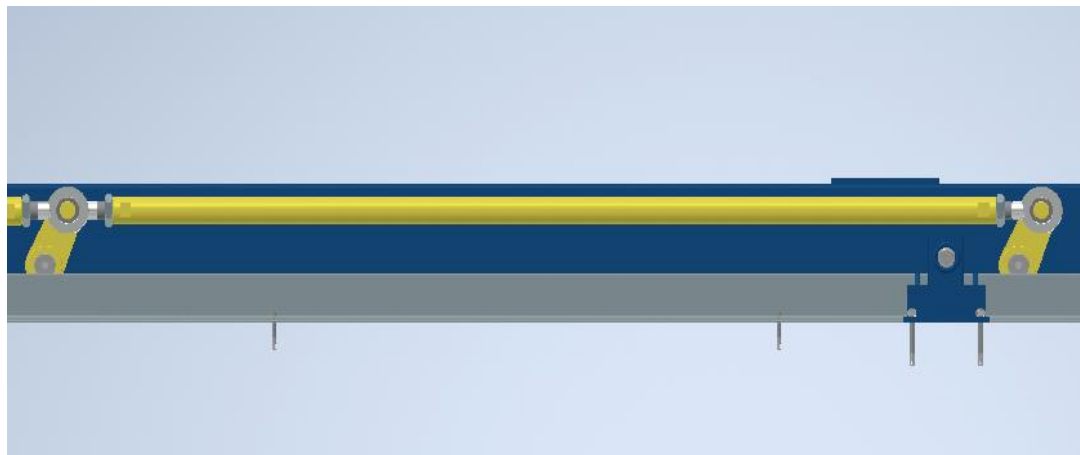


Figure 12: Grashof's parallelogram in the lifting mechanism

Being equal sides in opposite positions, we obtain a parallelogram: we recall, from the simplest geometric definition, that a parallelogram has opposite sides equal and parallel, meaning that they maintain the same inclination, hence angle with respect to any reference system. Consequently, it can be concluded that r21 and r31 have always the same angular position β and so does rB with respect to the frame link C21C31, keeping always an inclination of 0 radian (*Figure 12*).

2.3 The lifting mechanism: kinematic analysis

The final goal of our mechanical analysis includes also the motor dimensioning based on the given velocity profile, hence the determination of the torque needed to deliver such performance. For this reason, it is necessary to obtain a complete model of all positions, velocities and accelerations that each component assumes in the first half of the cycle, where the accelerations and velocities are greater, without being too abrupt or severe, as it would compromise stability and safety of the transported material. The collected data, relations and formulas collected in this step of the analysis will be very useful in the following steps of the research.

First, it is necessary to define a reference system for our subsystem. For a matter of simplicity, the axis centre of the speed reducer shaft was chosen as origin and a right-handed reference system was defined: the ***x axis*** pointing a rightwards direction parallel to the chassis basis surface, the ***y axis*** pointing upwards and perpendicularly to ***x*** and, consequently, the ***z axis*** pointing outwards along the motor shaft axis. In our model, this point also coincides with the centre of rotation C1 of arm R1 (*Figure 7*).

Since the mechanical system provided is subject to no motion and little solicitations along the ***z***-axis direction and the components could be approximated as rod-shaped objects, the system can be considered as a ***planar mechanism in the xy plane***.

As already mentioned, the external mechanism kinematic analysis was conducted according to the following intuition: by looking at the structure and at working principle, it is noticeable that the system is a typical example of two “four bar linkage mechanism” joined together by one common side (crank ***r21***) and with input in C1 (speed reducer angular velocity).

In particular, the right-hand side is the typical example limit case of Grashof’s law for the articulated quadrilateral, the Grashof’s parallelogram, which implies a series of simplifications for the model.

All the measurements related to the machine have been obtained according to the available drawings and components CAD files through Autodesk Inventor Professional software.

Amongst the main noteworthy dimensions, we can mention the main component lengths:

Component	<i>r1</i>	<i>r21=r31</i>	$\overline{C1C21}$	<i>r22=R32</i>	$\overline{C21C31}$	<i>rA</i>	<i>rB</i>
[mm]	80	150	1922,9	250	2700	1904	2700

Table 1: main components lengths

Considering the steady state setup of the machine, it was possible to collect fundamental data such as the initial positions, length of components, distances, angles with respect to our reference system.

In order to relate all the components, the angles values at steady state in time are obtained according to the following formulas:

- $\phi_0 = \cos^{-1}\left(\frac{X_{C1C2}}{C1C2}\right);$
- $\alpha_0 = \cos^{-1}\left(\frac{X_{A1A2}}{A1A2}\right);$
- $\beta_0 = \cos^{-1}\left(\frac{X_{C2A2}}{C2A2}\right) = \cos^{-1}\left(\frac{X_{C2A2}}{r_{21}}\right);$

Knowing the input acceleration and velocity profiles over a cycle time, it is possible to develop a system of equation calculating the variation of the linkage angles in time, hence predicting the variation of position in space of our points of interests in the mechanism, such as points of applications of forces and centres of gravity (or COGs) for all components.

The formulation of the model was developed according to these steps:

- Steady state condition definition.
- Velocity profiles and related accelerations.

2.3.1 The angular position derivation

Starting from the idle position (*Figure 13*) of the machine and the nominal lift / extrastroke lift (*Figure 14*) position, a general model for angle variation in time, as a function of input angular displacement was developed.

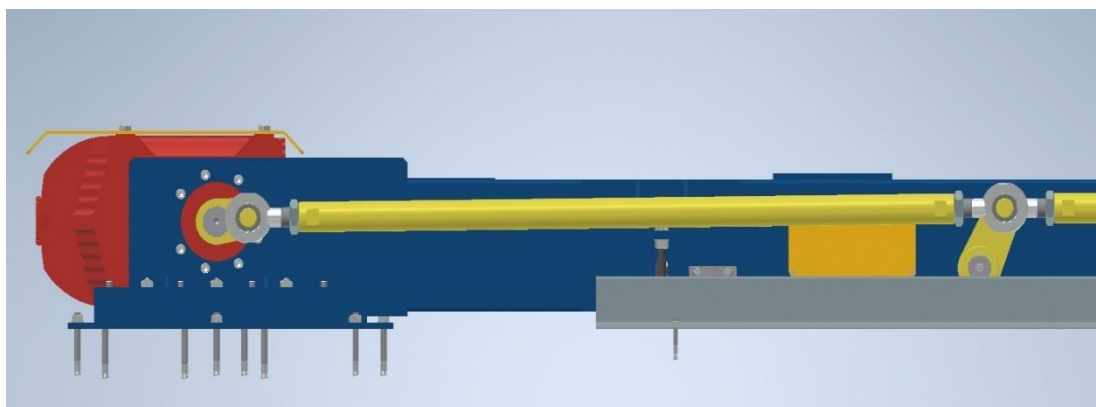


Figure 13: idle position

As stated before, the given input variable is the motor angular acceleration and the velocity profile it provides due to its variation in time and it is directly applied on arm r1 in the rotation centre C1.

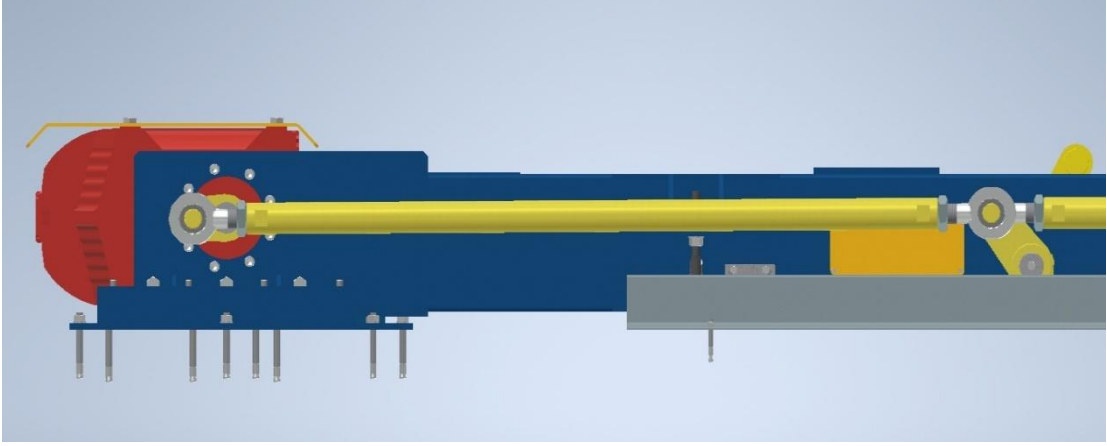


Figure 14: lifting mechanism in extrastroke lift position

Hence, we can state that:

- $\omega_{C1} = \dot{\theta} = \left[\frac{rad}{s^2} \right];$
- $\omega_{C1} = \dot{\theta} = \theta_0 + \dot{\theta} \cdot t = \left[\frac{rad}{s} \right];$
- $\omega_{C1} \cdot t = \theta = \theta_0 + \dot{\theta} \cdot t + \frac{1}{2} \cdot \dot{\theta} \cdot t^2 = [rad];$

In the case under examination (*Figure 15*), a trapezoidal profile with angular acceleration $\ddot{\theta}_{acc} = -3.7 \frac{rad}{s^2}$, $|\dot{\theta}_{acc}| = |\dot{\theta}_{dec}|$ and constant angular velocity $\dot{\theta}_{vel} = -1.85 \frac{rad}{s}$ is imposed.

The constant acceleration and deceleration time is trivial to be calculated, as

$$|\dot{\theta}_{acc}| = |\dot{\theta}_{dec}| = 3.7 \frac{rad}{s^2}$$

$$t_{acc} = t_{dec} = \left| \frac{\dot{\theta}_{max}}{|\dot{\theta}_{const}|} \right| = \frac{-1.85}{-3.7} s = 0,5 s$$

Regarding the constant velocity time t_{vel} , the total angular displacement of the motor crank θ_{tot} must be evaluated first.

	[rad]	[grad]	[rad]	[grad]	[rad]	[grad]
ANGULAR POSITION	β	β	δ	δ	θ	θ
idle position	1,13	65	0,00	0,00	-0,08	53,00
nominal lift	2,01	115,18	0,88	50,18	-2,17	-124,53
extrastroke lift	2,26	129,80	1,13	64,80	-3,11	-178,38

Table 2: angular positions in relevant configurations

The table above (*Table 2*) provides a summary of the values of the relevant angles in the mechanism at the beginning and at the end of the motion execution for both lifting procedures. Considering the biggest displacement, the extra stroke lift

$$\theta_{es} = |\theta_{es,f} - \theta_{es,i}| = |-3.11 - (-0.08)| = 3.03 \text{ rad};$$

Knowing the acceleration time and the acceleration value, we can evaluate the displacement obtained due to accelerated and decelerated motion:

$$\theta_{es,acc} = \left| \frac{1}{2} \ddot{\theta}_{acc} t_{acc}^2 \right| = \left| \frac{1}{2} (-3.7)(0.5)^2 \text{ rad} \right| = 0.46 \text{ rad}$$

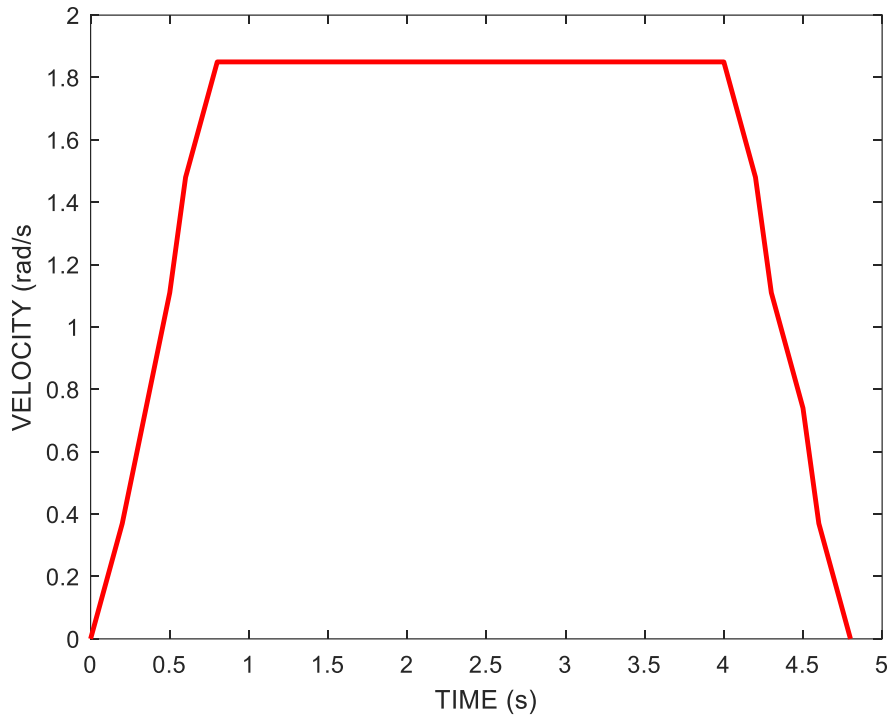


Figure 15: velocity profile for the lifting speed reducer

From here, the angular displacement during the constant velocity path θ_{vel} is defined as

$$\theta_{vel} = \theta_{tot} - 2\theta_{acc} = (3.03 - 2 \cdot 0.46) \text{ rad} = 2.11 \text{ rad}$$

And, by applying the general circular accelerated motion law

- $\dot{\theta}_{vel} = const = -1.85 \frac{rad}{s}$;
- $\ddot{\theta}_{vel} = \frac{d}{dt}(\dot{\theta}_{vel}) = 0 \frac{rad}{s^2}$;
- $\theta_{vel} = \theta_{vel,0} + \dot{\theta}_{vel} t_{vel} + \frac{1}{2} \ddot{\theta}_{vel} t_{vel}^2 \Rightarrow$
 $\Rightarrow \theta_{vel} = 0 + \dot{\theta}_{vel} t_{vel} + \frac{1}{2} 0 t_{vel}^2 \Rightarrow$
 $\Rightarrow t_{vel} = \frac{-\theta_{vel}}{\dot{\theta}_{vel}} = \frac{-2.11}{-1.85} = 1.183 s$

t_{vel} and t_{acc} are then subdivided into 20 and 5 units time intervals, that will be used as units for a discrete time analysis of the whole system.

[rad/s ²]	[rad/s]	[s]	[s]	[rad]	[s]	[s]
$\ddot{\theta}_{acc}$	$\dot{\theta}_{vel}$	t_{acc}	$\frac{t_{acc}}{5}$	$\theta_{es,acc}$	t_{vel}	$\frac{t_{vel}}{20}$
-3,7	-1,85	0,5	0,1	0,46	1,183	0,059

Table 3: kinematic parameters

Considering the hinge A1 between R1 and RA, the following relations hold:

- $\omega_{A1} = \omega_{C1} = \dot{\theta} = \left[\frac{rad}{s} \right]$;
- $\omega_{A1} = \omega_{C1} = \dot{\theta} = \dot{\theta}_0 + \dot{\theta} \cdot t = \left[\frac{rad}{s} \right]$;
- $X_{A1} = R1 \cdot \cos(\theta) = [mm]$;
 $\dot{X}_{A1} = -R1 \cdot \dot{\theta} \cdot \sin(\theta) = \left[\frac{mm}{s} \right]$;
 $\ddot{X}_{A1} = -R1 \cdot (\dot{\theta})^2 \cdot \cos(\theta) - R1 \cdot \ddot{\theta} \cdot \sin(\theta) = \left[\frac{mm}{s^2} \right]$;
- $Y_{A1} = R1 \cdot \sin(\theta) = [mm]$;

In our analysis, information about the values of θ , ϕ and r_A are provided, while we need to know the values of β and α in time, so that it will be possible to derive velocities and accelerations in the subsequent passages.

Since only two parameters incognita are present, a single closed loop equation of the mechanism is sufficient to solve the problem. In our case, we will use the description of the position of point A21 following two different approaches, considering the same starting point (C1) but different components measurements (Figure 16).

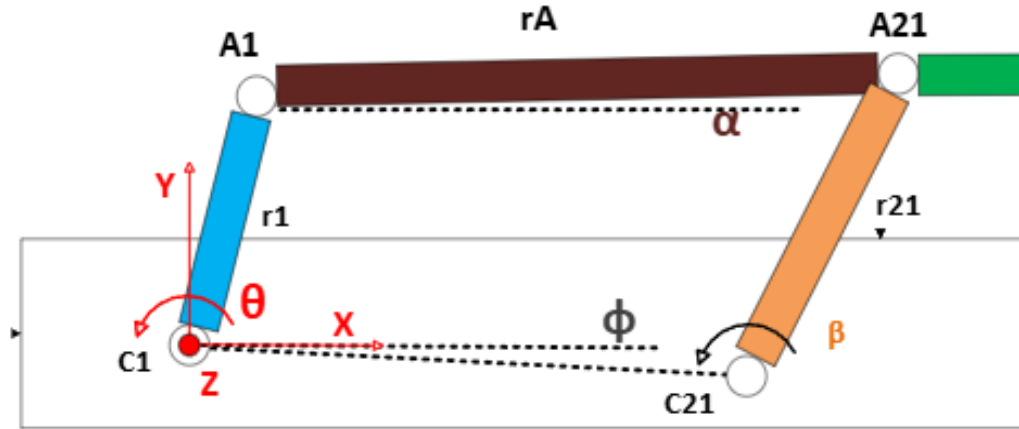


Figure 16: left four bar planar linkage

In particular, the motion laws of hinge A2, connecting r_A to r_{21} , can be described both in relation to rotation centre r_1 and r_2 , obtaining two systems of equations:

- $$X_{A21} = X_{\overline{C1C2}} + r_{21} \cdot \cos(\beta) = [mm];$$

$$X_{\overline{C1C2}} = const = [mm];$$

$$\dot{X}_{A2} = -r_{21} \cdot \dot{\beta} \cdot \sin(\beta) = \left[\frac{mm}{s} \right];$$

$$\ddot{X}_{A2} = -r_{21} \cdot (\dot{\beta})^2 \cdot \cos(\beta) - r_{21} \cdot \ddot{\beta} \cdot \sin(\beta) = \left[\frac{mm}{s^2} \right];$$
- $$Y_{A21} = Y_{\overline{C1C2}} + r_{21} \cdot \sin(\beta) = [mm];$$

$$Y_{\overline{C1C2}} = const = [mm];$$
- $$\omega_{C2} = \dot{\beta} = \left[\frac{rad}{s} \right];$$

$$\omega_{C2} = \dot{\beta} = \dot{\beta}_0 + \ddot{\beta} \cdot t = \left[\frac{rad}{s} \right];$$

$$\omega_{C2} \cdot t = \dot{\beta} = \beta_0 + \ddot{\beta} \cdot t = \left[\frac{rad}{s} \right];$$

And

- $X_{A2'} = X_{A1} + rA \cdot \cos(\alpha) = r1 \cdot \cos(\theta) + rA \cdot \cos(\alpha);$
 $\dot{X}_{A2'} = \dot{X}_{A1} - rA \cdot \sin(\alpha) = -r1 \cdot \dot{\theta} \cdot \sin(\theta) - rA \cdot \sin(\alpha);$
 $\ddot{X}_{A2'} = -r1 \cdot \ddot{\theta} \cdot \sin(\theta) - r1 \cdot \dot{\theta}^2 \cdot \cos(\theta) - rA \cdot (\dot{\alpha})^2 \cdot \cos(\alpha)$
- $Y_{A2'} = Y_{A1} + rA \cdot \sin(\alpha) = r1 \cdot \sin(\theta) + rA \cdot \sin(\alpha) = [mm];$
 $\dot{Y}_{A2'} = \dot{Y}_{A1} + rA \cdot \dot{\alpha} \cdot \cos(\alpha) = r1 \cdot \dot{\theta} \cdot \cos(\theta) + rA \cdot \dot{\alpha} \cdot \cos(\alpha) = \left[\frac{mm}{s} \right];$
 $\ddot{Y}_{A2'} = \ddot{Y}_{A1} + rA \cdot \ddot{\alpha} \cdot \cos(\alpha) - rA \cdot \dot{\alpha}^2 \cdot \sin(\alpha) = \left[\frac{mm}{s^2} \right];$
 $\ddot{Y}_{A2'} = -r1 \cdot (\dot{\theta})^2 \cdot \sin(\theta) + r1 \cdot \ddot{\theta} \cdot \cos(\theta) + rA \cdot \ddot{\alpha} \cdot \cos(\alpha) +$
 $-rA \cdot \dot{\alpha}^2 \cdot \sin(\alpha) = \left[\frac{mm}{s^2} \right];$

By imposing an equality on the corresponding position coordinates of the two systems:

- $X_{A2} = X_{A2'};$
- $Y_{A2} = Y_{A2'};$
- $RA^2 = RA^2 \cdot \cos^2(\alpha) + RA^2 \cdot \sin^2(\alpha);$

It follows that:

$$\begin{aligned} & (\overline{C1C2})^2 + R1^2 + R21^2 - 2 \cdot R21 \cdot \overline{C1C2} \cdot \cos(\theta - \phi) + 2 \cdot R21 \cdot \cos(\beta) \\ & \cdot (\overline{C1C2} \cdot \cos(\phi) - R1 \cdot \cos(\theta)) + \\ & + 2 \cdot R21 \cdot \sin(\beta) \cdot (\overline{C1C2} \cdot \sin(\phi) - R1 \cdot \sin(\theta)) = R31^2; \end{aligned}$$

By looking at the equation above, it can be noticed that it could be reduced by recalling the trigonometric relation:

$$k = a \cdot \cos(\beta) + b \cdot \sin(\beta);$$

Where:

- $a = 2 \cdot R21 \cdot (\overline{C1C2} \cdot \cos \phi - R1 \cdot \cos(\theta));$
- $b = 2 \cdot R21 \cdot (\overline{C1C2} \cdot \sin(\phi) - R1 \cdot \sin(\theta));$
- $k = RA^2 - R21^2 - R1^2 - (\overline{C1C2})^2 + 2 \cdot R1 \cdot \overline{C1C2} \cdot \cos(\theta - \phi);$

Moreover, it would be useful to obtain the following form:

$$\cos(\psi) \cdot \cos(\beta) + \sin(\psi) \cdot \sin(\beta) = k'$$

so that, by applying the trigonometric relation, it results that

$$\begin{aligned} \cos(x) \cdot \cos(y) + \sin(x) \cdot \sin(y) &= \cos(x - y) \Rightarrow \\ \Rightarrow \cos(\psi) \cdot \cos(\beta) + \sin(\psi) \cdot \sin(\beta) &= \cos(\psi - \beta); \end{aligned}$$

where ψ is a fictitious angle used for calculation purposes only. In order to do so, we multiply both members of equation by the factor $\frac{1}{\sqrt{(a^2+b^2)}}$, so that

$$\begin{aligned} \frac{1}{\sqrt{(a^2 + b^2)}} \cdot k &= \frac{1}{\sqrt{(a^2 + b^2)}} \cdot (a \cos(\beta) + b \sin(\beta)) \Rightarrow \\ \Rightarrow k' &= \cos(\psi) \cos(\beta) + \sin(\psi) \sin(\beta) = \cos(\psi - \beta) \end{aligned}$$

With

$$\begin{aligned} k' &= \frac{1}{\sqrt{(a^2 + b^2)}} k \\ \cos(\psi) &= a \cdot \frac{1}{\sqrt{(a^2 + b^2)}} \\ \sin(\psi) &= b \cdot \frac{1}{\sqrt{(a^2 + b^2)}} \end{aligned}$$

Hence, a final formulation for our unknown angle β is performed:

$$\beta = \psi \mp \cos^{-1} \left(\frac{k}{\sqrt{a^2+b^2}} \right), \text{ with}$$

- $\psi = \cos^{-1} \left(\frac{a}{\sqrt{a^2+b^2}} \right)$ if $b \geq 0$;
- $\psi = -\cos^{-1} \left(\frac{a}{\sqrt{a^2+b^2}} \right)$ if $b < 0$;

In order to find a trigonometric formulation for α , it is needed go back to our position equations for point A21 as a function of

- $rA \cdot \cos(\alpha) = \overline{C1C2} \cdot \cos(\phi) + r2 \cdot \cos(\beta) - r1 \cdot \cos(\theta)$;
- $rB \cdot \sin(\alpha) = \overline{C1C2} \cdot \sin(\phi) + r2 \cdot \sin(\beta) - r1 \cdot \sin(\theta)$;

And, by substituting the new equation for β , it is clear that:

- $\alpha = \cos^{-1} \left(\frac{c}{Ra} \right)$ if $c \geq 0$
- $\alpha = -\cos^{-1} \left(\frac{c}{Ra} \right)$ if $c < 0$,

$$\text{with } c = \overline{C1C2} \cos(\phi) + r2 \cos(\beta) - r1 \cos(\theta)$$

It can be concluded that, depending on the sign of b , hence on the value of β , we obtain only one possible value for α , which is depends on the sign of c .

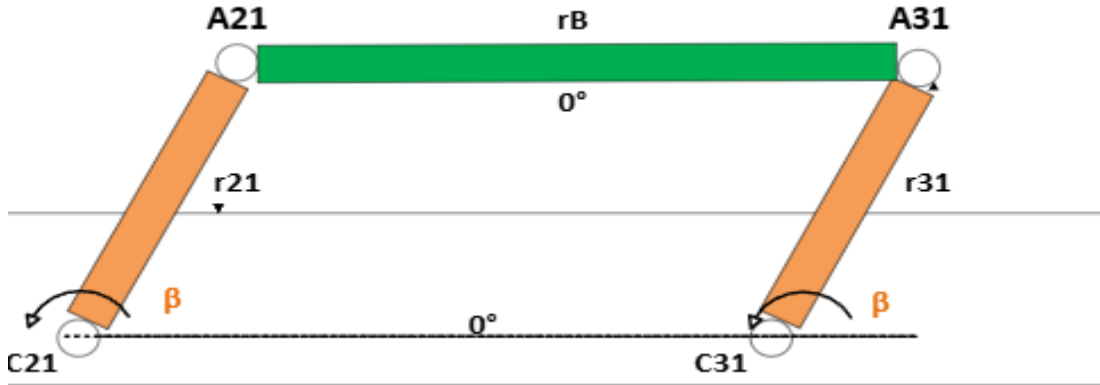


Figure 17: the right four bar planar linkage or Grashof's parallelogram in the lifting mechanism

For the right-hand parallelogram analysis, geometrical properties of the shape simplify a lot the calculations

- $X_{A31} = X_{A2} + rB \cdot \cos(0) = X_{\overline{C1C2}} + r21 \cdot \cos(\beta) + rB;$
 $Y_{A31} = Y_{A21} = Y_{\overline{C1C2}} + r21 \cdot \sin(\beta);$

Regarding the position of the lifting arms $r22$ and $r32$, we remember that they are coupled respectively $r21$ and $r31$ in the inner part of the chassis by means of a common shaft and with a shift of a relative angle δ_0 in angular position (Figure 17), such that

$$\delta = \beta - \beta_0; \quad \beta_0 = \text{const}$$

It follows that

- $X_{A22} = X_{\overline{C1C2}} + r22 \cdot \cos(\beta - \delta_0) = X_{\overline{C1C2}} + Rr22 \cdot \cos(\delta) = [mm];$
 $Y_{A22} = Y_{\overline{C1C2}} + r22 \cdot \sin(\beta - \delta_0) = Y_{\overline{C1C2}} + r22 \cdot \sin(\delta) [mm];$

And

- $X_{A32} = X_{\overline{C1C2}} + X_{\overline{C2C3}} + R32 \cdot \cos(\beta - \delta_0) = X_{\overline{C1C2}} + X_{\overline{C2C3}} + R32 \cdot \cos(\delta)$
 $X_{A32} = Y_{\overline{C1C2}} + Y_{\overline{C2C3}} + R32 \cdot \sin(\beta - \delta_0) = Y_{\overline{C1C2}} + R32 \cdot \sin(\delta)$

2.3.2 Angular velocities derivation

The analysis could be started by imposing the equality $\dot{X}_{A2} = \dot{X}_{A2'}$ from the position equations:

$$\Rightarrow r_{21} \cdot \dot{\beta} \cdot \sin(\beta) = r_1 \cdot \dot{\theta} \cdot \sin(\theta) + r_A \cdot \sin(\alpha);$$

And $\dot{Y}_{A2} = \dot{Y}_{A2'}$

$$\Rightarrow r_{21} \cdot \dot{\beta} \cdot \cos(\beta) = r_1 \cdot \dot{\theta} \cdot \cos(\theta) + r_A \cdot \dot{\alpha} \cdot \cos(\alpha);$$

By merging the two equations above

$$\Rightarrow r_1 \cdot \dot{\theta} \cdot e^{i\theta} + r_A \cdot \dot{\alpha} \cdot e^{i\alpha} = r_{21} \cdot \dot{\beta} \cdot e^{i\beta}$$

And by multiplying both members of by $e^{-i\alpha}$

$$\Rightarrow r_1 \cdot \dot{\theta} \cdot e^{i(\theta-\alpha)} + r_A \cdot \dot{\alpha} \cdot e^{i \cdot 0} = r_{21} \cdot \dot{\beta} \cdot e^{i(\beta-\alpha)}$$

Considering only the imaginary part of the equation,

$$\Rightarrow r_1 \cdot \dot{\theta} \cdot \sin(\theta - \alpha) = r_{21} \cdot \dot{\beta} \cdot \sin(\beta - \alpha) \Rightarrow$$

$$\Rightarrow \dot{\beta} = \frac{r_1}{r_{21}} \cdot \dot{\theta} \cdot \frac{\sin(\theta - \alpha)}{\sin(\beta - \alpha)}$$

We can repeat the same iter, by multiplying for $e^{-i\beta}$ instead, obtaining

$$\Rightarrow \dot{\alpha} = \frac{r_1}{r_A} \cdot \dot{\theta} \cdot \frac{\sin(\theta - \beta)}{\sin(\alpha - \beta)}$$

For the right -hand side of the mechanism, it is sufficient to recall that

- $\dot{X}_{A31} = \dot{X}_{A21} = -r_{21} \cdot \dot{\beta} \cdot \sin(\beta);$
 $\dot{Y}_{A31} = \dot{Y}_{A21} = r_{21} \cdot \dot{\beta} \cdot \cos(\beta);$

Regarding the angular velocity of the lifting arms, we simply apply the first derivative in time to

$$\delta = \beta - \beta_0; \quad \beta_0 = \text{const} \Rightarrow$$

$$\Rightarrow \dot{\delta} = \frac{\partial}{\partial t}(\beta - \beta_0) = \dot{\beta};$$

Hence, we can express the velocities of points A32 and A22 as:

$$\begin{aligned} \dot{X}_{A32} = \dot{X}_{A22} &= -r_{22} \cdot \dot{\beta} \cdot \sin(\beta) = -r_{32} \cdot \dot{\beta} \cdot \sin(\beta) \quad \dot{Y}_{A32} = \dot{Y}_{A22} \\ &= r_{22} \cdot \dot{\beta} \cdot \cos(\beta) = r_{32} \cdot \dot{\beta} \cdot \cos(\beta) \end{aligned}$$

2.3.3 Angular acceleration derivation

We can start from a formulation in the polar coordinates of A2 and imposing identity between the two equations:

- $X_{A2} = r1 \cdot e^{i\theta} + RA \cdot e^{i\alpha}$
- $X_{A2'} = r21 \cdot e^{i\beta} + \overline{C1C2} \cdot e^{i\phi}$

$$\Rightarrow r1 \cdot e^{i\theta} + rA \cdot e^{i\alpha} = r21 \cdot e^{i\beta} + \overline{C1C2} \cdot e^{i\phi}$$

Performing the second time derivative of the obtained formula, we obtain

$$\begin{aligned} \frac{\partial}{\partial t^2} (r1 \cdot e^{i\theta} + rA \cdot e^{i\alpha}) &= \frac{\partial}{\partial t^2} (r21 \cdot e^{i\beta} + \overline{C1C2} \cdot e^{i\phi}) \Rightarrow \\ \Rightarrow i \cdot r1 \cdot \dot{\theta} \cdot e^{i\theta} - r1 \cdot \dot{\theta}^2 \cdot e^{i\theta} + i \cdot rA \cdot \dot{\alpha} \cdot e^{i\alpha} - rA \cdot \dot{\alpha}^2 \cdot e^{i\alpha} \\ &= i \cdot r21 \cdot \dot{\beta} \cdot e^{i\beta} - r21 \cdot \dot{\beta}^2 \cdot e^{i\beta} \Rightarrow \end{aligned}$$

- Multiplying for $e^{-i\alpha}$:

$$\begin{aligned} \Rightarrow (i \cdot r1 \cdot \dot{\theta} - r1 \cdot \dot{\theta}^2) \cdot e^{i(\theta-\alpha)} + (i \cdot rA \cdot \dot{\alpha} - rA \cdot \dot{\alpha}^2) \cdot e^{i \cdot 0} \\ = (i \cdot r21 \cdot \dot{\beta} - r21 \cdot \dot{\beta}^2) \cdot e^{i \cdot (\beta-\alpha)} \end{aligned}$$

By considering the real part only,

$$\begin{aligned} \Rightarrow (i \cdot r1 \cdot \dot{\theta} - r1 \cdot \dot{\theta}^2) \cdot (\cos(\theta - \alpha) + i \cdot \sin(\theta - \alpha)) + i \cdot rA \cdot \dot{\alpha} - rA \cdot \dot{\alpha}^2 = \\ = (i \cdot r21 \cdot \dot{\beta} - r21 \cdot \dot{\beta}^2) \cdot (\cos(\beta - \alpha) + i \cdot \sin(\beta - \alpha)) \Rightarrow \\ \Rightarrow i \cdot r1 \cdot \dot{\theta} \cdot \sin(\theta - \alpha) + r1 \cdot \dot{\theta}^2 \cdot \cos(\theta - \alpha) + rA \cdot \dot{\alpha}^2 = r21 \cdot \dot{\beta} \cdot \sin(\beta - \alpha) + \\ + r21 \cdot \dot{\beta}^2 \cdot \cos(\beta - \alpha) \Rightarrow \\ \Rightarrow \dot{\beta} = \frac{r1 \cdot \dot{\theta} \cdot \sin(\theta - \alpha) - r1 \cdot \dot{\theta}^2 \cdot \cos(\theta - \alpha) - r21 \cdot \dot{\beta}^2 \cdot \cos(\beta - \alpha)}{r21 \cdot \sin(\beta - \alpha)} \end{aligned}$$

- Multiplying for $e^{-i\beta}$:

$$\begin{aligned} \Rightarrow (i \cdot r1 \cdot \dot{\theta} - r1 \cdot \dot{\theta}^2) \cdot e^{i(\theta-\beta)} + (i \cdot rA \cdot \dot{\alpha} - rA \cdot \dot{\alpha}^2) \cdot e^{i \cdot (\alpha-\beta)} = \\ = (i \cdot r21 \cdot \dot{\beta} - r21 \cdot \dot{\beta}^2) \cdot e^{i \cdot (0)} \end{aligned}$$

By considering the real part only,

$$\begin{aligned}
&\Rightarrow \left(i \cdot r_1 \cdot \dot{\theta} - r_1 \cdot \dot{\theta}^2 \right) \cdot (\cos(\theta - \beta) + i \cdot \sin(\theta - \beta)) + \\
&+ \left(i \cdot r_A \cdot \dot{\alpha} - r_A \cdot \dot{\alpha}^2 \right) \cdot (\cos(\alpha - \beta) + i \cdot \sin(\alpha - \beta)) = \left(i \cdot r_{21} \cdot \dot{\beta} - r_{21} \cdot \dot{\beta}^2 \right) \\
&\Rightarrow \\
&\qquad\qquad\qquad \Rightarrow \dot{\alpha} \\
&= \frac{r_{21} \cdot \dot{\beta}^2 - R_1 \cdot \dot{\theta} \cdot \sin(\theta - \beta) - r_1 \cdot \dot{\theta}^2 \cdot \cos(\theta - \beta) - r_A \cdot \dot{\alpha}^2 \cdot \cos(\alpha - \beta)}{r_A \cdot \sin(\alpha - \beta)}
\end{aligned}$$

For the right-hand side of the mechanism, it is sufficient to recall that

- $X_{A31}^{\dot{}} = X_{A21}^{\dot{}} = -r_{21} \cdot (\dot{\beta})^2 \cdot \cos(\beta) - r_{21} \cdot \dot{\beta} \cdot \sin(\beta)$
- $Y_{A31}^{\dot{}} = Y_{A21}^{\dot{}} = -r_{21} \cdot (\dot{\beta})^2 \cdot \sin(\beta) + r_{21} \cdot \dot{\beta} \cdot \cos(\beta);$

For what concerns the lifting cranks R22 and R32, we apply the second time derivative to the equation for angular displacement δ :

$$\frac{\partial}{\partial t^2}(\delta) = \dot{\delta} = \frac{\partial}{\partial t^2}(\beta - \beta_0) = \dot{\beta}$$

Hence, we can conclude that

- $X_{A32}^{\dot{}} = X_{A22}^{\dot{}} = -R_{32} \cdot (\dot{\beta})^2 \cdot \cos(\beta) - R_{32} \cdot \dot{\beta} \cdot \sin(\beta) = -R_{22} \cdot (\dot{\beta})^2 \cdot \cos(\beta) - R_{22} \cdot \dot{\beta} \cdot \sin(\beta)$
- $Y_{A32}^{\dot{}} = Y_{A22}^{\dot{}} = -R_{32} \cdot (\dot{\beta})^2 \cdot \sin(\beta) + R_{32} \cdot \dot{\beta} \cdot \cos(\beta) = -R_{22} \cdot (\dot{\beta})^2 \cdot \sin(\beta) + R_{22} \cdot \dot{\beta} \cdot \cos(\beta)$

2.4 The lifting mechanism: dynamic analysis

After having defined and obtained values for the angular displacements, velocities and acceleration for each element of our linkage, it is possible to proceed with the dynamic analysis of our system.

This step will be mainly functional to two goals of the project:

- Evaluation of the motor couple needed to deliver the requested performance in terms of velocities and accelerations, given the provided system.
- Evaluation of the maximum forces generated during a single cycle, with particular attention in evaluating the maximum stresses in critical components for dimensioning purposes, comparing the obtained results with the datasheet parameters of the actual chosen components.

The analysis was conducted by considering the forces and momenta applied on the single elements of the linkages by external constraints and inputs, together with contributions due to the mass (gravity and inertia forces).

A second analysis followed, considering the force exchanges and equilibrium in static conditions, for any possible angular position θ of the motor crank in our predefined range.

However, for convenience, only the dynamic analysis will be reported, as it is more complete and denser in terms of parameters taken into account. To obtain the equilibrium formulas in static conditions, it is sufficient to consider all both linear and angular velocities and acceleration as null, except for gravity acceleration.

As a general rule of thumb, it has been decided to consider a load distribution of 30% in the front and 70% in the rear portion of the lifting mechanism as a worst-case scenario, as from calculations it showed that the machine was more solicited in this configuration. For general knowledge, the following values will result

	[kg]			[kg]
	Load distribution			Load composition
	front	rear		
percentage	30%	70%	Lifted conveyor	741,5
For couple	511,8	1194,3	carbon fiber cart	622,7
For crank	255,9	597,2	glass load	192,0
			Extra load (cables, sensors,etc)	150,0

Table 4: Load distribution and composition on lifting mechanism

Link r1

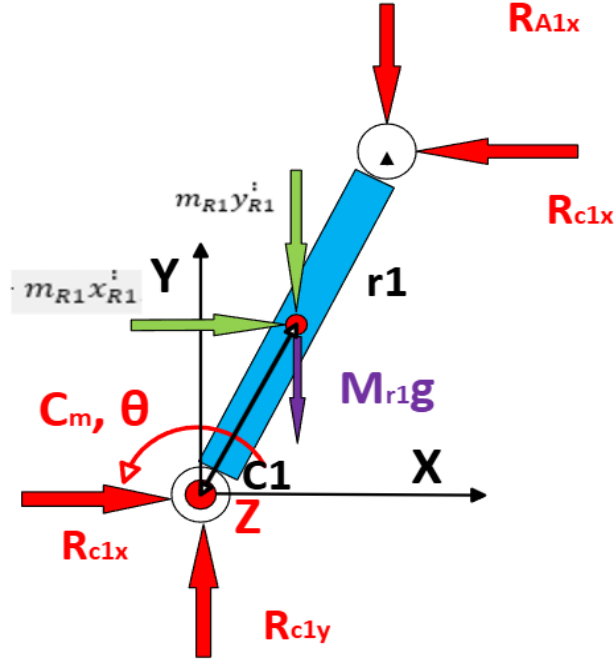


Figure 18: force analysis on crank r1

Crank r1 is fixed on speed reducer shaft of motor M1 by means of a key slot in C1 and transmits half the motor torque $C_m/2$ to the right-hand side of the mechanism. In C1, the reactions exerted on the bearings and on the shaft S1 are located. In the centre of gravity of the crank, located at a distance l_{r1} from the centre of rotation C1, both gravity force and inertia forces along x and y axis are acting. As in C1, the external reaction forces along the vertical and horizontal directions are acting on A1 and are transmitted to the bearings and to the crank pin. In this analysis, r1 rotates around C1 with rotating inertia I_{r1} and angular acceleration $\dot{\theta}$.

By looking at *Figure 18*, it follows that:

1. $R_{XC1} - R_{XA1} + m_{R1}\dot{x}_{R1} = 0 \Rightarrow R_{XA1} = R_{XC1} + m_{R1}\dot{x}_{R1}$;
2. $R_{YC1} - R_{YA1} - m_{R1}\dot{y}_{R1} = 0 \Rightarrow R_{YC1} - m_{R1}\dot{y}_{R1} = R_{YA1}$;
3. C1 \curvearrowright $C_m/2 - I_{r1}\dot{\theta} - m_{r1}(x_{r1}^i \sin(\theta) + (y_{r1}^i + g) \cos(\theta))l_{r1} - R_{yA1}r1 \cos(\theta) + R_{xA1}r1 \sin(\theta) = 0 \Rightarrow$
 $\Rightarrow \frac{C_m}{2} = I_{r1}\dot{\theta} + m_{r1}(r1 - l_{r1})(x_{r1}^i \sin(\theta) + (y_{r1}^i + g) \cos(\theta)) + R_{yC1}r1 \cos(\theta) - R_{xC1}r1 \sin(\theta)$;

Link rA

Connecting rod rA is subject to reaction forces in points A1 and A21, where the bearings of the eyelets are installed, while it is subject to inertia and gravity force in the centre of gravity, located at a distance l_{rA} from point A1 along the axis of rA. For the analysis, the rotation of the connecting rod was assumed around point A1 and with moment of inertia I_{rA} and angular acceleration $\ddot{\alpha}$.

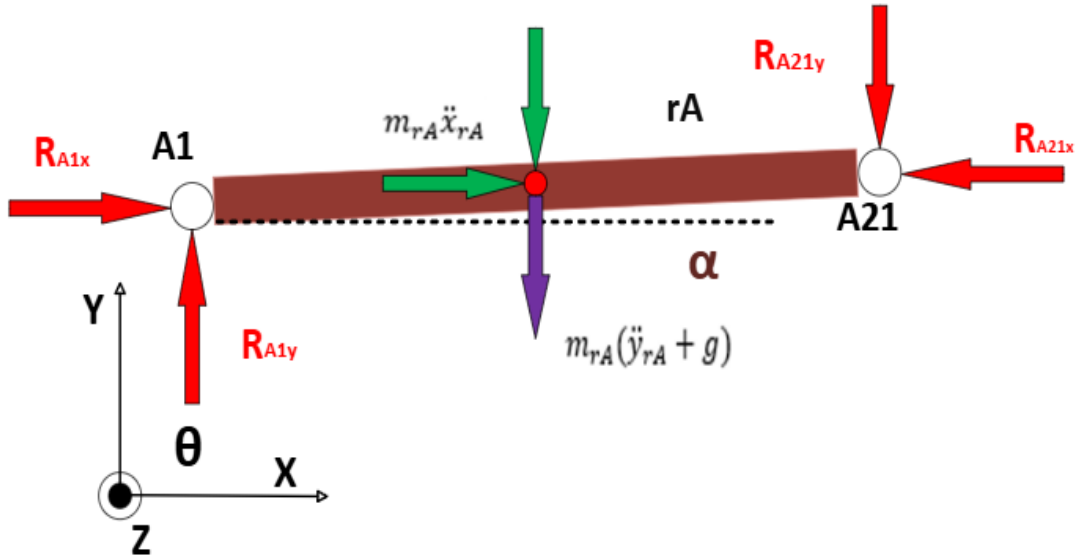


Figure 19: dynamic force analysis on link rA

By looking at Figure 19, it follows that

1. $R_{A1x} - R_{A2x} + m_{rA}\ddot{x}_{rA} = 0 \Rightarrow$
 $\Rightarrow -R_{A2x} = R_{A1x} + m_{rA}\ddot{x}_{rA};$
2. $R_{A1y} - R_{A2y} + m_{rA}(\ddot{y}_{rA} + g) = 0 \Rightarrow$
 $\Rightarrow R_{A2y} = R_{A1y} + m_{rA}(\ddot{y}_{rA} + g);$
3. $A1 \curvearrowright R_{A2x}rA \sin \alpha - m_{rA}l_{rA}(x_{rA}^{\dot{\cdot}} \sin(\alpha) + (y_{rA}^{\dot{\cdot}} + g) \cos(\alpha)) +$
 $-R_{A2y}rA \cos(\alpha) - I_{rA}\ddot{\alpha} = 0 \Rightarrow$
 $\Rightarrow R_{C1x} \sin(\alpha) + \frac{l_{rA}}{rA}\ddot{\alpha} + R_{C1y} \cos(\alpha) - m_{rA}(x_{rA}^{\dot{\cdot}} \sin(\alpha) + (y_{rA}^{\dot{\cdot}} +$
 $g) \cos(\alpha)) + -m_{rA} \left(1 - \frac{l_{rA}}{rA}\right) (x_{rA}^{\dot{\cdot}} \sin(\alpha) + (y_{rA}^{\dot{\cdot}} + g) \cos(\alpha));$

Link r21 & r22 on shafts S2

Crank r21 and r22 are both installed by means of key slots on shaft S2, so they could rotate together with a fixed relative angle in between, β_0 . With regards to r21, it has external reactions acting in point A21 and coming from connecting rods rA and rB, while the reaction forces on C2 are due to the interaction with constraints, such as bearings, shaft S2 and key shaft. R21 rotates around C2 with angular acceleration $\dot{\beta}$ and rotating inertia I_{r21} , while r22 with $\dot{\delta}$ and I_{r22} respectively. Moreover, crank r22 is subject to the partial mobile chassis load F_{W22} , which also contributes to the total

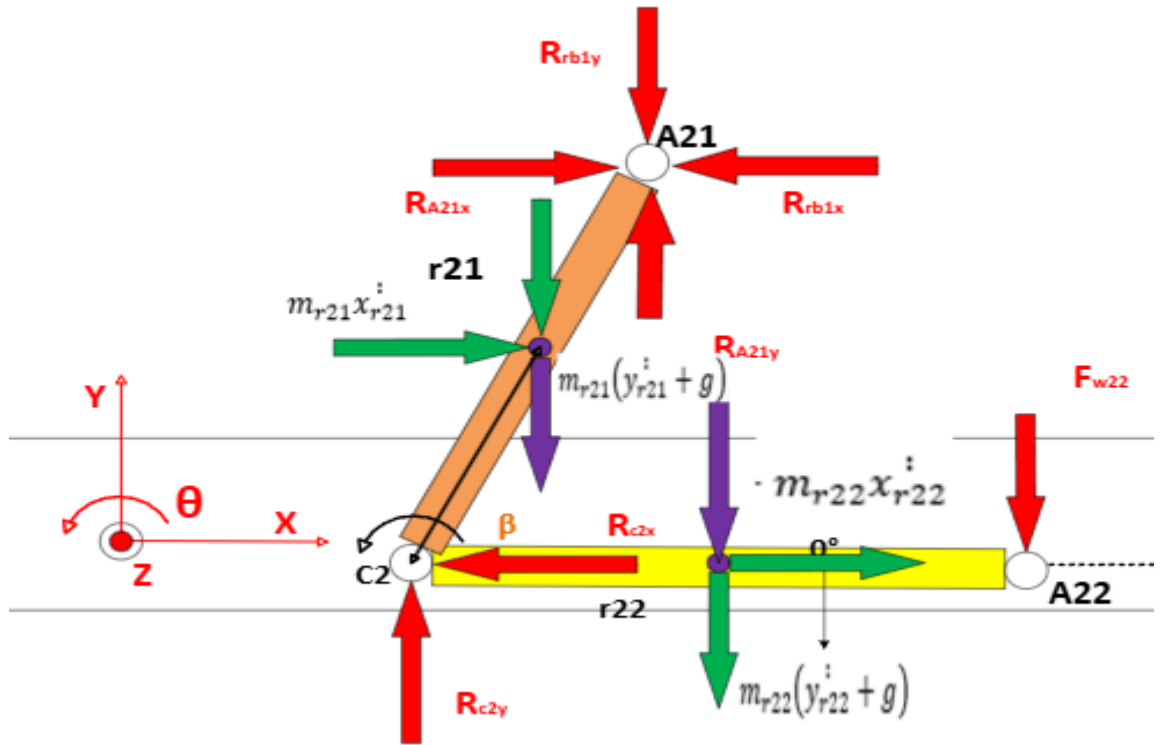


Figure 20: dynamic force analysis on link r21

momentum around shaft S2.

By looking at Figure 20, it follows that

1. $R_{A2x} - R_{RB1x} - R_{C2x} + m_{r22}x_{r22}^{\dot{\cdot}} + m_{r21}x_{r21}^{\dot{\cdot}} = 0 \Rightarrow$
 $\Rightarrow R_{C2x} = R_{C1x} - R_{RB1x} + m_{r21}x_{r21}^{\dot{\cdot}} + m_{r22}x_{r22}^{\dot{\cdot}} + m_{r1}x_{r1}^{\dot{\cdot}} + m_{rA}x_{rA}^{\dot{\cdot}}$
2. $R_{C2y} = -R_{C1y} + R_{RB1y} + m_{r21}(y_{r21}^{\dot{\cdot}} + g) + m_{r22}(y_{r22}^{\dot{\cdot}} + g) +$
 $m_{r1}(y_{r1}^{\dot{\cdot}} + g) + m_{rA}(y_{rA}^{\dot{\cdot}} + g) + F_{W22};$
3. $C2 \curvearrowright m_{r22}l_{r22}(x_{r22}^{\dot{\cdot}} \sin(\delta) + (y_{r22}^{\dot{\cdot}} + g) \cos(\delta)) +$
 $m_{r21}l_{r21}(x_{r21}^{\dot{\cdot}} \sin(\beta) + (y_{r21}^{\dot{\cdot}} + g) \cos(\beta)) + I_{r21}\dot{\beta} + I_{r22}\dot{\delta} +$
 $F_{W22}r22 \cos(\delta) + (R_{A2x} - R_{RB1x})r21 \sin(\beta) + (R_{RB1y} -$
 $R_{A2y})r21 \cos(\beta) = 0;$

Link rB

Connecting rod rB is subject to reaction forces in points A2 and A31, where the bearings of the eyelets are installed, while it is subject to inertia and gravity force in the centre of gravity, located at a distance l_{rB} from point A2 along the axis of rB. For the analysis, the rotation of the connecting rod was assumed around point A2 and with null angular acceleration.

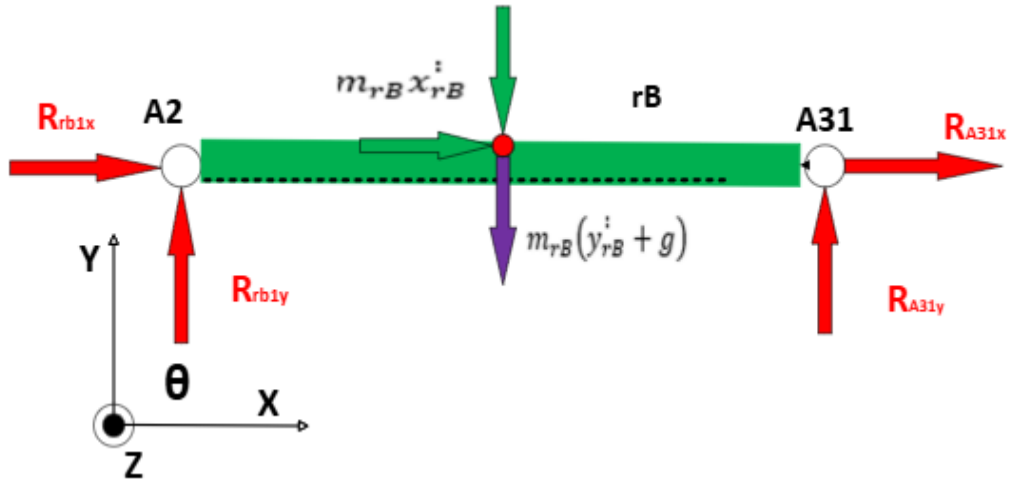


Figure 21: dynamic force analysis on link rB

By looking at *Figure 21*, it follows that

$$1. \quad R_{rB1x} + m_{rB} x_{rB}^{\ddot{}} - R_{A3x} = 0 \Rightarrow \\ \Rightarrow R_{A3x} = R_{rB1x} + m_{rB} x_{rB}^{\ddot{}};$$

$$2. \quad \Rightarrow R_{rB1y} - R_{A3y} - m_{rB}(y_{rB}^{\dot{}} + g) = 0 \Rightarrow \\ \Rightarrow R_{rB1y} = m_{rB}(y_{rB}^{\dot{}} + g) \left(1 - \frac{l_{rB}}{rB}\right);$$

$$3. \quad A2 \curvearrowright) - R_{A3y} \cdot rB - m_{rB}(y_{rB}^{\dot{}} + g)l_{rB} = 0 \Rightarrow \\ \Rightarrow R_{A3y} = -m_{rB}(y_{rB}^{\dot{}} + g) \frac{l_{rB}}{rB}$$

Link r31 & r32

As for shaft S2, rank r31 and r32 are both installed by means of key slots on shaft S3, so they could rotate together with a fixed relative angle in between, β_0 . With regards to r21, it has external reactions acting in point A31 and coming from connecting rod rB, while the reaction forces on C3 are due to the interaction with constraints, such as bearings, shaft S3 and key shaft. R31 rotates around C3 with angular acceleration $\dot{\beta}$ and rotating inertia I_{r31} , while r32 with $\dot{\delta}$ and I_{r32} respectively. Moreover, crank r32 is subject to the partial mobile chassis load F_{W32} , which also contributes to the total momentum around shaft S3.

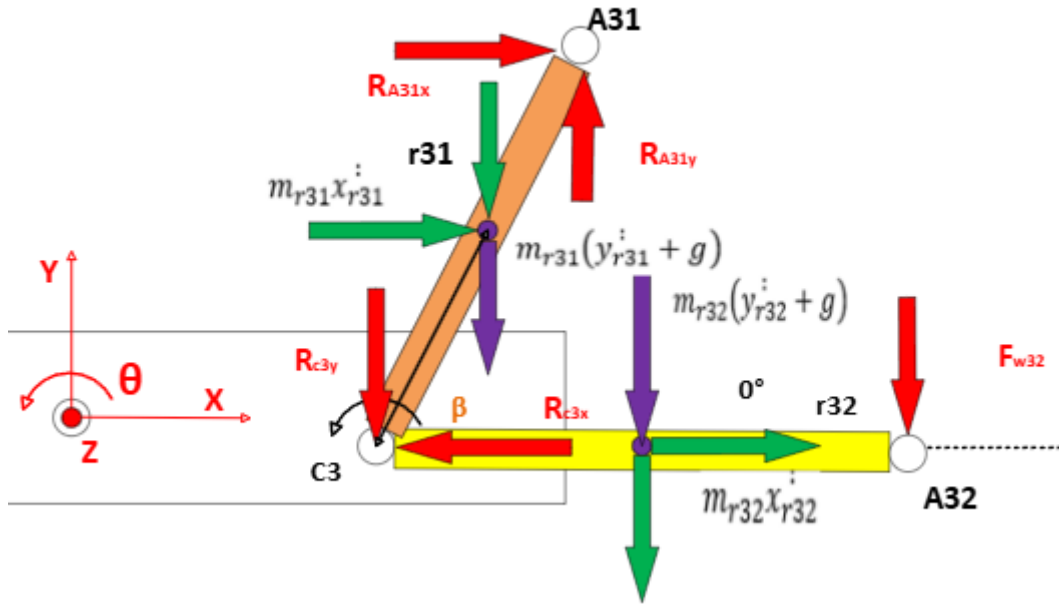


Figure 22: dynamic force analysis on links r31 & r32

By looking at Figure 22, it follows that:

1. $R_{A3x} - R_{C3x} + m_{r32}\ddot{x}_{r32} + m_{r31}\ddot{x}_{r31} = 0 \Rightarrow$
 $\Rightarrow R_{C3x} = R_{rB1x} + m_{rB}\ddot{x}_{rB} + m_{r32}\ddot{x}_{r32} + m_{r31}\ddot{x}_{r31} + m_{rA}\ddot{x}_{rA}$
2. $R_{A3y} - R_{C3y} - m_{r32}(\ddot{y}_{r32} + g) - m_{r31}(\ddot{y}_{r31} + g) - F_{W32} = 0 \Rightarrow$
 $\Rightarrow R_{C3y} = -m_{rB} \frac{l_{rB}}{r_B} (\ddot{y}_{rB} + g) - m_{r32}(\ddot{y}_{r32} + g) - m_{r31}(\ddot{y}_{r31} + g)$
 $- F_{W32}$
3. $C3 \cup) - (R_{A3x}r31 + m_{r31}\ddot{x}_{r31}l_{r31}) \sin(\beta) - m_{r32}\ddot{x}_{r32}l_{r32} \sin(\delta) +$
 $+ R_{A3y}r31 \cos(\beta) - m_{r31}(\ddot{y}_{r31} + g)l_{r31} \cos(\beta)$
 $- m_{r32}(\ddot{y}_{r32} + g)l_{r32} \cos(\delta) +$
 $- F_{W32}r32 \cos(\delta) - I_{r31}\dot{\beta} - I_{r32}\dot{\delta} = 0;$

By solving the provided systems of equations, it is not only possible to obtain numerical values in any time instant for all forces, reactions and momenta in the whole mechanism but also for the necessary motor torque profile, so that the provided velocities and accelerations performances are guaranteed.

As we can see from the graph above, at most 2000 Nm are needed in a single cycle. Comparing this value with the technical datasheet provided by Sew Eurodriver, manufacturer of the motors, it is possible to conclude that the choice of the motor is compatible with our needs, considering that the nominal torque at 60Hz is

1 PZ
 Motorid. ad assi paralleli
 FAZ97 DRN132S4/TH/EK8R/V



Velocità a 50Hz [r/min]	: 1464 / 13
Velocità a 60Hz [r/min]	: 1768 / 16
Rapporto di riduz. totale [i]	: 112,99 / Infinito
Coppia d'uscita max [Nm]	: 4300
Coppia d'uscita a 50Hz [Nm]	: 4050
Coppia d'uscita a 60Hz [Nm]	: 3360

Figure 23: datasheet parameters of lifting motor from manufacturer

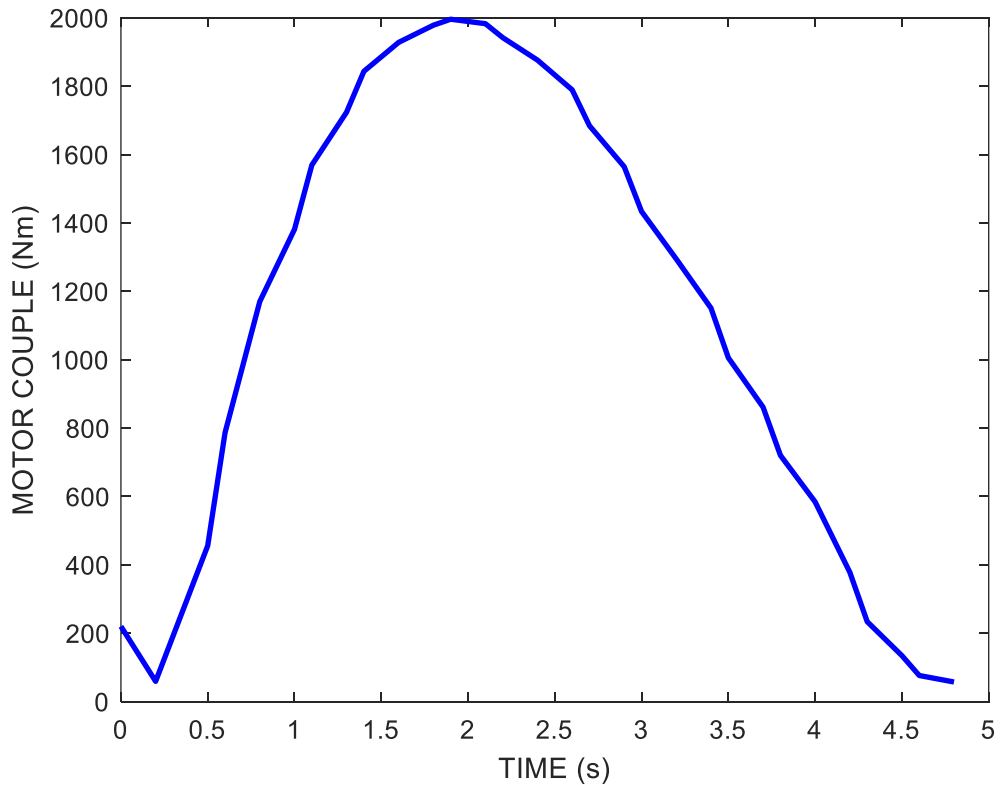


Figure 24: motor couple C_m variations during half cycle

2.5 The lifting mechanism: dimensioning of critical elements

The dimensioning procedure took into account different possible weight distributions of the moving elements of the machine and of the maximum load on the lifting mechanism itself.

Regarding the machine at steady state and unloaded, we always have the weight contributions due to the mobile chassis, the moving cart and the carbon fibre comb, with a total of 1364,2 kg. To this value, 150 kg of extra load are added, taking into account additional components such as sensors, cables, etc.

For the maximum load condition, a glass load equivalent to 3 glass slabs with volume of $1200 \times 1600 \times 10 \text{ mm}^3$ and density of $2.5 \times 10^{-6} \text{ kg/mm}^3$ are considered, with a total of 192 kg.

A comprehensive weight of about 1706,2 kg could be accounted as an average load for the lifting mechanism. However, the load is not distributed uniformly among the whole mechanism during a single cycle execution, hence the need to

[KG]	
component	Load composition
Lifted conveyor	741,5
carbon fibre cart	622,7
glass load	192,0
Extra load (cables, sensors, etc)	150,0
Total	1706,2

Table 5: loads on the mobile chassis

By looking at the obtained general dynamic model, it was possible to observe that with a load distribution of 30% in the front of the machine and 70% in the back, the following values of forces are found, showing a greater number of mechanical solicitations and higher magnitude of forces, especially in the central part of the lifting mechanism, as expected.

Hence the dimensioning procedure took into account the machine forces values for the configuration aforementioned, so that the maximum forces were taken into account for the safety factors calculations.

2.5.1 Connecting rods bearings

The dimensioning analysis begins with the verification of the eyelets joining the connecting rods and the crank. Specifically, they are also defined as maintenance-free rod end with male thread and sliding contact surface in a combination of steel and PTFE fabric.

As a first step, for the ball bearings verification it was necessary to evaluate the maximum resultant forces for each crank pin, hence points A1, A21, A31, to see if they were actually able to withstand the resultant of the exchanged forces.

The static (C_0) and dynamic (C) basic load ratings could be retrieved from the technical datasheet (Figure 25) provided by the bearing manufacturer: these values must be compared with the maximum resultant forces applied on the bearings themselves.

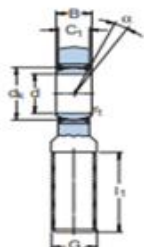
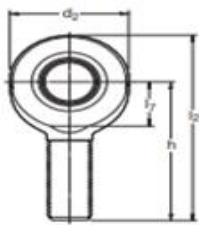
1 Product information			2 Recommendations			3 Product data					
Page 4			Page 16			Maintenance-free rod ends with male thread, with sliding contact surface combination steel/PTFE fabric d 35 – 70 mm					
											
Principal dimensions			Angle of tilt		Basic load ratings		Mass	Designations			
d	d ₂ max	G 6g	B	C ₁ max	h	α	C	C ₀	kg	–	left-hand thread
mm						degrees	kN				
35	84	M 36×3	25	22	130	6	224	110	1,30	–	SAA 35 TXE-2LS SAL 35 TXE-2LS
40	94	M 39×3	28	24	150	6	280	140	1,85	–	SAA 40 TXE-2LS SALA 40 TXE-2LS
45	104	M 42×3	32	28	163	7	360	200	2,45	–	SAA 45 TXE-2LS SALA 45 TXE-2LS
50	114	M 45×3	35	31	185	6	440	245	3,30	–	SAA 50 TXE-2LS SALA 50 TXE-2LS
	114	M 52×3	35	31	195	6	440	235	3,90	–	SAA 50 TXE-2LS SAL 50 TXE-2LS

Figure 25: technical datasheet of the eyelets with bearings

For what concerns the reaction forces, in our case it is sufficient to calculate the modulus of the resultant starting from their components along the coordinate axis, according to the formula

$$R = \sqrt{R_x^2 + R_y^2}.$$

Specifically, for each link, the following calculations followed:

Link R1

$$R_{A1} = \sqrt{R_{A1y}^2 + R_{A1x}^2}$$

Link RA

$$R_{RA} = \sqrt{R_{RAy}^2 + R_{RAx}^2}$$

Link R21

$$R_{A21,R} = \sqrt{(R_{RB1x} - R_{RA2x})^2 + (R_{RB1y} - R_{RA2y})^2} = \sqrt{R_{A21y}^2 + R_{A21x}^2}$$

Link RB

$$R_{A31} = \sqrt{R_{A3y}^2 + R_{A3x}^2}$$

Link R31

$$R_{RA} = \sqrt{R_{RAy}^2 + R_{RAx}^2}$$

Using these relations in the excel datasheet, the maximum values for each reaction resultant were obtained and compared to the known basic loads, both for static and dynamic cases:

	[kN]	[kN]	[mm]
Components	C	Co	d
Bearings	440	245	50
Force	dynamic	static	
$R_{A1,max}$	16,25	17,23	
$R_{A2,max}$	16,25	17,24	
$R_{BA2,max}$	4,84	4,60	
$R_{A3,max}$	4,84	4,60	

Table 6: maximum resultant loads

Hence it is possible to conclude that the bearings are verified for our application.

2.5.2 Connecting rods threads verification

After the verification on the bearings, it is necessary to evaluate the amount of stress exerted on the threaded profile and check whether they are in the expected security level or not.

First of all, it is necessary to derive the normal and shear forces exerted on both connecting rods.

Connecting rod rA

Looking at **Figure 26**, it is intuitive to understand how the reaction forces are related to the normal and shear ones for the two eyelets involved.

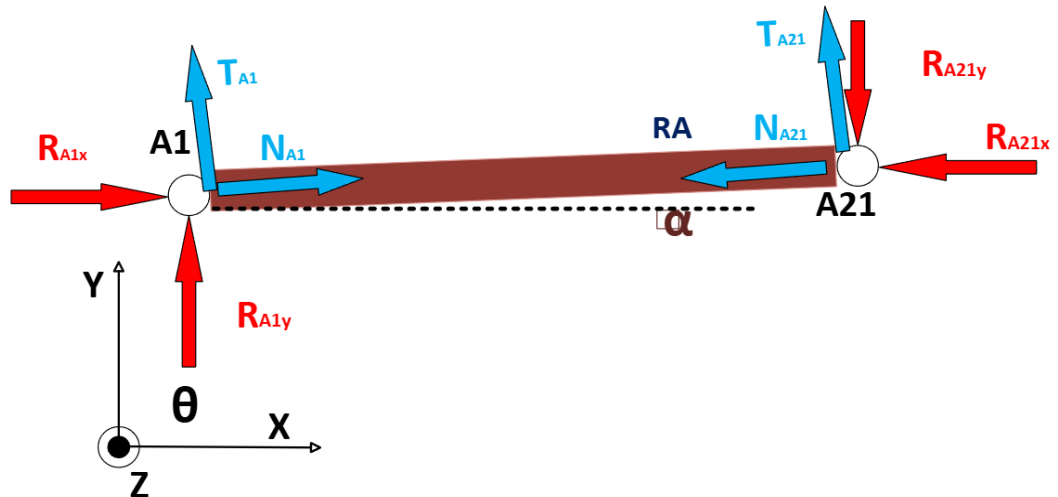


Figure 26: Normal and shear forces distribution along rA

Using basic trigonometric knowledge, the following relations are derived for both eyelets:

A1

- $N_{A1} = -(R_{A1y} \sin(\alpha) + R_{A1x} \cos(\alpha));$
- $T_{A1} = -(R_{A1x} \cos\left(\frac{\pi}{2} + \alpha\right) + R_{A1y} \cos(\alpha));$

A21

- $N_{A21} = -(R_{A2y} \sin(\alpha) + R_{A2x} \cos(\alpha));$

- $T_{A21} = -(R_{A2x} \cos\left(\frac{\pi}{2} + \alpha\right) + R_{A2y} \cos(\alpha));$

Connecting rod rB

Eyelets on connecting rod rB are simpler to be analysed, as the connecting rod always maintain a horizontal position, hence the algebraic sum of horizontal and vertical forces allow direct computation of normal and shear components.

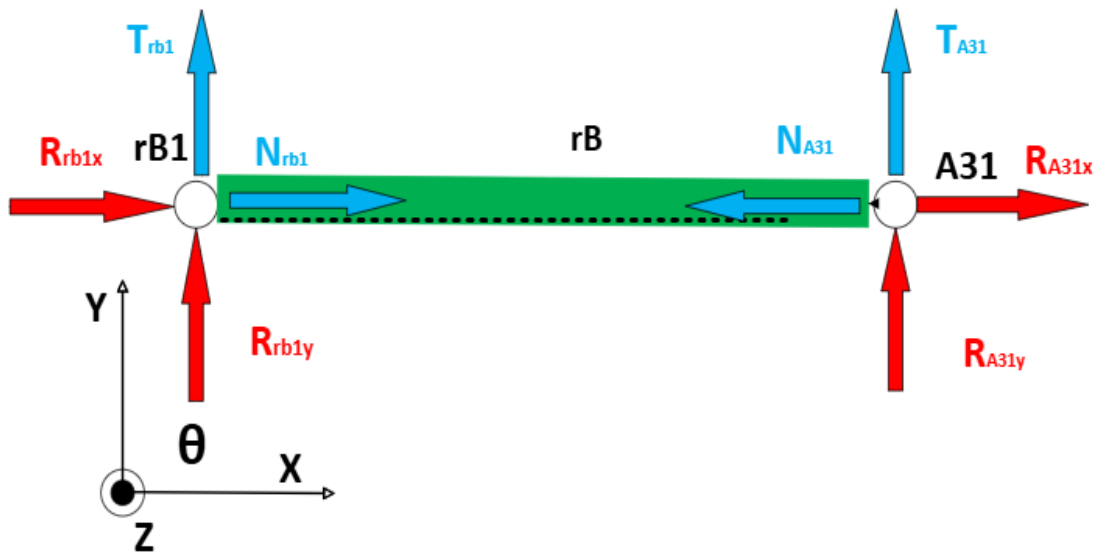


Figure 27: Normal and shear forces distribution along rB

Using basic trigonometric knowledge, the following relations are derived for both eyelets:

RB1

- $N_{A1} = -R_{A3x};$
- $T_{A1} = -(R_{A1x} \cos\left(\frac{\pi}{2} + \alpha\right) + R_{A1y} \cos(\alpha));$

A31

- $N_{A31} = -R_{A31x};$
- $T_{A31} = -R_{A31y};$

After calculating all the normal and shear forces during a whole cycle on the four eyelets, the following maximum components are collected:

	[N]	[N]	[N]	[N]
Eyelet	$N_{max,dyn}$	$N_{max,sta}$	$T_{max,dyn}$	$T_{max,sta}$
RA1	16246	17229	177	178,91
RAA2	16253	17236	183	179,29
RBRB	4834	4588	259	262,84
RA3	4835	4588	266	262,84

Table 7: maximum normal and shear forces acting on eyelets

Once the maximum resultant forces acting on each eyelet are obtained, it is possible to proceed to calculations of the maximum normal and shear stress for yield test on the threaded coupling, according to our knowledge of the theory and the technical datasheet of the component:

- $F_s = \sigma_s \cdot A_t \approx \sigma_s \cdot \frac{\pi \cdot (0.9 \cdot d)^2}{4} \Rightarrow$
 $\Rightarrow \sigma_s = F_s \frac{4}{\pi \cdot (0.9 \cdot d)^2} = \text{normal stress};$

- According to Von Mises criterion:

$$F_t = 0.577 \cdot \sigma_s \cdot \pi \cdot 0.9 \cdot d \cdot 0.75 \cdot h \Rightarrow$$

$$\Rightarrow \tau_{VM} = 0.577 * \sigma_s = \frac{F_t}{\pi \cdot 0.9 \cdot d \cdot 0.75 \cdot h} = \text{Von Mises shear stress};$$

and

$$\tau = \frac{1}{0.75 \cdot \pi \cdot d_r \cdot h} \cdot \frac{F}{d_r \cdot h} = 0.424 \cdot \frac{F}{d_r \cdot h} = 0.424 \cdot \frac{F}{d_r \cdot p \cdot n} = \text{shear stress};$$

- $\sigma_{id,VM} = \sqrt{\sigma_{id}^2 + 3\tau^2};$

- $Sf = \text{safety factor} = \frac{\sigma_{max,yield}}{\sigma_{id,VM}},$

- with:

- $h = \text{length of the threaded connection} = 80\text{mm}$ instead than nominal value 90 mm for safety reasons;
- $\sigma_{max,yield} = 345 \text{ Mpa}$ from table;
- $d_r = \text{core diameter of the thread} \approx d = \text{nominal diameter} = 45 \text{ mm};$
- both male and female thread are made of hardened steel E355

It is noteworthy to highlight that almost all the contribution is given by the horizontal component of the reactions, along the x axis of our reference system, given also the fact that both connecting rod maintain an inclination around or at 0 rad for the whole cycle duration.

	MPa	MPa	MPa	MPa	MPa	MPa	MPa	MPa	MPa	MPa	MPa
	σ_{dyn}	σ_{sta}	$\tau_{VM,dyn}$	τ_{dyn}	$\tau_{VM,sta}$	τ_{sta}	$\sigma_{id,dyn}$	$\sigma_{id,sta}$	$SF_{yeld,dyn}$	$SF_{yeld,sta}$	
RA1	12,6 1	13,3 7	7,28	1,92	7,7	2,1 7	18	19	19,35	18	
RAA2	12,6 2	13,3 8	7,28	1,92	7,7	2,1 7	18	19	19,34	18	
RBR B	3,75	3,56	2,16	0,57	2,0	0,5 8	5	5	65,04	5	
RA3	3,75	3,56	2,17	0,57	2,0	0,5 8	5	5	65,02	5	

Table 8: maximum values of stress and safety factors

2.5.3 Motor crank dimensioning

The motor crank analysis will involve the dimensioning of the pin (Figure 28) which connects the crank with connecting rod rA, as the pin will couple with the eyelet in point A1. To proceed with a correct dimensioning, it is important to collect some data about the crank r1 and the pin. From the CAD file in Autodesk inventor and the Excel spreadsheet, the following information are retrieved:

- $d_{critic} = 45$ mm;
- $q = 35$ mm = length of the surface on which R_{A1} acts;
- $R_{A1,max,dyn} = 16247,2$ N
- $R_{A1,max,sta} = 17228,7$ N

Starting from these parameters, the coefficient of linear distributions for the maximum value of R_{A1} are obtained, both for static and dynamic cases.

- $K_{FA1,sta} = \frac{R_{A1,max}}{\Delta z} = \frac{17228,7}{35} = 492249$ N/m;
- $K_{FA1,dyn} = \frac{R_{A1,max,dyn}}{\Delta z} = \frac{16247,2}{35} = 464205$ N/m;

Considering **Figure 28**, the force analysis on the pin is performed according to the following formulation:

1. For $0 \leq l_z \leq 30$
 - $N = 0$;
 - $T = 0$;
 - $M_x = 0$;

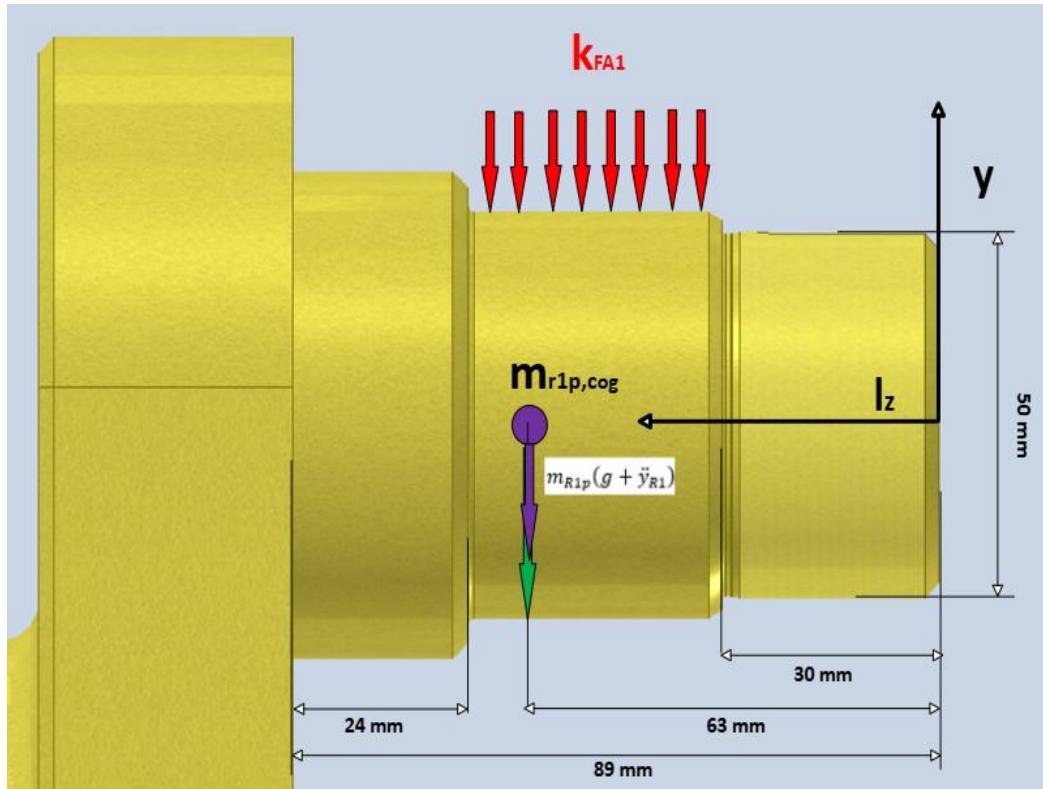


Figure 28: force distribution on pin of motor crank *r1*

2. For $30 \leq l_z \leq 53$
 - $N = 0$;
 - $T - K_{FA1}(l_z - 30) = 0 \Rightarrow$
 $\Rightarrow T = K_{FA1}(l_z - 30)$;
 - $M_x - K_{FA1}(l_z - 30) \left(\frac{l_z - 30}{2} \right) = 0 \Rightarrow$
 $\Rightarrow M_x = K_{FA1}(l_z - 30) \left(\frac{l_z - 30}{2} \right)$;
3. For $53 \leq l_z \leq 65$
 - $N = -m_{R1p}\ddot{x}$;
 - $T - K_{FA1}(l_z - 30) - m_{R1p}(g + \ddot{y}) = 0 \Rightarrow$
 $\Rightarrow T = K_{FA1}(l_z - 30) + m_{R1p}(g + \ddot{y}) = 0$;

- $M_x - K_{FA1}(l_z - 30) \left(\frac{l_z - 30}{2} \right) - m_{R1p}(g + \ddot{y}_{R1})(l_z - 53) = 0 \Rightarrow$
 $\Rightarrow M_x = K_{FA1}(l_z - 30) \left(\frac{l_z - 30}{2} \right) + m_{R1p}(g + \ddot{y}_{R1})(l_z - 53);$

4. For $65 \leq z \leq 89$

- $N = -m_{R1p}\ddot{x};$
- $T - K_{FA1}q - m_{R1p}(g + \ddot{y}) = 0 \Rightarrow$
 $\Rightarrow T = K_{FA1}q + m_{R1p}(g + \ddot{y}) = 0;$
- $M_x - K_{FA1}(l_z - 30) \left(\frac{q}{2} \right) - m_{R1p}(g + \ddot{y}_{R1})(z - 53) = 0 \Rightarrow$
 $\Rightarrow M_x = K_{FA1}(l_z - 30) \left(\frac{q}{2} \right) + m_{R1p}(g + \ddot{y}_{R1})(l_z - 53);$

Using the model above and combining it with all the forces and moments combinations that occur during a single cycle, it is possible to have a complete overview of the forces and moments acting in time along the whole pin.

$l_z < 30$			$30 < l_z < 53$		
	dynamic	static		dynamic	static
N	0,0	0,0	N	0,0	0,0
T	0,0	0,0	T	10677	10677
M_x	0,0	0,0	M_x	122,8	122,8
l_z	24,0		l_z	53,0	

$53 < l_z < 65$			$65 < l_z < 89$		
	dynamic	static		dynamic	static
N	0,0	0,0	N	0,0	0,0
T	16265	16265	T	16265	16265
M_x	284,5	301,7	M_x	674,90	715,63
l_z	65,0		l_z	89,0	

Table 9: motor crank pin force analysis results

By varying the value of l_z , it is possible to find the critical point at which the greatest amount of force is acting. As one might have been predicted, the point is located in the intersection of the pin with the crank body ($l_z = 89 \text{ mm}$), where the two pieces are welded together.

Consequently, combining the information collected so far and some theoretical recalls, the following safety factor evaluation is obtained:

- $W_f = \text{section modulus of a solid circular beam} = \frac{\pi d_{crit}^3}{32}$;
- $A = \text{cross section area} = \frac{\pi d_{crit}^2}{4}$;
- $\sigma = \frac{M_x}{W_f} = \text{normal stress due to bending moment } M_x$;

	[Nm]	[Nm]	[N]	[N]	[Mpa]	[Mpa]	[Mpa]	[Mpa]
	max $M_{bend,dyn}$	max $M_{bend,sta}$	$T_{max,dyn}$	$T_{max,sta}$	σ_{dyn}	σ_{sta}	τ_{dyn}	τ_{sta}
r1	675	716	16265	16265	55,00	58,31	10,23	10,23

Table 10: maximum forces, moments and stress components acting on pin of crank r1

	[Mpa]	[Mpa]	[m^3]		[Mpa]		
	$\sigma_{id,dyn}$	$\sigma_{id,sta}$	Wf	A	Re_{yeld}	SF _{yeld,dyn}	SF _{yeld,sta}
r1	58	61	1,23E-05	0,002	700	12,12	11,49

Table 11: maximum ideal stresses and safety factors acting on pin of crank r1

As last step, a finite element model simulation was performed by means on AutoDesk Inventor software, using the CAD models of the machine available in the company database.

The simulation was conducted to verify the stress distribution obtained at the highest torque delivered, especially in the key region, which usually is the most solicited during this kind of interactions.

In particular,

[s]	[rad]	[Nm]	[N]	[N]	[N]	[N]	[N]	[N]
time	θ	Cm	$R_{C1,x}$	$R_{C1,y}$	R_{C1}	$R_{A1,x}$	$R_{A1,y}$	R_{A1}
0,91	-1,23	-1995,79	-13024,3	-581,8	13037,3	-13024,6	-643,5	13040,51

Table 12: data related to the highest torque point in lifting mechanism

Upon selecting the surface interested in the mechanical behaviour simulation and the grain dimension, along with magnitude, direction and point of application of the force on the workpiece, the simulation is launched and the result in the picture below is obtained:

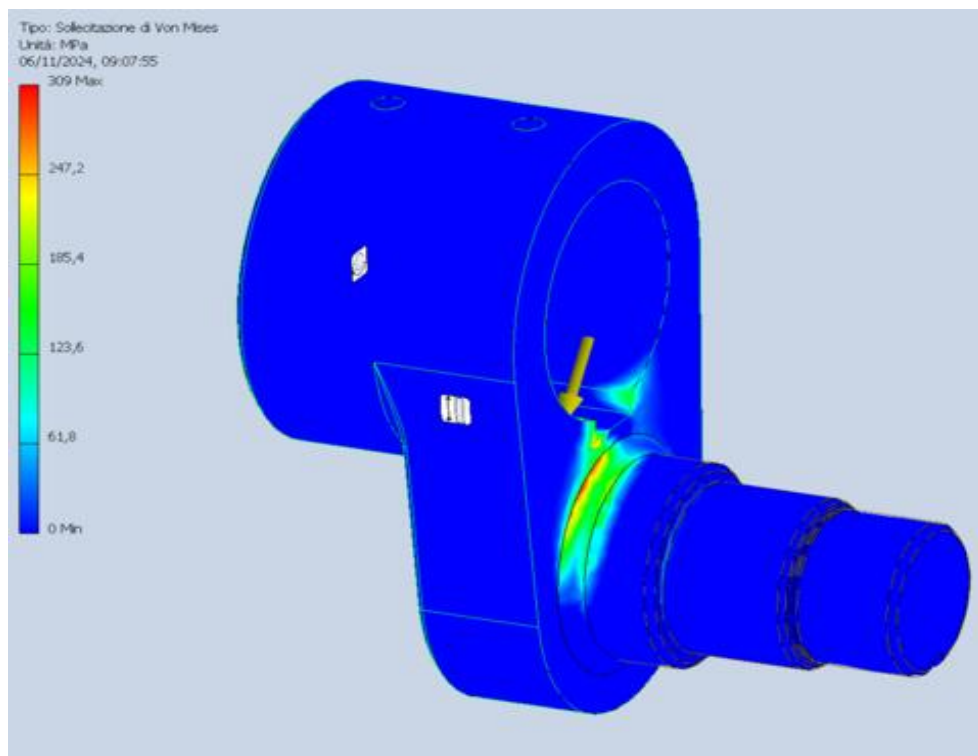


Figure 29: FEM analysis on crank r1

As it can be seen (**Figure 29**), tolerant levels of stress are reached, considering the of steel E355, with some small peaks that can be mitigated by the presence of the weldings joining the crank pin to the crank itself. For simulation purposes and in order to avoid software issues, weldings were temporarily excluded from the FEM analysis itself.

2.5.4 Lifting arm r22 dimensioning

30 % front - 70% back	
Reaction	[kN]
$R_{A2,tot}$	26,9
R_{C2}	30,3
R_{A3}	11,3
R_{C3}	13,0

70 % front - 30% back	
Reaction	[kN]
$R_{A2,tot}$	11,6
R_{C2}	13,0
R_{A3}	26,0
R_{C3}	30,0

Table 13: comparison between a 30%-70% and a 70%-30% load distribution

As already explained, first an evaluation of all reactions in a single cycle time is performed, in order to find the case in which the highest forces act on the component under analysis. To do so, a force balance calculation is brought out.

Force Balance

- $R_{C22x} + m_{r22}\ddot{x}_{r22} = 0 \Rightarrow$
 $R_{C22x} = -m_{r22}\ddot{x}_{r22};$
- $R_{C22y} + m_{r22}(\ddot{y}_{r22+g}) + F_{w22} = 0 \Rightarrow$
 $\Rightarrow R_{C22y} = -m_{r22}(\ddot{y}_{r22} + g) - F_{w22};$
- $C22 \cup: -m_{r22}(\ddot{y}_{r22} + g)l_{22}\cos\delta - m_{r22}\ddot{x}_{r22}\sin\delta - F_{w22}r_{22} - I_{22}\ddot{\delta} = 0$

Secondly, the coefficient of distributed force is calculated for the reaction force acting radially on a section of the crank pin, in particular in the bearing:

$$K_{Fw22} = \frac{F_{w22}}{q_{w22}} = \frac{5852.13}{60} = 97535 \text{ , } q_{w22} = 60 \text{ mm};$$

The force and bending moment evaluation is executed according to the scheme below (Figure 30) as it is observable, there is no notable contribution along the z axis direction, as expected by our a priori assumptions. Moreover, contributions along the x directions are negligible, as it has been proved from calculation on the excel datasheet model.

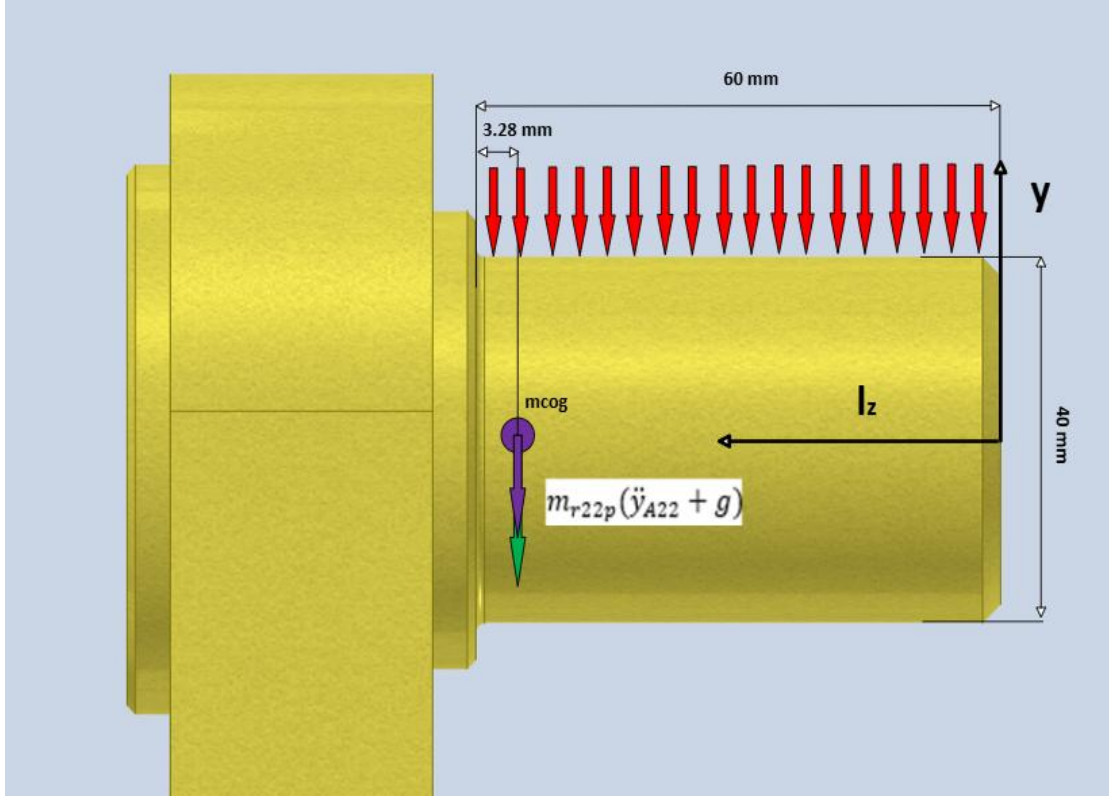


Figure 30: force distribution on pin of lifting crank r22

For $0 \leq l_z \leq 56,72$

- $N = 0;$
- $T - K_{FW22} l_z = 0 \Rightarrow$
 $\Rightarrow T = K_{FW22} l_z;$
- $M_x - K_{FW22} \frac{l_z^2}{2} = 0 \Rightarrow$
 $\Rightarrow M_x = K_{FW22} \frac{l_z^2}{2};$

For $56,72 \leq l_z \leq 60$

- $N = 0;$
- $T - K_{FW22} l_z - m_{r22p} (\ddot{y}_{A22} + g) = 0 \Rightarrow$
 $\Rightarrow T = K_{FW22} l_z - m_{r22p} (\ddot{y}_{A22} + g);$
- $M_x - K_{FW22} \frac{l_z^2}{2} - m_{r22p} (\ddot{y}_{A22} + g) (l_z - 50) = 0 \Rightarrow$
 $\Rightarrow M_x = K_{FW22} \frac{l_z^2}{2} + m_{r22p} (\ddot{y}_{A22} + g) (l_z - 50);$

For $60 \leq l_z \leq 65$

- $N = 0$;
- $T - K_{FW22}q - m_{r22p}(\ddot{y}_{A22} + g) = 0 \Rightarrow$
 $\Rightarrow T = K_{FW22}q + m_{r22p}(\ddot{y}_{A22} + g)$;
- $M_x - K_{FW22} \frac{l_z^2}{2} - m_{r22p}(\ddot{y}_{A22} + g)(l_z - 50) = 0 \Rightarrow$
 $\Rightarrow M_x = K_{FW22} \frac{l_z^2}{2} + m_{r22p}(\ddot{y}_{A22} + g)(l_z - 50); 3$

As on the previous analysis, all the possible forces and moments combinations acting on the pin during the cycle time are inserted in the model, allowing to find the variation of resultant normal, shear forces and moments on the pin, as a function of the displacement along the pin l_z . Among the results, the most significant data is displayed in tables below:

$l_z < 56,72$			$56,72 < l_z < 60$			$60 < l_z < 65$		
	dinamic a	statica		dinamic a	static a		dinamic a	statica
N	0,0	0,0	N	0,1	0,0	N	0,1	0,0
T	5532,2	5532,2	T	5864	5864	T	5864	5864,2808
M_x	156,9	156,9	M_x	176	176	M_x	205	205
l_z	56,7		l_z	60,0		l_z	65,0	

Table 14: crank r22 pin force analysis results

Even in this case, the biggest amount of shear force and bending moment is located at the intersection of the pin with the body of the crank, where the two pieces are joined and welded together. From the values at $l_z=65$ mm, the stress data are calculated as in 2.5.3.

	[Nm]	[Nm]	[N]	[N]	[MPa]	[MPa]	[MPa]	[MPa]
	max $M_{bend,dyn}$	max $M_{bend,sta}$	$T_{max,dyn}$	$T_{max,sta}$	σ_{dyn}	σ_{sta}	τ_{dyn}	τ_{sta}
r22	205	205	5864	5864	32,61	32,61	4,6667	4,6666

Table 15: maximum forces, moments and stress components acting on pin of crank r22

	[Mpa]	[Mpa]	[m^3]	[m^2]	[Mpa]	[Mpa]
	$\sigma_{id,dyn}$	$\sigma_{id,sta}$	Wf	A	Re_{yeld}	SF _{yeld,dyn}
r22	34	34	6,28319E-06	0,001	700	20,83

Table 16: maximum ideal stresses and safety factors acting on pin of crank r22

At last, a FEM analysis is performed on the crank pin, imposing a rotation constraint in the shaft slot and applying a vertical load F_{w22} on the pin itself, as it represents the maximum load applied during a single cycle. By looking at the colour legenda, the value of stress in the pin/body intersection is pretty close to the calculated σ_{id} .

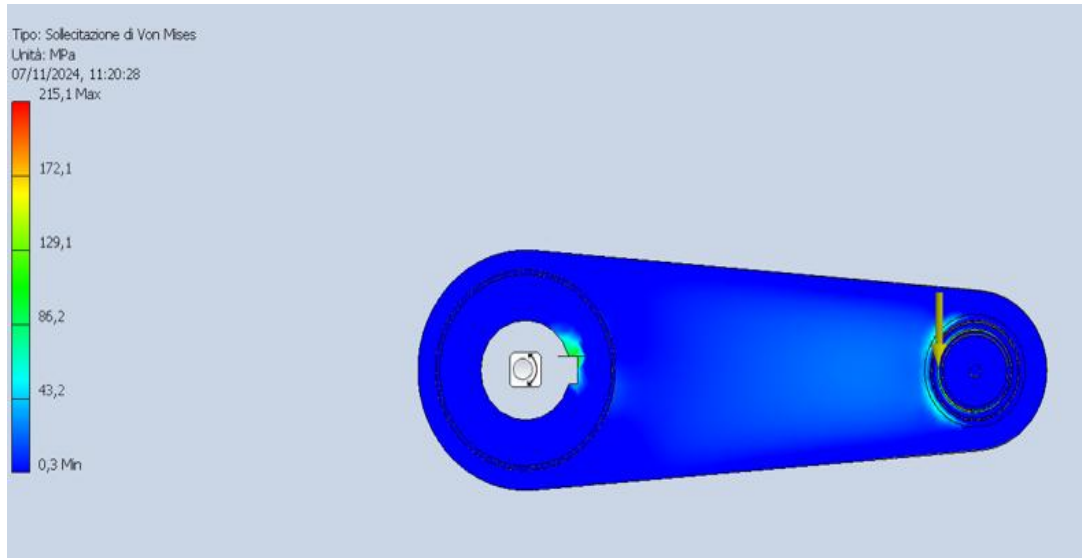


Figure 31: FEM analysis on lifting crank r22

2.5.5 Crank r21 dimensioning

Being the linking element between the two four bar planar linkages that made up half of the lifting mechanism, crank r21 is one of the most solicited elements, as it receives reactions from connecting rod rA on the left and rB on the right. For this reason, a stress analysis is conducted on this element too.

First, the resultant reaction force on the pin is calculated by means of the formula, as previously stated:

$$R_{A21,R} = \sqrt{(R_{RB1x} - R_{RA2x})^2 + (R_{RB1y} - R_{RA2y})^2} = \sqrt{R_{A21y}^2 + R_{A21x}^2};$$

- $R_{A21,R,dyn} = 16253,9 \text{ N};$
- $R_{A21,R,sta} = 17236,5 \text{ N};$

Subsequently, from the CAD model, the length of the surface on which force $R_{A21,R}$ is acting, q_{A21} , is obtained.

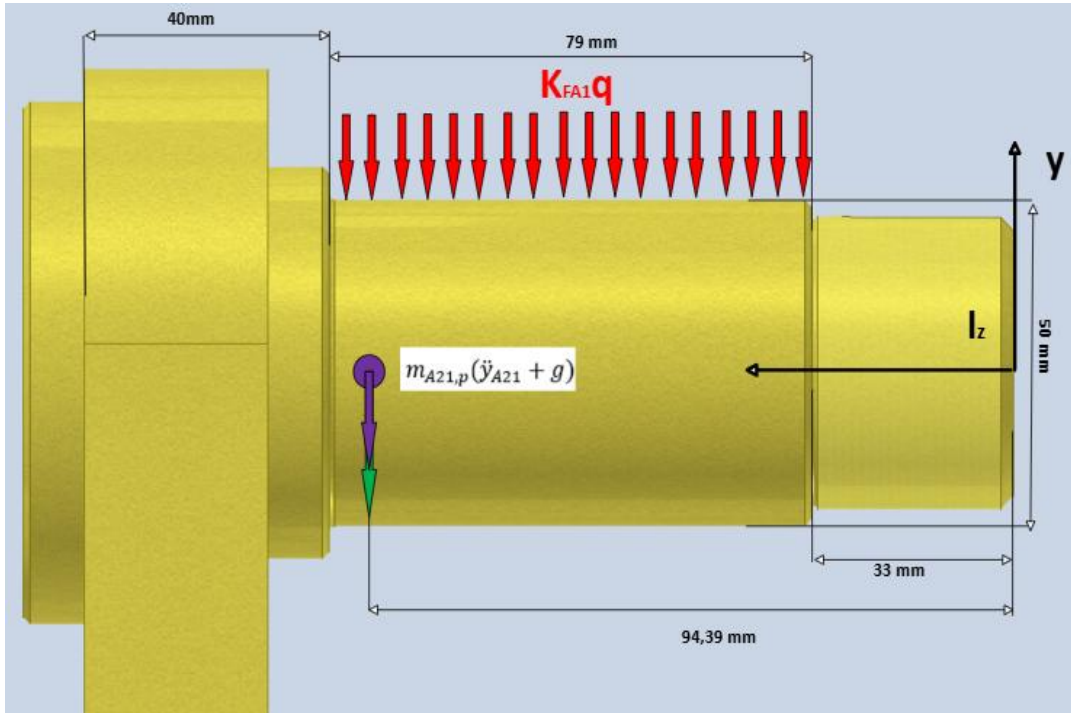


Figure 32: force distribution on pin of crank r21

Hence, the linear coefficient of distributed force is obtained, as follows:

$$K_{RA21,R} = \frac{R_{A21,R,max}}{q_{A21}}, \quad q_{A21} = 79 \text{ mm};$$

- $K_{RA21,R,dyn} = 205745 \frac{N}{m}$;
- $K_{RA21,R,sta} = 218183 \frac{N}{m}$;

Considering Figure 32, the force analysis on the pin is performed according to the following formulation:

For $0 \leq l_z \leq 33$

- $N = 0$;
- $T = 0$;
- $M_x = 0$

For $33 \leq l_z \leq 94,39$

- $N = 0$;
- $T = K_{RA21,R}(d - 33)$;
- $M_x = K_{RA21,R} \frac{(d-33)^2}{2}$;

For $94,39 \leq l_z \leq 112$

- $N = m_{A21,p} \ddot{x}_{A21}$;
- $T = K_{RA21,R}(l_z - 33) + m_{A21,p}(\ddot{y}_{A21} + g)$;
- $M_x = K_{RA21,R} \frac{(l_z - 33)^2}{2} + m_{A21,p}(\ddot{y}_{A21} + g)(l_z - 94,39)$;

For $112 \leq d \leq 152$

- $N = 0$;
- $T = K_{RA21,R}q + m_{A21,p}(\ddot{y}_{A21} + g)$;
- $M_x = K_{RA21,R}q \left(l_z - 33 - \frac{q}{2} \right) + m_{A21,p}(\ddot{y}_{A21} + g)(l_z - 94,39)$;

Using the model above and combining it with all the forces and moments combinations that occur during a single cycle, it is possible to have a complete overview of the forces and moments acting in time along the whole pin.

$l_z < 33$			$33 < l_z < 94,39$			$94,39 < l_z < 112$			$112 < l_z < 152$		
	dynami c	stati c		dynamic	static		dynamic	static		dynami c	static
N	0,0	0,0	N	0,0	0,0	N	0,0	0,0	N	0,0	0,0
T	0,0	0,0	T	12631	1339 4	T	16283	17265	T	16283	1726 5
M_x	0,0	0,0	M_x	388	411	M_x	643	681	M_x	1294	1372
l_z	33,0 mm		l_z	94,4 mm		l_z	112,0 mm		l_z	152,0 mm	

Table 17: crank r21 pin force analysis results

As expected, the biggest amount of shear force and bending moment is located at the intersection of the pin with the body of the crank, where the two pieces are joined and welded together. From the values at $l_z=152$ mm, the stress data are calculated as in 2.5.3.

	[Nm]	[Nm]	[N]	[N]	[MPa]	[MPa]	[MPa]	[MPa]
	max $M_{bend,dyn}$	max $M_{bend,sta}$	$T_{max,dyn}$	$T_{max,sta}$	σ_{dyn}	σ_{sta}	τ_{dyn}	τ_{sta}
RA22	805	854	16283	17265	65,63	69,59	8,29	8,79

Table 18: maximum forces, moments and stress components acting on pin of crank r1

[Mpa]	[Mpa]	[m^3]	[m^2]	[Mpa]
$\sigma_{id,dyn}$	$\sigma_{id,sta}$	Wf	A	Re_{yeld}
67	71	1,23E-05	0,002	700
				$SF_{yeld,dyn}$
				10,42

Table 19: maximum ideal stresses and safety factors acting on pin of crank r21

At last, a FEM analysis is performed on the crank pin, imposing a rotation constraint in the shaft slot and applying an almost horizontal load $R_{A21,R,max}$ on the pin itself, as it represents the maximum load applied during a single cycle.

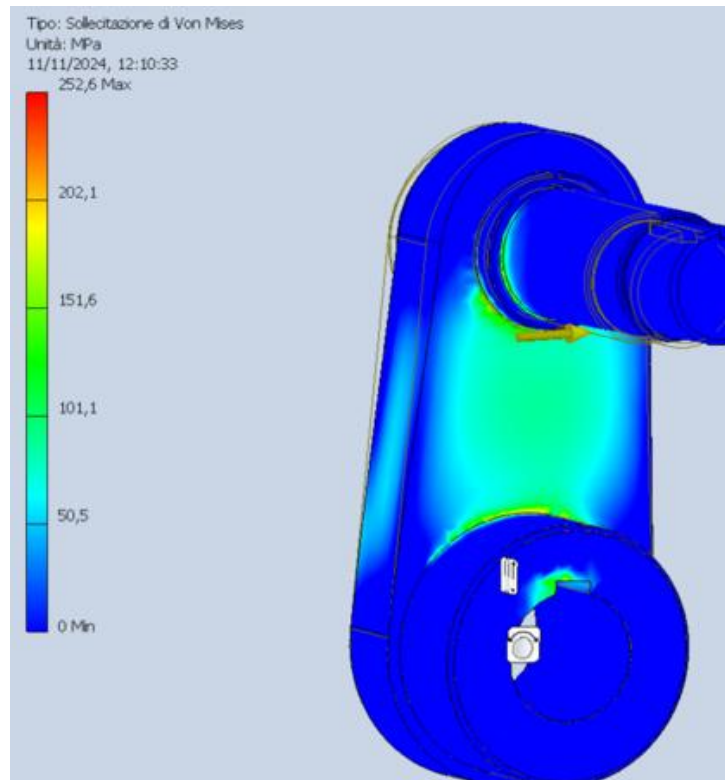


Figure 33: FEM analysis on crank r21

By looking at the colour legend, the mean value of stress in the pin/body intersection is pretty close to the calculated σ_{id} , with spikes due to the removal of welding in the junction areas.

2.5.6 Shaft S2 bearing verification

After concluding the analysis on the relevant cranks, the study moved on other relevant components, such as shaft S2 and its bearings.

Shaft S2 is located inside a hub in the fixed chassis by means of two roller bearings (Figure 34). On the outer side, crank r21 is installed, while, on the inner one, crank r22 is found. Consequently, during a cycle, the shaft will be solicited on both extremes simultaneously so a force analysis is fundamental to verify that suitable bearings are chosen.

Thank to our previous analysis, integrated in the Excel spreadsheet, we have already the general variation of applied forces on the two rotation points for the two cranks r21 and r22, namely C21 and C2.

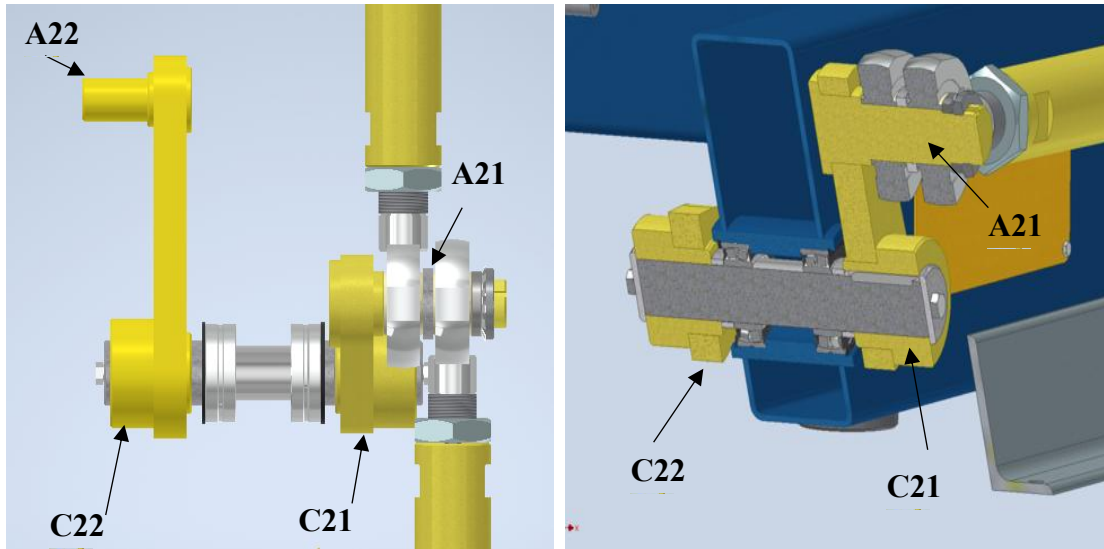


Figure 34: on the left, shafts s2 with cranks r21 and r22 installed; on the right, section view of bearings on shaft S2

By looking at figure **Figure 35**, the following relations are derived:

- $R_{s2x} = T_{s2x} = R_{c21,x} - R_{c22,x}$;
- $R_{s2y} = T_{s2y} = R_{c22,y} - R_{c21,y}$;
- $M_{sx} = (R_{c22,x} + R_{c21,x}) \frac{l_s}{2}$;
- $M_{sy} = (R_{c22,y} + R_{c21,y}) \frac{l_s}{2}$;

Subsequently, from the Excel spreadsheets, the maximum values for the forces on the outer side are considered to calculate the linear coefficient of distributed forces on the bearing, as the forces are higher in magnitude on that side.

- $F_{c21x,max,dyn} = -11367,5 \text{ N} \Rightarrow K_{f,c21x,dyn} = \frac{R_{c21x,max,dyn}}{q} = -152584,1 \frac{\text{N}}{\text{m}}$;
- $F_{c21x,max,sta} = -12625,6 \text{ N} \Rightarrow K_{f,c21x,sta} = \frac{R_{c21y,max,sta}}{q} = -169470,7 \text{ N/m}$;

- $F_{c21y,max,dyn} = 6862,2 \text{ N} \Rightarrow K_{f,c21y,dyn} = \frac{R_{c21y,max,dyn}}{q} = 92110 \frac{\text{N}}{\text{m}};$
 $F_{c21y,max,sta} = 6884,8 \text{ N} \Rightarrow K_{f,c21x,sta} = \frac{R_{c21y,max,sta}}{q} = 92413,5 \frac{\text{N}}{\text{m}};$
- $q = 74,5 \text{ mm};$

By looking at the models below (**Figure 35**), the dynamic analysis is performed.

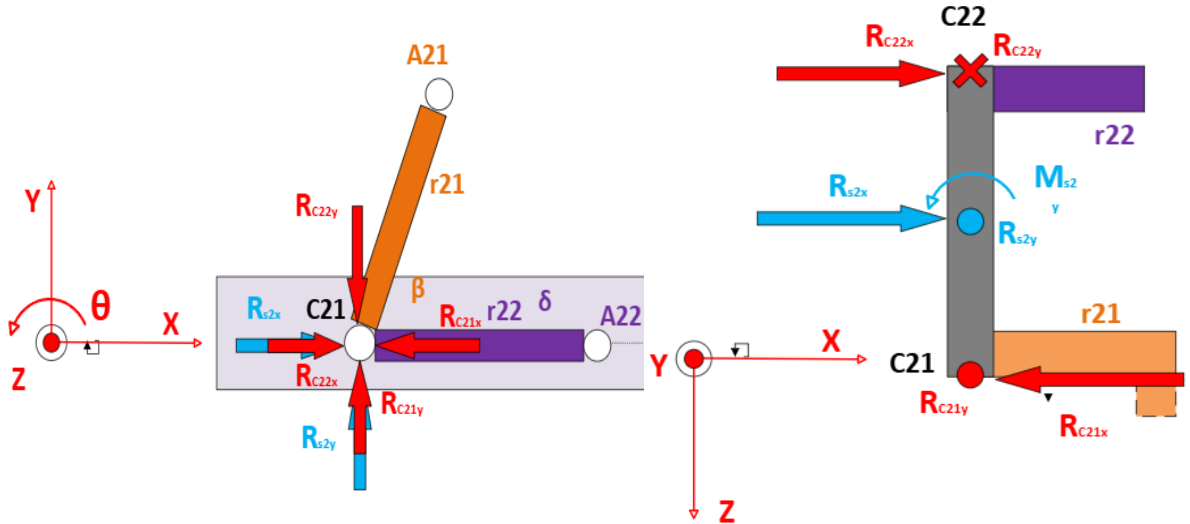


Figure 35: force distribution along shaft S2

For $0 \leq l_z \leq 74,5$

- $N = 0;$
- $T_y = K_{f,c21y} l_z;$
- $T_x = K_{f,c21x} l_z;$
- $M_{xc21} = K_{f,c21y} \frac{l_z^2}{2};$
- $M_{yc21} = K_{f,c21x} \frac{l_z^2}{2};$

For $74,5 \leq l_z \leq 89$

- $N = 0;$
- $T_y = K_{f,c21y} q;$
- $T_x = K_{f,c21x} q;$
- $M_{yc21} = K_{f,c21x} q \left(l_z - \frac{q}{2} \right);$
- $M_{xc21} = K_{f,c21y} q \left(l_z - \frac{q}{2} \right);$

Then, using the model above and combining it with all the forces and moments combinations that occur during a single cycle, it is possible to have a complete overview of the forces and moments acting in time along the whole pin.

$l_z < 74,5$			$74,5 < l_z < 102,12$		
	dynamic	static		dynamic	static
N	0,0	0,0	N	0,0	0,0
T_y	6862,2	13278,2	T_y	8197,8	0,0
T_x	-11367,5		T_x	-13580,0	
M_{xc21}	255,6	256,5	M_{xc21}	355,1	356,3
M_{yc21}	-423,4	-470,3	M_{yc21}	-588,3	-653,4
l_z	74,5		l_z	89,0	

Table 20: force analysis results on shaft S2

From the above analysis it is found that the highest reactions are located at distance $l_z = 89 \text{ mm}$ from C21 and along shaft S2. Hence the equivalent radial reactions are calculated for both static and dynamic case, using the relation

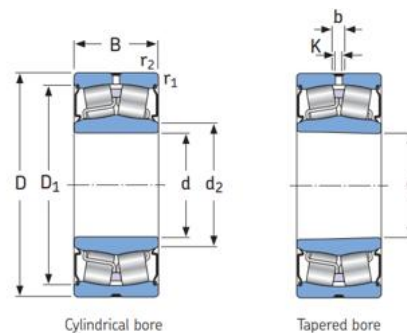
$$T_{eq} = \sqrt{T_x^2 + T_y^2}$$

- $T_{eq,dyn} = \sqrt{T_{x,dyn}^2 + T_{y,dyn}^2} = 13,6 \text{ kN}$
- $T_{eq,sta} = \sqrt{T_{x,sta}^2 + T_{y,sta}^2} = 15,1 \text{ kN}$

By looking at the bearing datasheet from the manufacturer (Figure 36), at the row corresponding to $d = 50 \text{ mm}$, the basic load ratings values are found and could be compared to the equivalent shear forces on the bearings. It is concluded that the bearings are abundantly dimensioned for our application (Table 21).

	[kN]	[kN]
	Dynamic	static
Basic load rating	104	108
T_{eq}	13,6	15,1

Table 21: equivalent shear forces acting on the shaft



Principal dimensions	Basic load ratings		Fatigue load limit P_u	Limiting speed	Mass	Designations Bearings with cylindrical bore
	dynamic	static				
d D B	C	C_0	kN	r/min	kg	-
25 52 23	49	44	4,75	3 600	0,26	BS2-2205-2CS/VT143
30 62 25	64	60	6,4	2 800	0,34	BS2-2206-2CS/VT143
35 72 28	86,5	85	9,3	2 400	0,52	BS2-2207-2CS/VT143
40 80 28	96,5	90	9,8	2 200	0,57	BS2-2208-2CS/VT143
90 38	150	140	15	1 900	1,2	BS2-2308-2CS/VT143
45 85 28	102	98	10,8	2 000	0,66	BS2-2209-2CS/VT143
100 62	183	183	19,6	1 500	1,4	BS2-2309-2CS/VT143
50 90 28	104	108	11,8	1 900	0,7	BS2-2210-2CS/VT143

Figure 36: roller bearing datasheet

2.5.7 Lifting bearings dimensioning

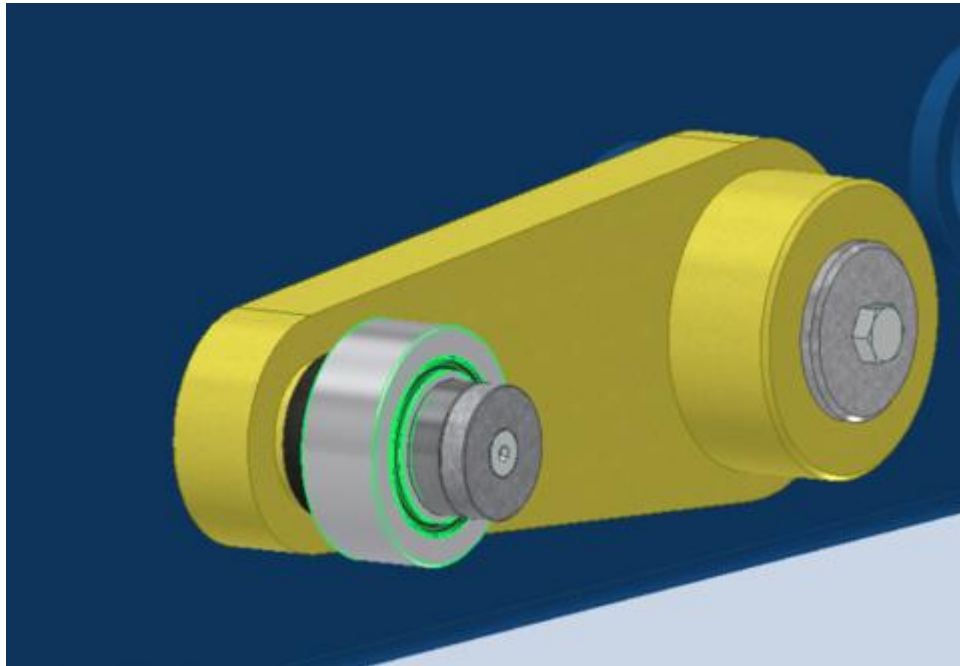


Figure 37: lifting bearing on crank r22

The bearing analysis is then extended to the bearings that act as coupling element between the lifting cranks on the fixed chassis and the hubs on the mobile chassis, which is lifted.

As for the previous bearing verifications, it is necessary to derive the equivalent reactions on the bearing itself and then compare the value with the basic rate loadings provided by the manufacturer on the datasheet.

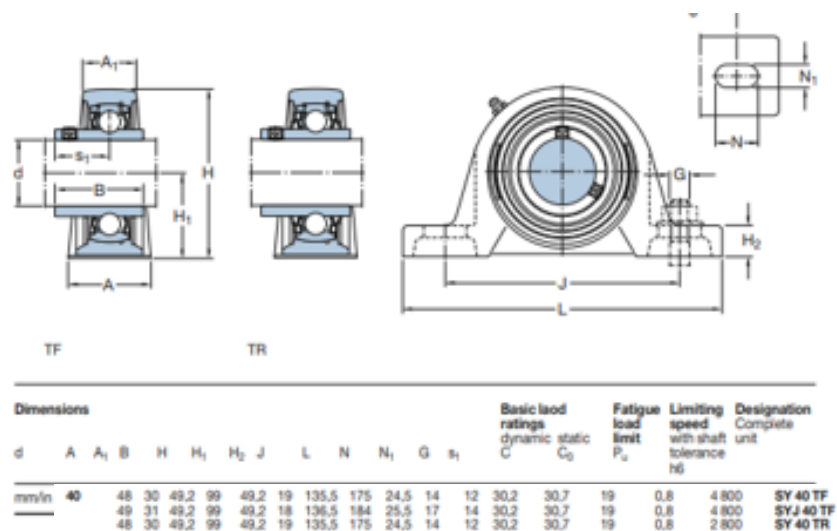


Figure 38: datasheet for front bearing on lifting crank r32

As previously mentioned, considering the maximum admissible load for each bearing, it is reasonable to consider, for a worst case scenario, a load distribution of 70%-30% between front and rear or viceversa, hence the 70% of load, distributed between each couple of lifting arms, will be considered.

Since, as already known, this amount of load per crank is equal to about 5,9 kN for both static and dynamic conditions, confronting this values with the basic rate loading allows to conclude that the bearings are verified for the application .

Dimensioni principali & prestazioni		ILN1	ILN1
d	40 mm	Diametro del foro	
D	80 mm	Diametro esterno	
B	32 mm	Larghezza, anello interno	
C _{r w}	45.000 N	coefficiente di carico dinamico, radiale	
C _{0r w}	60.000 N	coefficiente di carico statico, radiale	

resultant		
Rear bearing		
	dynamic	static

Figure 39: datasheet for rear bearing on crank r22

Force resultant	5,9	5,9

Table 22: basic load rating and loads for lifting bearings

2.5.8 Radial load on speed reducer shaft

As the last step in our motor analysis, the radial load exerted on the speed reducer motor shaft is analysed. In order to verify it, it is sufficient to evaluate the resultant force acting on C1 as

$$R_{C1} = \sqrt{R_{C1x}^2 + R_{C1y}^2}$$

And compare it with the maximum radial force admitted from the motor datasheet (Figure 40).

Being $R_{C1} \leq R_{C1,max}$, the speed-reducer is verified for our application.

Carico radiale di uscita ammissibile per n=1400	40000 N
--	---------

Figure 40: maximum radial load speed reducer on lifting mechanism

[kN]	[kN]
R_{max}	R_{C1}
40	16,25

Table 23: comparison maximum admissible radial load and the maximum found

2.6 The translating mechanism: analytical approach

The second relevant subsystem in the walking beam transfer machine is the horizontal translation mechanism, which allows to transport the designated glass slabs from the main line to the secondary one.

It consists in a modified belt conveyor system, in which the load is not transported on the toothed belt itself, as it usually happens, but is connected to the belt by means of

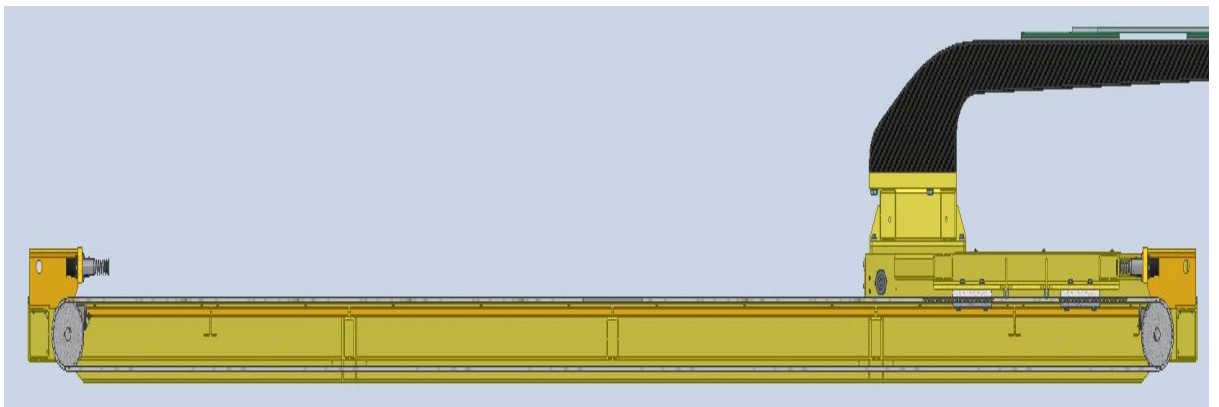


Figure 41: section view of the translating mechanism

adjustable male clamps: the motion of the elastic belt, due to the rotation of the driving pulley P1 and driven pulley P2, allows the motion of the cart and, so, the translation of the comb and its load. In particular, the cart is a steel E355 chassis, with 4 v-roller wheels that slides on complementary rails. The specific V-shape simplifies grease lubrication from the carters, in which the wheels are hosted: the lubricant flows on the wheels from above by means of an injector and then on the rails, under which specific lubricant collectors are placed. In this way, not only the wheels are kept greased, but also the guides, contributing to friction reduction. For each v-roller, a matching round wheel is present under the guide, in order to prevent the cart to tilt or turn over because

of abrupt accelerations, changes in the load distribution on the comb or external interactions.

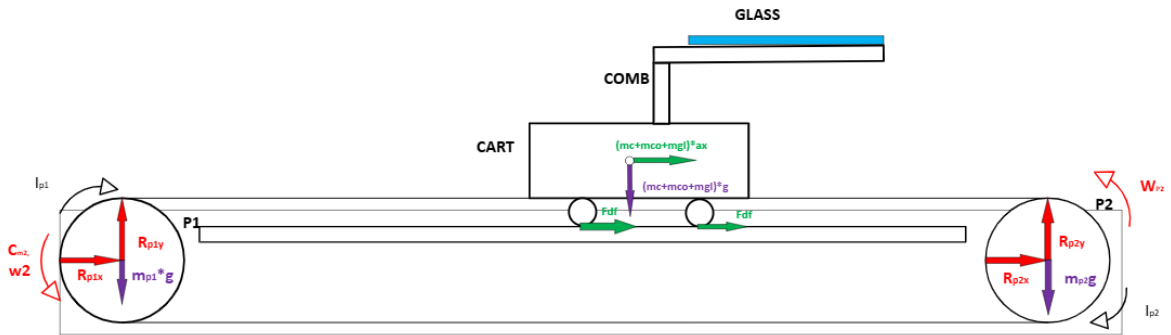


Figure 42: scheme of the horizontal translation mechanism

P1 and P2 are identical toothed pulleys, so it follows that $r_{P1} = r_{P2} = r_P = \frac{D_P}{2}$, $m = m_{P2} = m_P$ and so do the inertias $I_{P1} = I_{P2} = I_P$. As they match with the open-ended belt, they share the same pitch $p = 20\text{mm}$, while the width is such to keep the belt in position.

[mm]	[mm]	[mm]
diameter	pitch	width
159,2	20,0	25,0

Table 24: relevant parameters for pulleys P1 and P2

2.7 The translating mechanism: kinematic approach

From a kinematic point of view, the working principle is very simple. The driving pulley P1 receives the torque from the speed reducer of secondary motor M2 and starts rotating following a trapezoidal velocity profile, with acceleration $\dot{\theta}_{P1,T}$ until angular velocity $\theta_{P1,T}$, a short time interval maintaining constant velocity and then decelerating with the same magnitude of $\dot{\theta}_T$.

[rpm]	[rad/s]	[rad/s^2]	[s]	[rpm]	[rad/s]	[rpm^2]	[rad/s^2]
$\dot{\theta}_{M2,T}$	$\ddot{\theta}_{M2,T}$	w	t_{acc}	$\dot{\theta}_{P1,T}$	$\ddot{\theta}_{P1,T}$		
2438	255,3	124,5	12,9	189,0	19,8	5500,4	9,6

Table 25: kinematic parameters of the translating mechanism

Regarding the input parameters, the motor velocity and accelerations are known, as well as the reduction ratio of the speed reducer. From these parameters, the calculation of the pulley cinematic data could proceed.

- $w = \text{reduction ratio} = 12.9 = \frac{\dot{\theta}_{M2,T}}{\dot{\theta}_{P1,T}} = \left| \frac{\ddot{\theta}_{M2,T}}{\ddot{\theta}_{P1,T}} \right| \Rightarrow$
 $\Rightarrow \dot{\theta}_{P1,T} = \frac{\dot{\theta}_{M2,T}}{12.9} = \frac{2438}{12.9} \text{ rpm} = 189 \text{ rpm} = 19.8 \frac{\text{rad}}{\text{s}};$
 and
 $\Rightarrow \ddot{\theta}_{P1,T} = \left| \frac{\ddot{\theta}_{M2,T}}{12.9} \right| = \frac{124.5}{12.9} \text{ rad/s} = 9.6 \frac{\text{rad}}{\text{s}};$
- $\theta_{P1,T}(t) = \dot{\theta}_{P1,T} * t + \theta_0;$
 $\dot{\theta}_{P1,T}(t) = \ddot{\theta}_{P1,T} * t + \dot{\theta}_0;$
 $\ddot{\theta}_{P1,T}(t) =$
 - $9.6 \frac{\text{rad}}{\text{s}^2}$ for $t \in [0, t_{p,acc}];$
 - $0 \frac{\text{rad}}{\text{s}^2}$ for $t \in [t_{p,acc}, t_{p,const} + t_{p,dec}];$
 - $-9.6 \frac{\text{rad}}{\text{s}^2}$ for $t \in [t_{p,const} + t_{p,dec}, t_{p,tot}];$

The tangential velocity of the pulley P1 in the point of contact with the pulley corresponds to the velocity of the translation of the belt-cart couple, hence it is possible to relate the rotating motion parameters of the pulley with the rectilinear motion ones of the belts, as follows:

- $x_T = \theta_T r_P = (\dot{\theta} t + \theta_0) r_P;$
 $\dot{x}_T = \dot{\theta}_T r_P = (\dot{\dot{\theta}} t + \dot{\theta}_0) r_P;$
 $\ddot{x}_T = \ddot{\theta}_T r_P =$
 - $767.9 \frac{\text{mm}}{\text{s}^2}$ for $t \in [0, t_{T,acc}];$
 - $0 \frac{\text{mm}}{\text{s}^2}$ for $t \in [t_{T,acc}, t_{T,dec}];$
 - $-767.9 \frac{\text{mm}}{\text{s}^2}$ for $t \in [t_{T,dec}, t_{T,tot}];$

Knowing the velocities profiles parameters (*Figure 43*) and the total horizontal displacement, it is intuitive to derive the time intervals for each phase of the trapezoidal profile by means of the motion laws:

- $\dot{x}_{T,const} = 1575 \frac{mm}{s}$;
- $\dot{x}_{T,acc} = |\dot{x}_{T,dec}| = 797.9 \frac{mm}{s^2}$;
- $x_{T,TOT} = \frac{1}{2} \dot{x}_{T,acc} t_{T,acc}^2 + \frac{1}{2} |\dot{x}_{T,dec}| t_{T,dec}^2 + \dot{x}_{T,const} t_{T,const} = 4316 \text{ mm}$;
- $t_{T,acc} = \frac{\dot{x}_{T,const} - 0}{\dot{x}_{T,acc}} = t_{T,dec} = \frac{0 - \dot{x}_{T,const}}{\dot{x}_{T,dec}} = 2.1 \text{ s}$;
- $t_{T,const} = \frac{x_{T,TOT} - 2 \frac{1}{2} \dot{x}_{T,acc} t_{T,acc}^2}{\dot{x}_{T,const}} = 0.69 \text{ s}$;

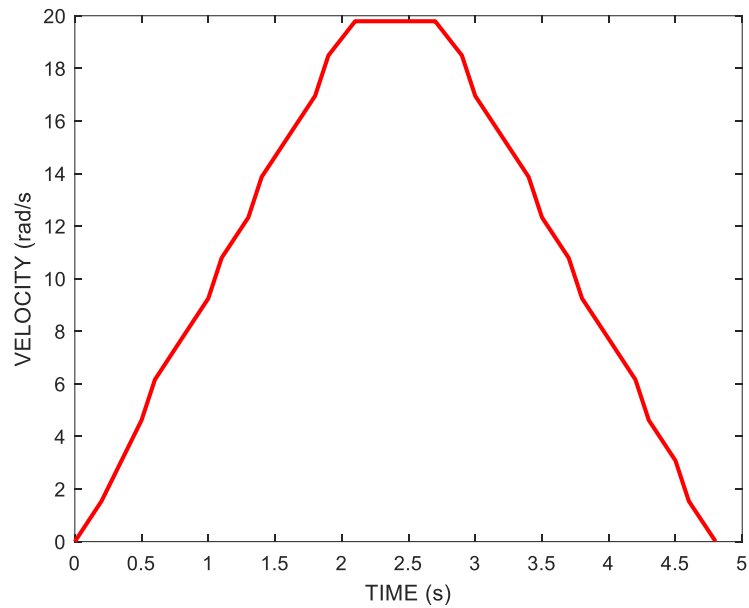


Figure 43: velocity profile for the translating speed reducer

After this premise, the dynamic analysis can be performed.

2.8 The translating mechanism: dynamic approach

The dynamic analysis has as main goal to quantify the amount of torque necessary to deliver the requested performance, as well as determining the forces and momentums involved for the component dimensioning.

Driving pulley P1

The dynamic analysis begins from the evaluation of the forces acting on the driving pulley P1, that receives the motor torque by means of the speed reducer, with reduction ratio $w=12.9$, while it is kept in position by reaction forces R_{P1x} and R_{P1y} acting in the centre of the pulley. Tension T1 is the tight side tension, while T2 is the slack side tension and they both account for the variation of tension on the two sides of the pulley due to the preload and the transversal tensions., F_u and F_{pl} specifically.

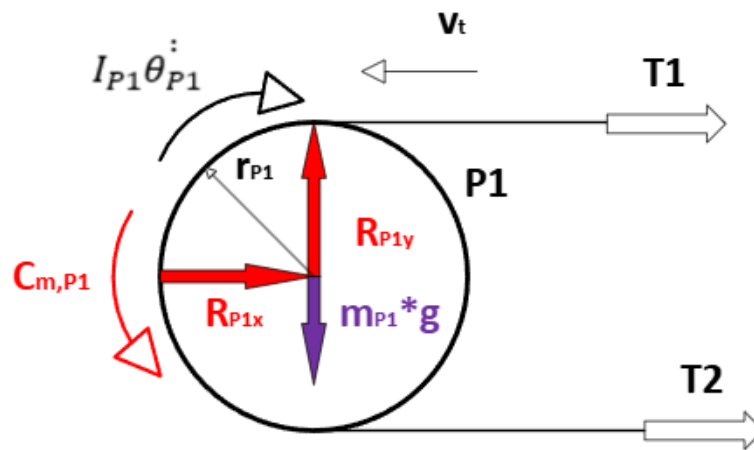


Figure 44: dynamic analysis pulley P1

- $C_{m,P1} - I_{P1} \dot{\theta}_{P1} + (T_2 - T_1) D_p / 2 = 0 \Rightarrow$
 $\Rightarrow T_1 - T_2 = F_u = 2 \frac{(C_{m,P1} - I_{P1} \dot{\theta}_{P1})}{D_p};$
- $T_1 = F_{PL} + \frac{F_u}{2};$
- $T_2 = F_{PL} - \frac{F_u}{2}$
- $R_{P1x} = F_{PL};$
- $R_{P1y} = m_{P1} g;$

Driven pulley

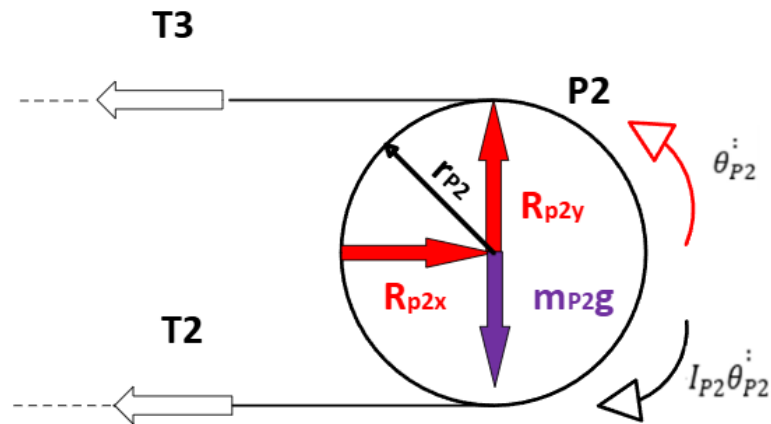


Figure 45: dynamic analysis pulley P2

The driven pulley P2 is a passive element in the mechanism as it is subject to the transmission motion of the belt due to the motor torque. The reaction forces R_{P2y} and R_{P2x} balance tensions T2, T3 and the weight of the belt and of the pulley P2 itself.

- $R_{P2y} = m_{P2}g = m_{P1}g = R_{P1y}$;
- $R_{P2x} = T_3 + T_2$;
- $-I_{P2}\dot{\theta}_{P2} + \frac{(T_3 - T_2)D_P}{2} = 0 \Rightarrow$
 $\dot{\theta}_{P2} = \frac{(T_3 - T_2)D_P}{2I_{P2}}$;
- $I_{P1} = I_{P2}$;

Cart with carbon fibre comb

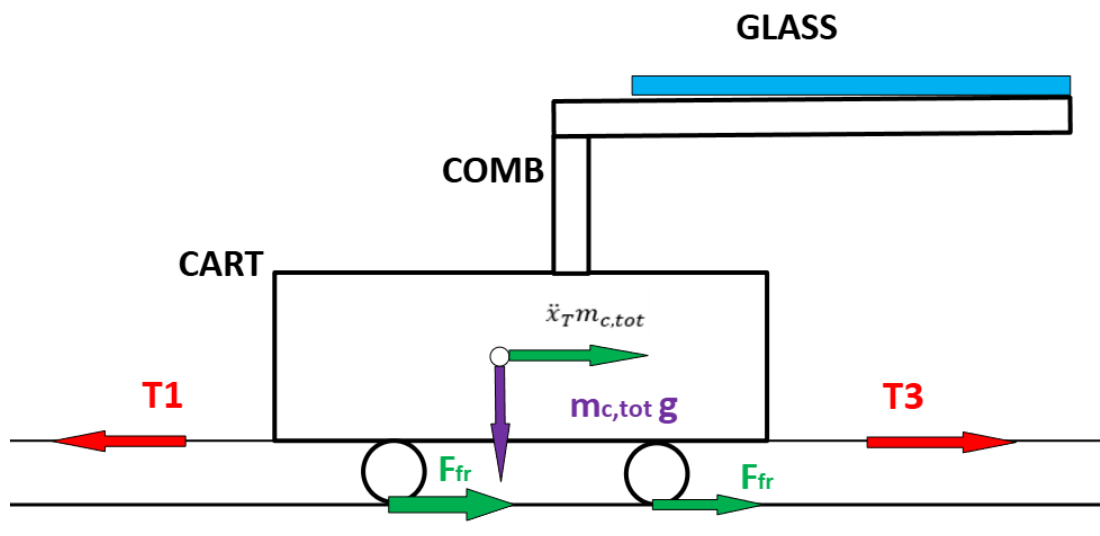


Figure 46: dynamic analysis cart

With regards to the cart analysis (*Figure 46*), since the carbon fibre comb can be considered ideally stable and rigid, it is considered as a unique body with the cart and so, the total weight given by the comb and its load could be directly applied in the centre of mass of the cart. This will represent the only relevant vertical force acting in this section of the analysis, but will be important in the evaluation of the horizontal forces, specifically sliding friction. Horizontally, the belt tension T_1 must account for the contribution due to inertia, preloading tension and sliding friction, both in the static and dynamic cases.

	mass [kg]
m_{cart}	622,7
m_{glass}	192,0
$m_{c,tot}$	814,7

Table 26: total load composition

Static friction case

- $F_{sf} = -(m_{c,tot})g\mu_s$, with $\mu_s = 0.6$ for steel on steel interaction;
- $T_1 = T_3 + m_{c,tot}(g\mu_s + \ddot{x}_T)$;
- $F_{PL} = 2F_U$;

Dynamic friction case

- $\mu_d = 0.015 \approx 0$ for greased steel on steel interaction;
- $T_1 = T_3 + m_{c,tot}(g\mu_d + \ddot{x}_T) = T_3 + \ddot{x}_T m_{c,tot}$
- $F_{PL} = 2F_U$;

V-Roller

The v-rollers will be subject to friction and weight forces mainly. In particular, the total load plus cart weights will be considered as equally divided amongst the four rollers.

Static friction case

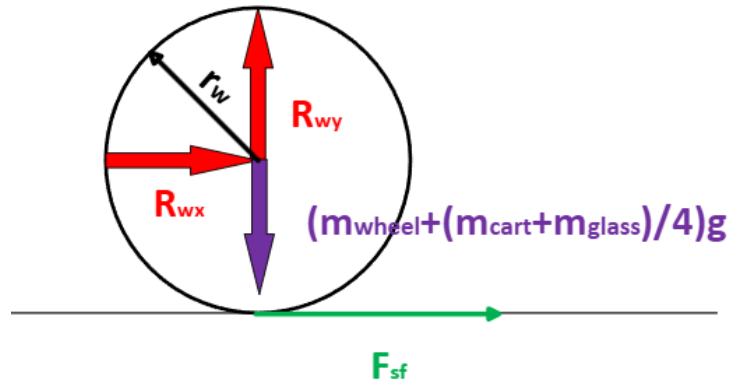


Figure 47: static friction case in v-roller dynamic analysis

- $F_{s,fr} = (m_{c,tot})g\mu_s$;
- $T1 = F_{s,fr} + (m_{c,tot})\dot{x}_T = T_3 + m_{c,tot}(g\mu_s + \ddot{x}_T)$;

At steady state, when the cart is not in motion, static friction is acting between the steel surface, with an assumed coefficient of about $\mu_s = 0.15$ for a steel-steel greased interaction:

- $R_{wx} = -F_{sf}$;
- $F_{sf} = -\left(\frac{m_{cart} + m_{glass}}{4} + m_{wheel}\right)g\mu_s$;
- $R_{wy} = \left(\frac{m_c + m_g}{4} + m_{wheel}\right)g$;

dynamic friction case

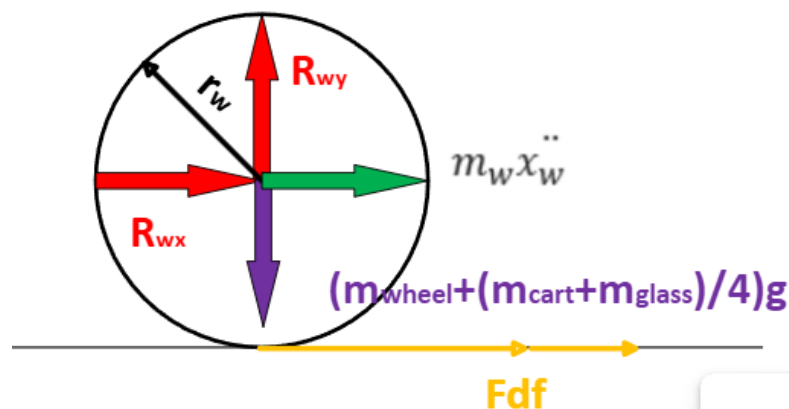


Figure 48: dynamic friction case in v-roller dynamic analysis

- $R_{wx} = -(F_{df} + F_v + m_w \dot{x}_w) = -\left(\frac{m_{cart+m_{glass}}}{4} + m_{wheel}\right)g\mu_d + m_w \ddot{x}_w$;
- $F_{df} = \left(\frac{m_{cart+m_{glass}}}{4} + m_{wheel}\right)g\mu_d$;
- $R_{wy} = \left(\frac{m_{cart+m_{glass}}}{4} + m_{wheel}\right)g$;

By combining together the single dynamic analysis on components, it is possible to obtain the value of the driving torque $C_{m,P1}$, provided by motor M2 by means of a speed reducer, as function of all the forces and moments involved.

1 PZ
Motorid. a coppia conica
KA47 DRN90L4/BE2HR/TH/EK8R



Velocità a 50Hz [r/min]	: 1461 / 120
Velocità a 60Hz [r/min]	: 1767 / 145
Rapporto di riduz. totale [i]	: 12,19 / Infinito
Coppia d'uscita max [Nm]	: 375
Coppia d'uscita a 50Hz [Nm]	: 120
Coppia d'uscita a 60Hz [Nm]	: 99

Figure 49: datasheet parameters for translating motor from manufacturer

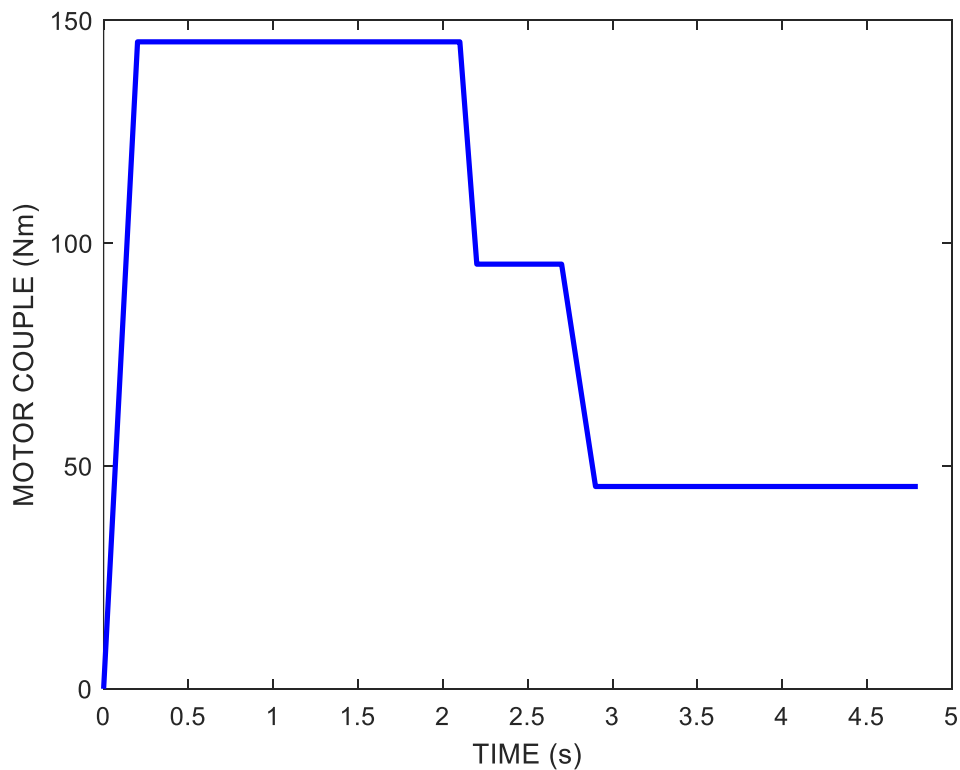


Figure 50: driving torque $C_{m,P1}$ of the translating mechanism

2.9 The translating mechanism: component dimensioning

2.9.1 Toothed belt

For the toothed belt dimensioning process, it was necessary to have a look at the datasheet from the manufacturer. Our model of choice is a Megalinear High-Performance open ended toothed belt (AT20X100-HP-NFT), with width $b=100$ mm and a weight of 906 gr/m for about 8m of length.

From the manufacturer documentation, it is possible to obtain crucial information about the parametrization of the belt, forces and the theory behind the design phase. In particular, for linear motion and conveying application, the peripheral force F_u and preload tension F_{pl} could be quantified by knowing the masses involved.

Specifically, the following formulations hold:

$$F_u = m_{c,TOT}(\ddot{x}_T + g\mu),$$

where μ =generic sliding friction coefficient;

As already highlighted, considering a lubricated steel-steel contact of the v-rollers on the rail, it follows that the dynamic friction is negligible with respect to the static one ($\mu_d \ll c$). A similar discussion holds for the rolling friction μ_r , whose impact is very small than the sliding one.

Consequently, the maximum transversal force $F_{u,max}$ will be given by considering the static sliding friction coefficient at the start of motion

$$F_{u,max} = m_{c,TOT}(\ddot{x}_{T,ACC} + g\mu_s) = 1823,3 \text{ N}$$

For linear motion conveyors, the manufacturer suggests to adopt a preload tension such that

$$F_{pl} = 2F_{u,max} = 3646,6 \text{ N};$$

As it is known from general knowledge about belt transmission systems with pulleys, by analysing the two ends of the belt pulley wrapped around a single pulley, it is always possible to identify a slack side and a tight side. The following relations holds, considering the contribution of inertial forces:

- $C_{mP1} - I_{P1}\ddot{\theta}_{P1} + (T_2 - T_1)\frac{D_{P1}}{2} = 0 \Rightarrow$
 $\Rightarrow T_1 - T_2 = \frac{C_m - I_{P1}\ddot{\theta}_{P1}}{\frac{D_{P1}}{2}},$
- $T_1 = F_{pl} + \frac{F_{u,max}}{2};$
 $T_2 = F_{pl} - \frac{F_{u,max}}{2};$
- where:
 - b = belt width=100 mm;
 - C_s = safety factor;
 - $z_m=12= n^\circ$ of teeth of the pulley in mesh;
 - $F_{p,spec}$ = tooth resistance=[N/cm];
 - $F_{u,max}$ = peripheral force= [N];

By substitution, it is trivial to conclude that

$$\Rightarrow T_1 - T_2 = F_{pl} + \frac{F_{u,max}}{2} - \left(F_{pl} - \frac{F_{u,max}}{2} \right) = \frac{C_m - I_{P1}\ddot{\theta}_{P1}}{\frac{D_{P1}}{2}} \Rightarrow$$

$$\Rightarrow F_{u,max} = \frac{C_m - I_{P1}\ddot{\theta}_{P1}}{\frac{D_{P1}}{2}};$$

Once that the transversal force for our transmission is obtained, it is possible to derive the minimum width of the belt needed for the chosen application, by considering some additional application-related parameters, as follows:

$$b = \frac{F_{u,max}C_s 10}{F_{p,spec}z_m}$$

- b = belt width=100 mm;
- C_s = safety factor;
- $z_m=12= n^\circ$ of teeth of the pulley in mesh;
- $F_{p,spec}$ = tooth resistance=[N/cm];
- $F_{u,max}$ = peripheral force=[N];

From the a priori information of the design, $z_m = 14 \Rightarrow 12$ as 12 is considered by the manufacturer as the maximum possible number of teeth in mesh that must be accounted in calculations.

Also, the values of the safety factor C_s and the tooth resistance $F_{p,spec}$ to be chosen is coded by tables provided by the manufacturer, depending on the belt application. In our case, we consider a steady load along the belt, as the tension is kept almost continuously along the belt, while the maximum speed reached is known as $\theta_T=189$ rpm.

TABLE 4 - SAFETY FACTOR	
Steady Load	1

Figure 51: security factor for a conveyor belt subject to steady load

Hence

$$C_s = 1$$

and

TOOTH RESISTANCE										
RPM (1/min)	0	20	40	60	80	100	200	300	400	500
$F_{p,spec}$ (N/cm)	147	144	142	139	137	135	126	119	112	107

Figure 52: tooth resistance for AT20 open belt based on angular velocity

$$F_{p,spec} = 126 \frac{N}{cm};$$

By substituting the parameters obtained above, it results that the minimum admissible belt width is:

$$b_{min} = \frac{F_{u,max} C_s 10}{F_{p,spec} z_m} = \frac{1823,3 * 1 * 10}{126 * 12} = 12 \text{ mm};$$

However, it is also important to verify that the belt is actually able to withstand the resultant traction load applied, which is given by

$$T_{max} \geq \frac{F_u}{2} + F_{PL} C_s = 4558,3 \text{ N}$$

The AT20 HP belt with 50 mm width is the closest belt from the manufacturer to a 36 mm width. For this choice, it is seen that

$$T_{max} = 16000 N \geq 4558,3 N$$

So, a 50 mm width version of the same belt would be sufficient to account for the application requests. However, it was chosen to over-dimension the belt to a 100 mm width, so that it could be used for more demanding loads and tensions.

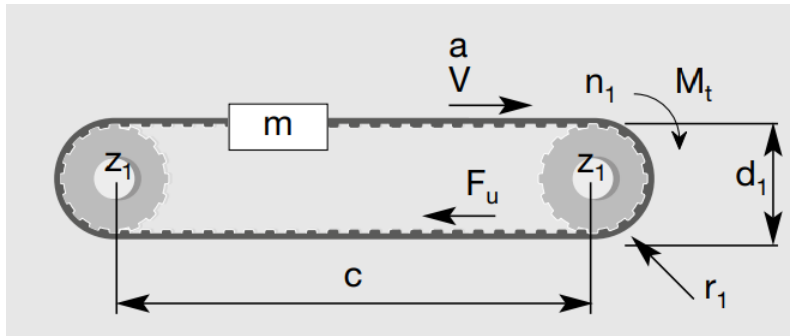


Figure 53: belt conveyor model provided by belt manufacturer

2.9.2 V-shaped rollers

From the manufacturer datasheet, it is immediate to retrieve the maximum load in dynamic conditions and along the radial and axial direction. By calculating the resultants of the reaction forces on the v-shaped rollers, the greatest one for each case is considered and compared to the maximum admissible. As there are no solicitations along the z axis of our reference system, no contribution is present along the axial direction of the rollers.

[kN]	[kN]	[kN]	[kN]	[kN]	[kN]
C_{dyn}	$C_{eff,dyn}$	$C_{max,ax}$	$C_{eff,ax}$	$C_{max,rad}$	$C_{eff,ax}$
130	7,98	41	0	15,3	4,49

Tipo		Carichi dinamici (N)		Carichi limite (N)		Fattori di carico		Coppia di serraggio (2) (Nm)	Massa (kg)
		C_w (5)		radiale F_r	assiale F_a	X	Y		
RKY 52	RKYR 52	41 000		11 900	4 800	1	3.7	80	0.6
RKY 62	RKYR 62	46 000		19 000	8 300	1	3.5	160	0.9
RKY 72	RKYR 72	66 000		30 000	12 300	1	3.2	300	1.6
RKX 90C	RKXR 90C	130 000		41 000	15 300	1	3.8	450	2.8
RKX 110C	RKXR 110C	185 000		55 000	20 900	1	3.9	450	4.9

Figure 54: v-roller wheels datasheet compared to the obtained results

2.10 Results

The analysis of the main mechanisms of the walking beam has been a quite challenging yet fascinating section of the project, as it explored many aspects of mechanics and allowed to put into practice some prior knowledge, acquired during my bachelor degree, plus some recent knowledge, acquired in the mechatronics field.

Specifically, for the lifting mechanism the velocity and dynamic models have been derived and integrated inside an Excel spreadsheet, so that the torque variation during the cycle could be obtained as a function of the exchanged forces. Hence the suitability of the chosen motor was confirmed.

By means of the same Excel calculations, it was possible to verify all the critical components, such as cranks, threads and bearings. No one of them shew particular issues for the application.

Subsequently, a Finite Element Method analysis was performed in Autodesk Inventor, confirming the results of the calculations.

A similar approach was adopted for the translating mechanism, as first kinematics and dynamics were studied in details and, the, modelled on an Excel spreadsheet. Also in this case, relevant graphs about the torque variation in time were obtained and the translation motor was verified. A dimensioning of the belt and of the cart roller wheels was performed and even there no issues were found.

In this case, no FEM analysis was necessary as the components are certified by the manufacturer.

In general, all chosen components for the walking beam were found compliant with the requirements and type of application and all the analysis were fully completed.

Chapter 3 Rockwell Automation PLC

3.1 Studio 5000 intro

Studio 5000x is a software suite included in the offer of Allen-Bradley, an electronics manufacturer which is part of the Rockwell Automation group: it is as a complementary tool to the hardware belonging to the Allen-Bradley's **Logix 5000** controllers, as it allows to program and adapt them to any need during the designing, developing and debugging phases of any industrial environment, either simple or complex.

This is possible thanks to the many features that Studio 5000x offers, not to mention the wide number of resources and online courses to approach and get to know the programming environment.

Programming Languages

The program allows to use almost all the programming languages and techniques, such as Ladder logic (LD), structured text (ST), function block (FBD) and sequential function charts (SFC). For the purpose of the project, ladder logic and structured text were used.

3.1.1 Programming modules

The software is made up by many modules, each one with a specific purpose in defining and organizing the system that is going to be developed. Among them, it is worth to mention: Motion Control, Logix designer and RsLinx Classic.

Motion Control allows to directly program and control drives and actuators in the system connected to the Logix Controller, managing them accordingly to motion axis and motion parameters. By means of Direct Kinematix commands it is possible to directly send motion commands to the interested actuators, without need of routines or programming code.

RsLinx Classic is useful to define the connections and communications between all the PLC units present in the plant network, such as controllers, actuators, sensors, HMI devices.

Logix designer is the main module in studio 5000 as it is where the programming code is written, debugged and executed. From there it is possible to monitor the whole system, having a full overview in real time on the processes, variables involved, routines and subroutines in execution and errors. In particular, it contains a diagnostics

system that detect errors and warns about possible undesired outcomes from programmed instructions, as well as a debugging tool to check step by step the effect of each command on the plant. Moreover, it allows to virtually simulate the plant before connecting to the actual electronic instruments, even in absence of the physical hardware, as it has happened for some simulations of this project.

3.1.2 Connections

In this project, Studio 5000 was connected via **Ethernet/IP** to a generic PLC controller available, as the ControlLogix Controller 5580 was not available at the time of the simulations. However, as already mentioned, studio 5000x has a feature that allows to simulate the plant connecting to a different PLC from the designated one, even just for debugging and simulation purposes. It is also possible to use connection protocols such as **ControlNet**, **DeviceNet**, and **Modbus**, while **FactoryTalk** ensures compatibility and integration with other third party softwares and devices.

3.1.3 Kinetix Motion instructions

The Kinetix Motion library is a set of instructions included in the family of Logix 5000 controllers for drives and offer a wide range of possibilities in the control of single and multi-axis systems. CIP (Control and Information Protocol) drivers allow communication between hardware and software, importing tags in PLC software control applications related to the drives themselves.

In general, every motion instruction presents mnemonic tags that act as memories in relation to the instruction execution. The values are stored upon a new iteration of the instruction under analysis.

The main tags are:

.EN (Enable)	It is set when the rung makes a false-to-true transition and remains set until the instruction message transaction is completed and the rung goes false.
.DN (Done)	It is set when the instruction has been correctly executed without errors
.ER (Error)	It is set to indicate that the instruction detected an error, such as if you specified an unconfigured axis.
.PC (Process Complete)	It is set once the instruction has been executed and completed, if even with errors;

.IP (In Progress)	It is set when the instruction is still being executed
-------------------	--

Table 27: tags for bits

Here is a list of some of the main used along the motion programming development.

MSO (Motion Servo On)

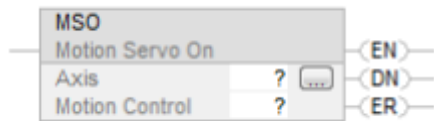


Figure 55 MSO function block

The Motion Servo On (MSO) instruction activates the drive amplifier for the specified axis and to activate the axis' servo control loop.

Motion Axis Shutdown (MASD)

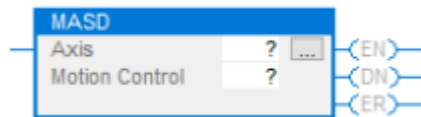


Figure 56 MASD function block

Motion Axis Shutdown (MASD) instruction forces a specified axis into the Shutdown state, in which the drive output is disabled, servo loop deactivated, and any available or associated OK solid-state relay contacts open. The axis remains in the Shutdown state until either an Axis or Group Shutdown Reset is executed. Moreover, it clears all motion processes in progress and status bits.

Another characteristic of the Shutdown state is that any instruction that initiates axis motion is blocked from execution. Attempts to do so result in an execution error. Only by executing one among a Motion Axis Shutdown Reset (MASR), a Motion Group Shutdown Reset (MGSR), or a Motion Coordinate Shutdown Reset (MCSR), motion can be executed again.

Motion Axis Shutdown Reset (MASR)

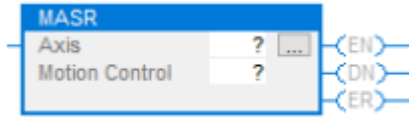


Figure 57: MASR function block

Just as the Motion Axis Shutdown (MASD) instruction forces the targeted axis into the Shutdown state, the MASR instruction takes the axis out of the Shutdown state into the Axis Ready state. This feature could also close the E-Stop string that controls main power to the drive system and, thus, permit the customer to reapply power to the drive.

Motion Servo Off (MSF)

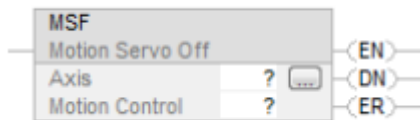


Figure 58: MSF function block

The MSF instruction directly and immediately turns off drive output and disables the servo loop on any physical servo axis. With CIP motion, this places the axis in the Stopped state described in Motion State Instructions. The MSF instruction also disables any motion planners that may be active at the time of execution and requires no parameters besides the designated axis. It can be also used to turn servo action off when the axis must be moved by hand and, since the position continues to be tracked even with servo action off, when the servo loop is turned on again, the axis is again under closed-loop control, at the new position.

Motion Servo On (MSO)

The MSO instruction directly activates the drive and enables the configured servo loops associated with a physical servo axis. It can be used anywhere in a program but should not be used while the axis is moving: if this is attempted, an Axis in Motion error is generated. The MSO instruction automatically enables the specified axis by activating the drive and the associated servo loop: the resulting state of the axis is referred to as the Running state. The most common use of this instruction is to activate the servo loop for the specified axis in its current position in preparation for commanding motion. The Done (.DN) bit is not set immediately, but only after the request is completed.

Motion Axis Stop (MAS)

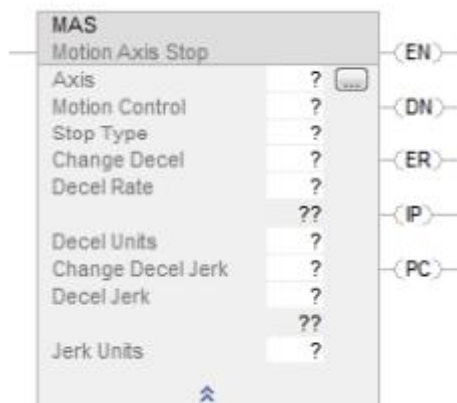


Figure 59: MAS function block

Use the MAS instruction when you want a decelerated stop for any controlled motion in process for the axis, without disabling the servo loop. A trapezoidal profile is always used for MAS with Stop Type=ALL for the deceleration regardless of the programmed profile type. The instruction could be used to stop a specific motion process such as jogging, moving, or gearing, stop the axis completely or to abort a test or tune process.

Motion Axis Home (MAH)

The MAH instruction is used to calibrate the absolute position of the specified axis. Servo axes that the axis can be homed using Active, Passive, or Absolute Homing Mode configuration. The MAH instruction sets the HomedStatus bit upon successful completion of the configured homing sequence: this bit indicates that an absolute machine reference position has been established. When the axis Homing Mode is configured as Active (project case), the physical axis is first activated for servo operation. As part of this process, all other motion in process are cancelled and relative status bits are cleared. The axis is then homed using the configured Home Sequence, which may be Immediate, Switch, Marker (project case), or Switch-Marker. In the Marker Home Sequence, the axis is jogged in the configured Home Direction and then, after the position is redefined based on detection of the home event, it is automatically moved to the configured Home Position.

Motion Axis Move (MAM)

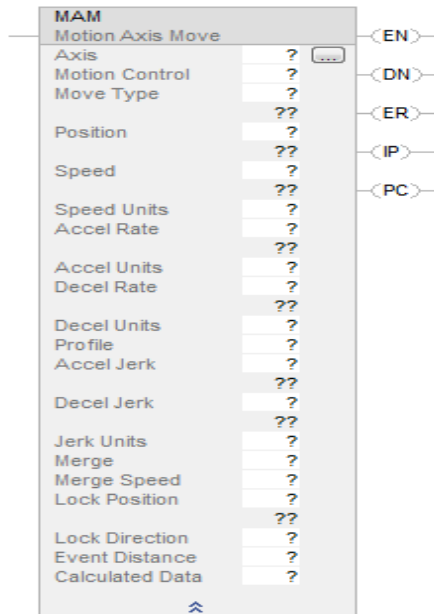


Figure 60: MAM function block

The Motion Axis Move (MAM) instruction allows the execution of a specific axis motion based on the parameters reported on the instruction block, with a high level of personalization.

Besides selecting the axis interested and the related motion instruction, it is possible to choose the type of motion among a variety: absolute, relative, shortest path, rotary positive or negative and many more, depending on the approach to the programmed environment or personal preference. The same choice of convention could be applied to the position slot.

Then, a parametrization section is left for speed, acceleration, jerk values and units (unit of choice, % of time or % of maximum).

The last slots are used for extra options that allow, for instance, to overwrite the MAM motion on that axis on any motion currently in process on the axis itself or locking the motion direction.

3.2 Software development in Studio 5000

3.2.1 Main architecture

After a short overview of the software Studio 5000 and the possibilities that it opens, especially through the Kinetix Motion libraries, the software development started.

First of all, in order to start a project in Studio 5000, it is needed to configure the PLC architecture that it is expected to be implemented in the project and on which it is supposed to work on. This is a crucial step to allow proper communication through the expected communication connection between software and hardware, even during the developing, testing and debugging phases. Failure in defining the correct PLC controller will result in possible malfunctioning while running the code or just the impossibility to properly connect to the PLC infrastructure, hence preventing the download of our code instructions on the control system itself.

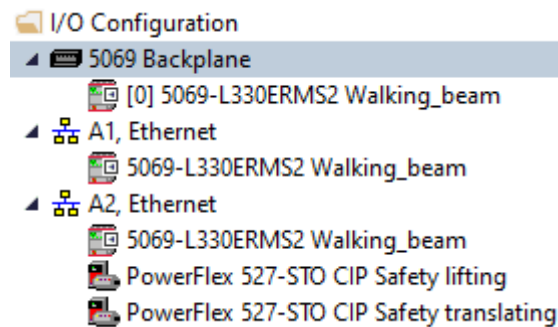


Figure 61: tree of devices in the network

In the case under analysis, a 5069 Backplane chassis was chosen to host as first module a Compact GuardLogix 5380 Safety Controller by Allen-Bradley, with Ethernet/IP protocol connections: It is the brain of the machine PLC system, as it takes decisions (output signals) on the basis of the received data (input signals), depending on the programming code downloaded on it. In particular, the dual IP feature allows using port A1 for maintenance/service connection and port A2 for the I/O control of the machine: besides the few position sensors on board, port A2 is used to connect to the two PowerFlex 527-STO CIP Safety drives, one for each axis drive of the machine: the lifting motor and the translating one. The setup of an IP address is a required step to proceed with the further steps, as it allows to setup the communication between devices on the same Ethernet/IP network; a private network configuration with IP 192.168.1.2 was chosen for the controller. At last, the time synchronization must be enabled on the controller, so that all movements are synchronized and correctly executed in time.

3.2.2 Motion groups

In order to assign the CIP drives to the designated axis, it is necessary to define the motion groups first, which is a collection of different axes that are controlled as single unit. Only a single motion group per project can exist and it is comprehensive of just two motion axes in this project: `Axis01_lifting` and `Axis_02_translating`. Both axes present a similar configuration, as both have a position loop control approach and a tracking application type, which assures an accurate positioning on the

motor and, hence, of the machine, by means of a Position Integrator Hold; the control conditions on velocity and acceleration are relaxed instead.

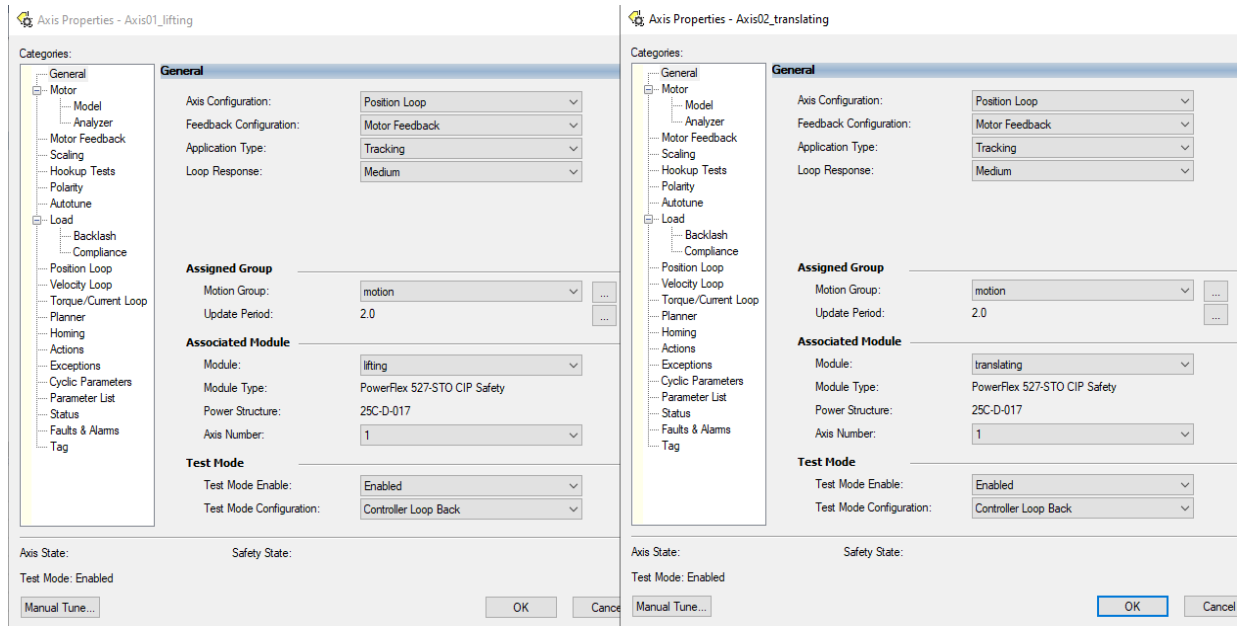


Figure 62: general properties for both axis

Subsequently, the motor setup for each axis is defined by using nameplate datasheet parameters provided by the manufacturer, as the motors are produced by a different company and so they are not included in the Rockwell Automation catalogue.

Axis01_lifting

For the lifting motor, the following parameters are inserted from the manufacturer datasheet. The only parameter that needs to be calculated is the pole count, as it is not mentioned on the technical sheet.

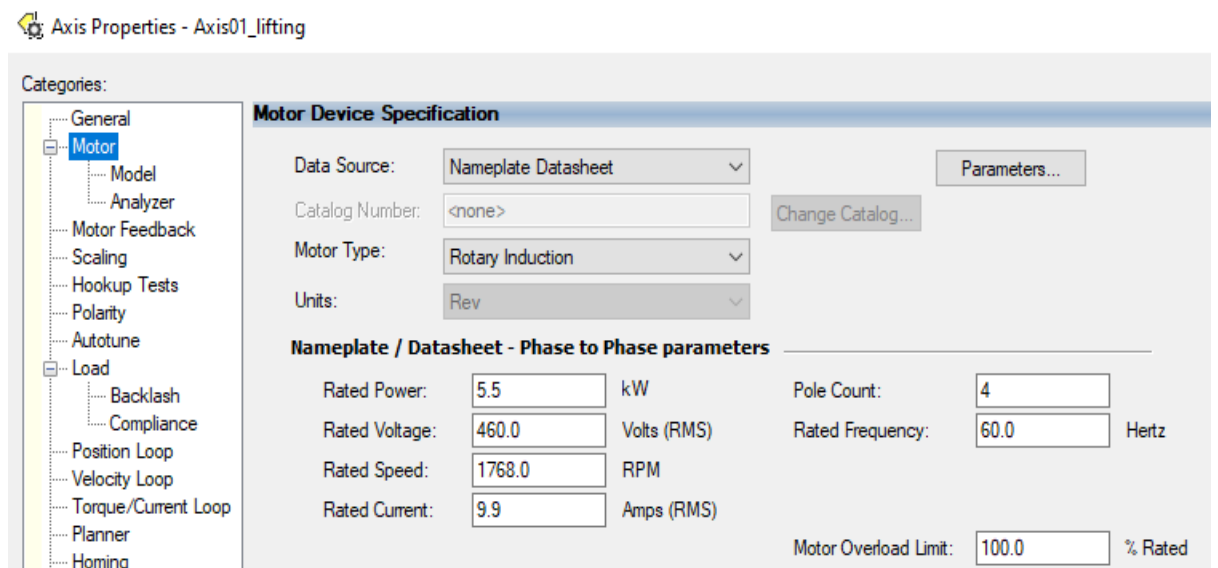


Figure 63: Axis01 motor specifications

This value could be inversely derived by knowing the rated frequency and speed of the motor, as stated by the formula

$$w_n = 120 \cdot \frac{f}{P} \Rightarrow$$

$$\Rightarrow P = 120 \cdot \frac{f}{w_n} = 4, \text{ with:}$$

- w_n = angular speed in rpm;
- f = nominal frequency;
- $P = n^\circ$ of poles;

After, the scaling section is filled and, as the name suggests, it is dedicated to define how the actuation transmission from the motor is delivered: linear actuation, direct coupling or rotary transmission (project case).

Rotary transmission is related to any transmission system pairing the load with the output shaft of the motor, such a speed reducer. Hence, the transmission ratio I/O $\frac{\omega_{m1}}{\omega_\theta} = 123$ is added as a parameter.

The scaling section allows to define a personalized unit of measurement related to rotation, inserting the name and the ratio existing between the chosen unit and a single revolution of the output shaft. In this case, grades were chosen as units, with a ratio of 360 grades per 1 Load revolution. The travel section instead offers the possibility to define constraints on the allowed travel of the axis by imposing 3 travel modes: Unlimited, Limited and Cyclic.

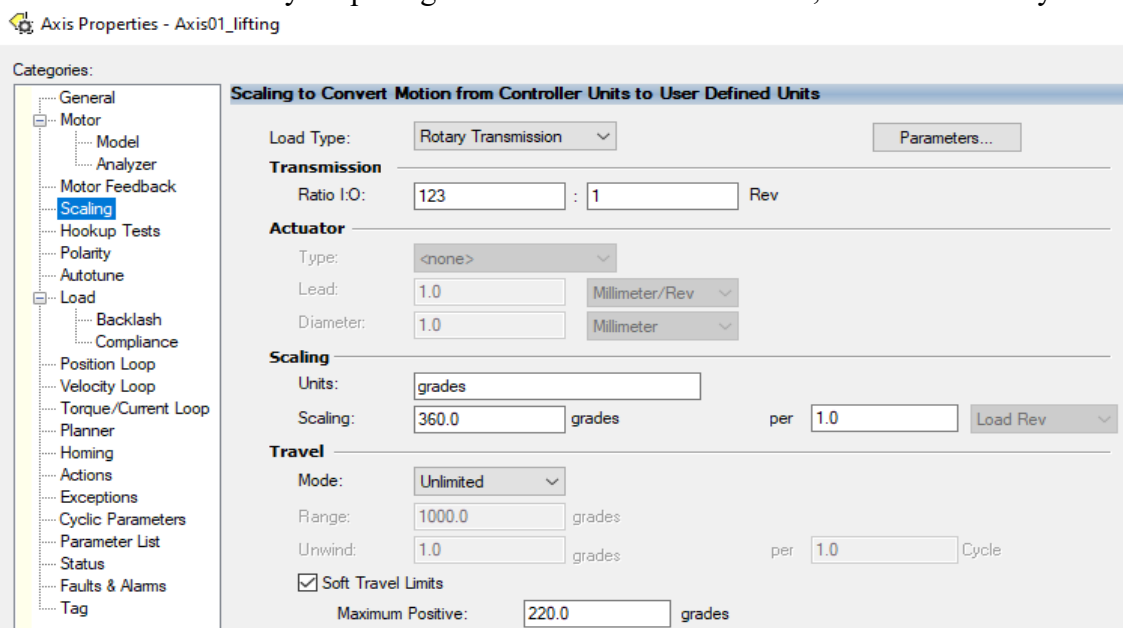
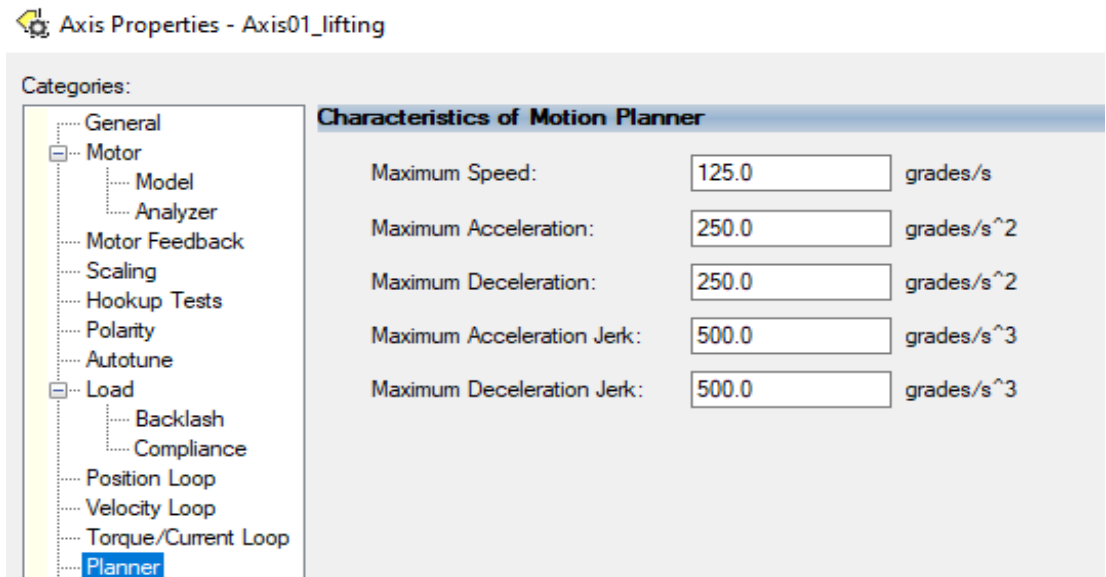


Figure 64: Axis01 scaling settings

Since it is not necessary to strongly constraint the travelling capability of our axis, the choice fell on the unlimited travel mode, with the imposition of Soft Travel Limits, to



make sure that the axis wouldn't exceed two specific angular positions, specifically at 220° and -10°, measured with respect to the XZ plane and along a clockwise direction.

The planner section could be used to define the maximum values for the motion planner of our axis, avoiding in this way to reach undesired velocities or accelerations. For this application, the constraints were considered as the maximum value for the parameter + 10% of its value, rounded to the closest integer multiple of 5.

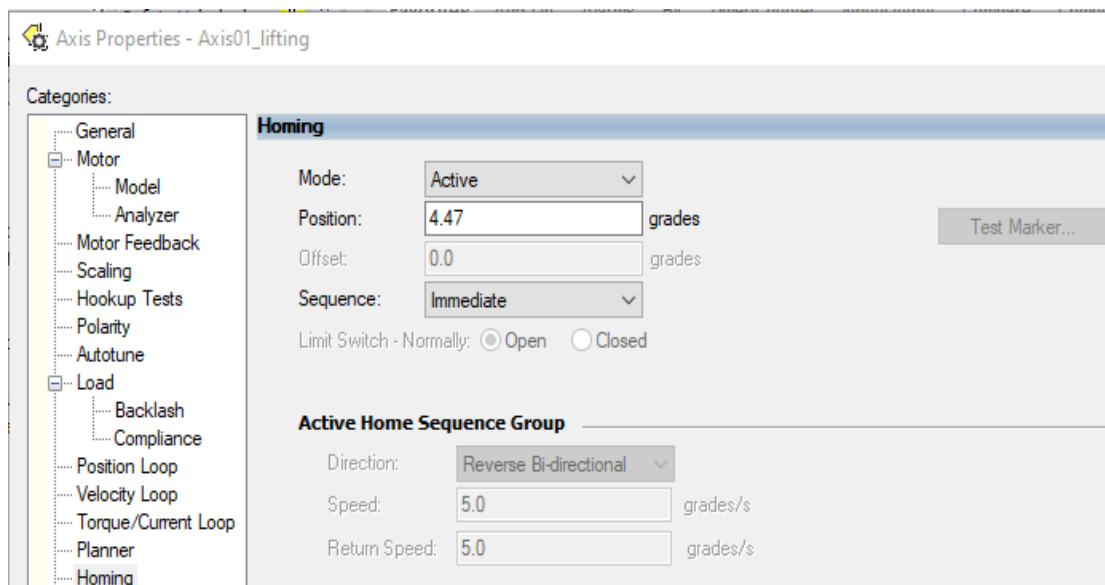


Figure 65: homing settings

At last, an active homing procedure is setup. If the machine was already assembled and connected to the PLC, the marker mode would be chosen, as it would allow to actively find the home marker automatically; being it not possible, the immediate

homing procedure was selected, homing immediately via software the axis at the desired home position (4.47°).

3.3 Axis02_translating

With regards to general setup of the motion axis, the same setup of Axis01_lifting was used, as we are dealing with the same exact necessities. Being also the motor M2 from a third part manufacturer, the nameplate datasheet elements were entered in the motor section, allowing its correct parametrization.

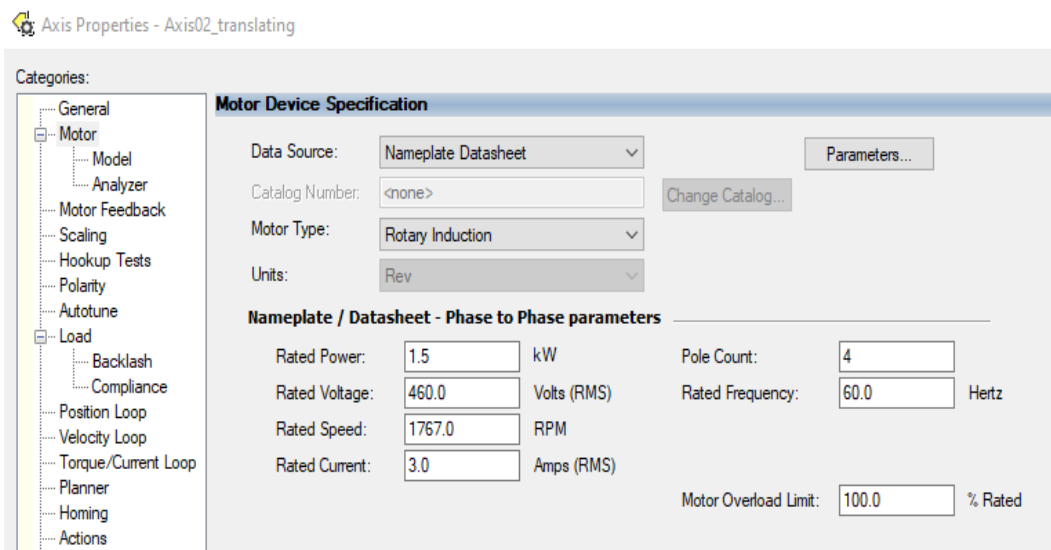


Figure 66: axis02 motor setup

Similarly, the scaling section was filled in with the corresponding reduction ratio $\frac{\omega_{m2}}{\omega_{\theta}} = 16$ and imposing a soft travel constraint of 6000 grades to limit the travel

position achievable during motion.

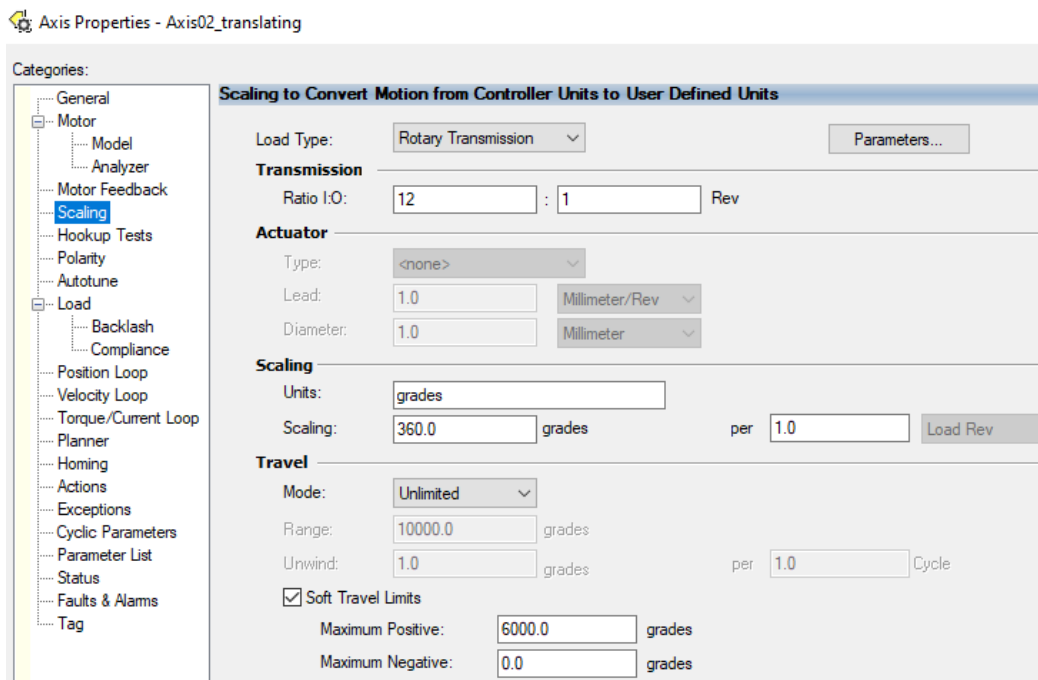


Figure 67: axis02 scaling settings

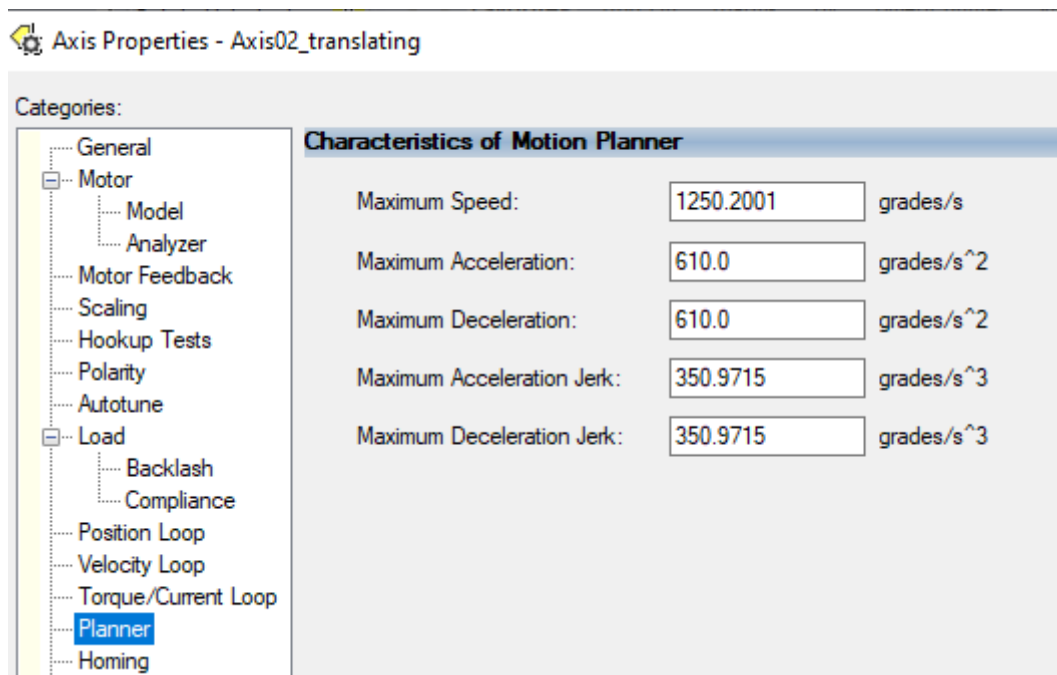


Figure 68: axis02 motion planner settings

Even the planner section was filled in using the same criteria that in Axis01_lifintg, as the maximum values + 10% were considered, rounding at the closest integer multiple of 5.

Regarding the home procedure, the homing position was defined at 0° and will be reached through an active and immediate homing procedure, hence a software redefinition of position.

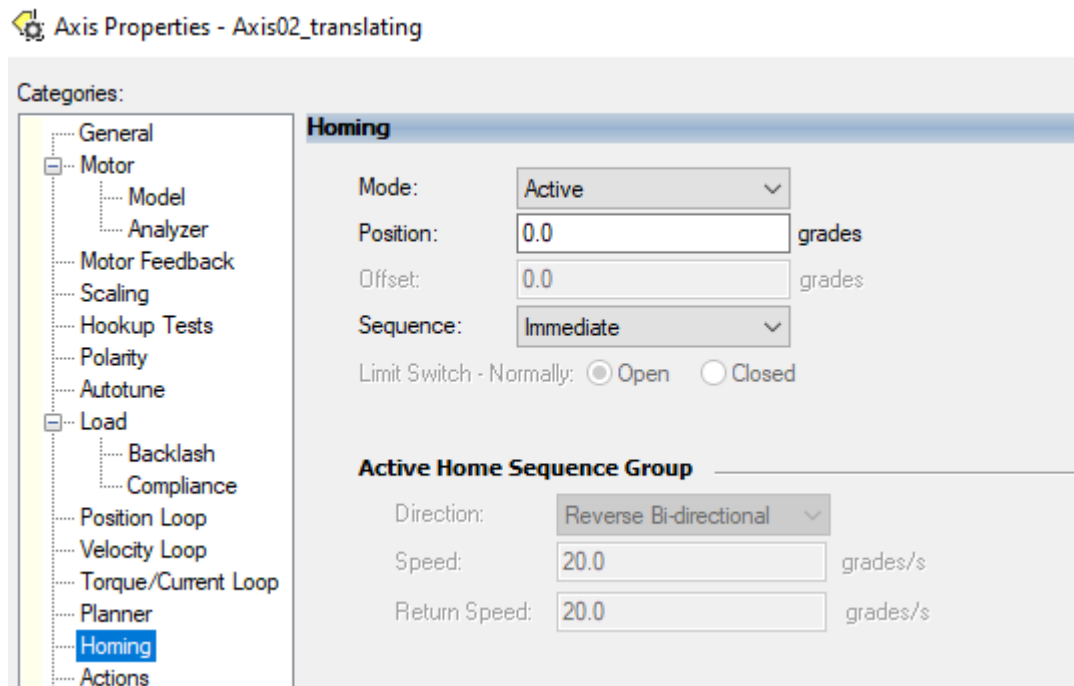


Figure 69: axis02 homing settings

Once that both axes were explicitly defined, the coding phase of the project could start.

3.4 Main routine

After having had a first approach to libraries and commands available in Studio 5000, the designing process of the main routine began. The main routine is the first piece of code that is approached both by the designer and the viewer, as it could provide a general idea and overview of the coding logic behind the program.

Usually, it presents some essential lines of ladder code related to preliminary checks, HMI and I/O interactions that could either allow or prevent the execution of some portions of code.

In this case, due to linearity and relatively low presence of subroutines, the main routine contains also the step-by-step code for the motion execution, according to the sequence explained during the kinematic analysis.

Rung 0-1-2 are used for HMI and security purposes, signalling the presence of errors through solenoids connected to lights and preventing the program to be executed in absence of power supply or in the presence of critical errors.

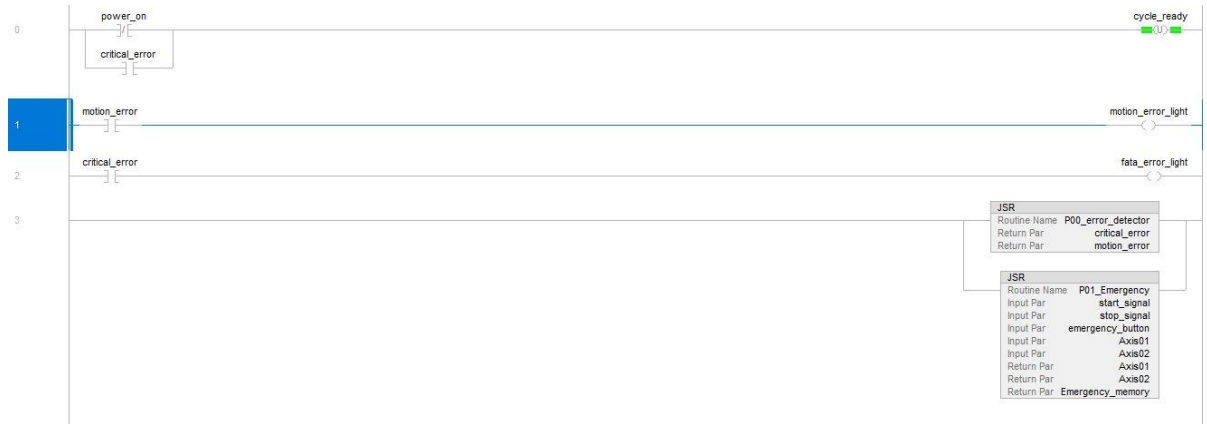


Figure 70: first rungs of main routine

Rung 3 contains two permanently supplied subroutines, P00_error_detector and P01_emergency.

3.5 P00_error_detector

This subroutine has been designed to receive as input all the fault error flags from the motion axis and send as an output a Boolean value associated to a latched memory.

To latch the memory, a several amount of normally open contacts, each one for an error fault signal, have been put in parallel: it is sufficient that just one is true to latch the memory and return a critical error and motion error flag to the main routine.



Figure 71: P00_error_detector

To unlatch the memory and turn off the error flag output in the main routine, there is a series of normally closed contacts, each for any error flag: if all error flags are false, the memory is unlatched and the critical error output flag is not true anymore.



Figure 72: step 10-20 main routine

3.6 P01_emergency

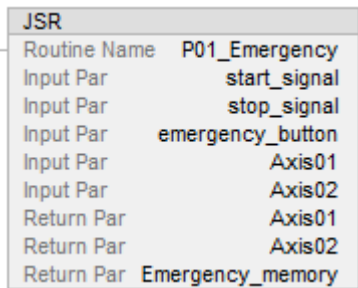


Figure 73: P01_emergency subroutine function block

This subroutine has been designed to receive as input the emergency, start and stop buttons signals and all the motion axis information and send as an output a Boolean value associated to a latched memory, relative to emergency state.

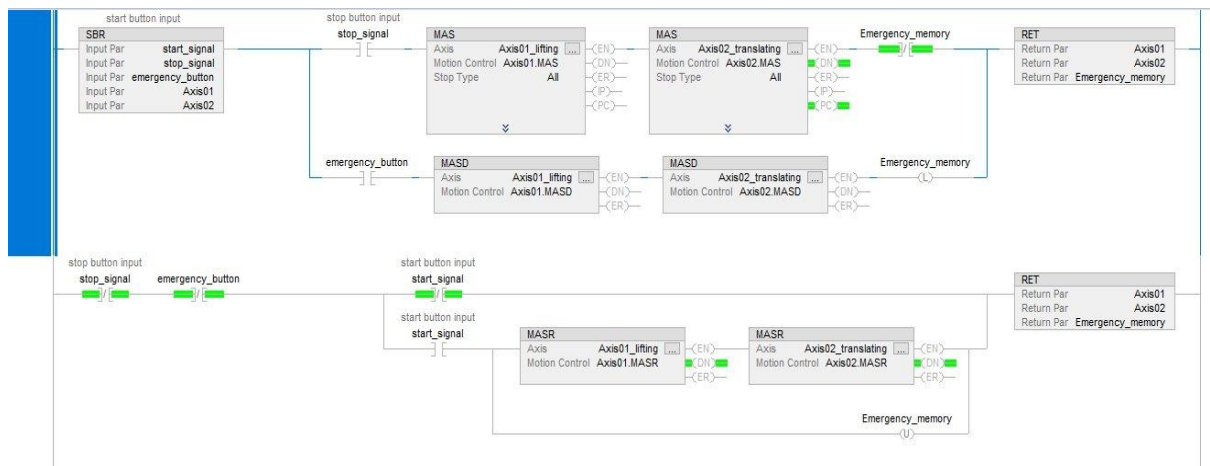


Figure 74: P01_emergency structure

To latch the memory (line 0), it is sufficient to press the emergency button: the normally open contact associated becomes true, the MASD (Motion Axis Shutdown) commands are executed, disabling the drive output, deactivating servo loop, and any available or associated OK solid-state relay contacts are opened.

To unlatch the memory and turn off the emergency flag output in the main routine, it is sufficient to press the start button, executing the MASR (Motion Axis Shutdown Reset) commands and unlatching the emergency memory.

In line 0, there is also another path, which is activated when the stop button is pressed:

It executes the MAS (Motion Axis Stop) commands, which stops the axis without disabling the servo and the drive.

3.7 Main routine

From rung 4, a specific programming path is followed for each rung, to ensure the correct launch of subroutines and motion sequence in the expected time instant and conditions. Among these conditions, a not-negative integer variable “STEP” is added to guarantee an order in commands execution. In particular, each rung from 4 to 10 has a structure that could be divided into 3 parts: general requirements, specific requirements and command execution

The general requirement part is generally made up by a series of two normally closed contacts for the “Emergency_memory” and “critical_error” variables. If only one of the two is true, the respective contact opens, avoiding the start of execution of the commands present in the rung itself. This is a precautional measure to prevent the program to continue running even in case of critical situations.

Subsequently, the specific part includes parallel ladder logic paths, different for each rung, allowing the launch of the subroutine or command only when specific requirements are met. In general, there is always a path with an EQ (equal) command, that compares the actual value of the variable "STEP" with a certain reference: if the equality is true, the path is unlocked, otherwise not. A parallel path with a normally open contact, called “override”, allows to jump to command execution even if the specific conditions are not met.

At last, the command execution part, which includes JSR (Jump to subroutine), to launch the subroutine, and move commands to change the value of the “step” variable.

In the case of rung 4, the specific requirements are either the pression of the stop button, manual override or STEP=0 and at least one of the steady state/home positions are not met. Any of these conditions bring to the execution of the subroutine P02_initialize.

3.8 P02_initialize



Figure 75: P02_initialize calling rung

The subroutine receives as input the data related to the motion axis, the active cycle status and the step value variable and sends as output the new value of the latter and executes a series of commands to initialize the state of the machine. Rung 0 resets the flags related to the MAM (Motion Axis Move) command for both axes by means of a FLL command.

Rung 1 checks if the machine is in steady state/ home positions. If the machine is in the correct position, the execution returns to the main routine, otherwise the subroutine step value is changed and execution proceeds at rung 2.



Figure 76: P02_initialize structure

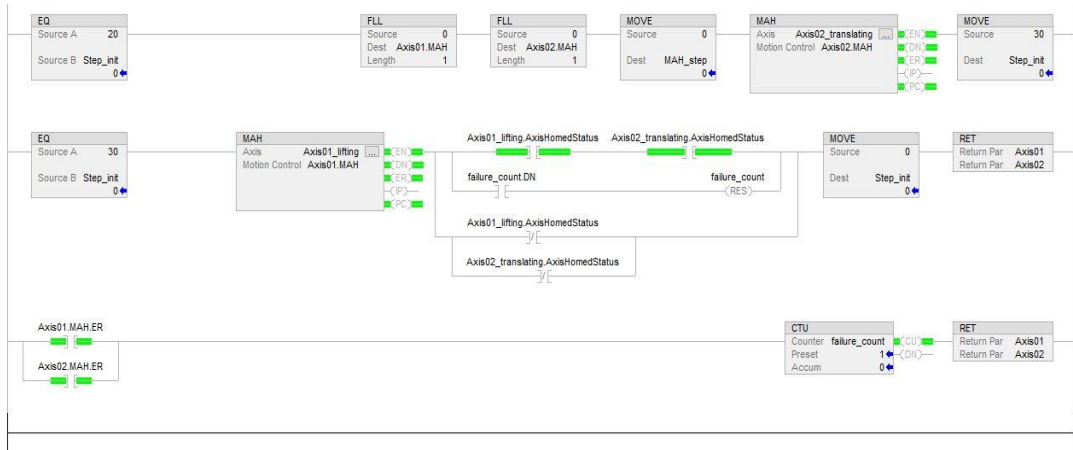


Figure 77: P02_initialize structure

At rung 2 the FLL command resets the arrays relate to MAH instructions for both axes and executes again a MAH motion on axis02 before increasing the subroutine step value, so that instruction execution could proceed on rung 3.

Rung 3 allows the execution of the MAH instruction for axis 01 and, depending on the specific case path, returns to the main routine upon resetting of the subroutine STEP variable.

The three cases account for:

- Both axes successfully at home;
- One of the axes is not at home;
- The failure counter is equal 1 (failure_count.DN=TRUE) and reset of the counter is provided;

Rung 4 is executed only if the error bit on the MAH instruction for any of the axes is true: in that case, the counter is increased from 0 to 1, setting the failure_count.DN=TRUE.



Figure 78: step 10-20 structure

3.9 Main routine (Step 0-20)

In rung 5, the specific requirement is represented by the operating mode selected: nominal_lift or extralift. The rung provides the latching of the cycle_ready variable and, if the equality check is successful, sets the value of Step variable from 0 to 10;

Subsequently in rung 6, by satisfying the equality constraint or manual override, subroutine P05_startup is launched.

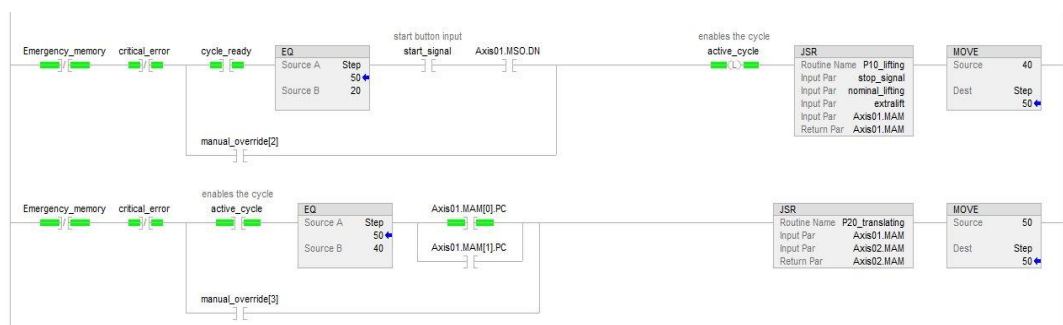
3.10 P05_startup

This subroutine simply provides the execution of the commands MSO (Motion Servo On) for both axes, which enables the servo motors of the axis;

3.11 Main routine (Step 40-60)

Rung 7, upon manual overriding or start_signal reception from the HMI and successful activation of servo motors, latches the active_cycle memory and launches the P10_lifting subroutine. Step variable moves from 40 to 50.

If P10_lifting is successfully completed, rung 8 executes subroutine P20_translating. The check is performed through open contacts referred to either Axis01.MAM of nominal or extra lifts. Upon successful completion, step variable is increased from 50 to 60.



P10_lifting and P20_translating

These two subroutines have the same purpose, resetting the flags from previous MAM and executing a new one, using the information stored in designated vectors for MAM operations, which consists in data related to positions, velocities and accelerations. P10_lifting presents two options, depending on the desired lifting movement selected at rung 5: nominal lifting or extralift.

Main routine (step 50-60)

Rung 9 uses different specific requirement paths to launch subroutine P30_homing. The first specific requirement is based on the present of active servo motors and the detection, via proximity sensor, of the translation position 1, corresponding to the position reached at the end of the lifting + horizontal translations concatenated motion, hence half of the cycle. The second and third specific requirements refer to the bit AxisHomedStatus, which is given by the respective markers on the two axes' engines and expresses if the axis is in the assigned position or not. If the two axes are not in the expected homed position at step 50, the P30_homing subroutine is launched.

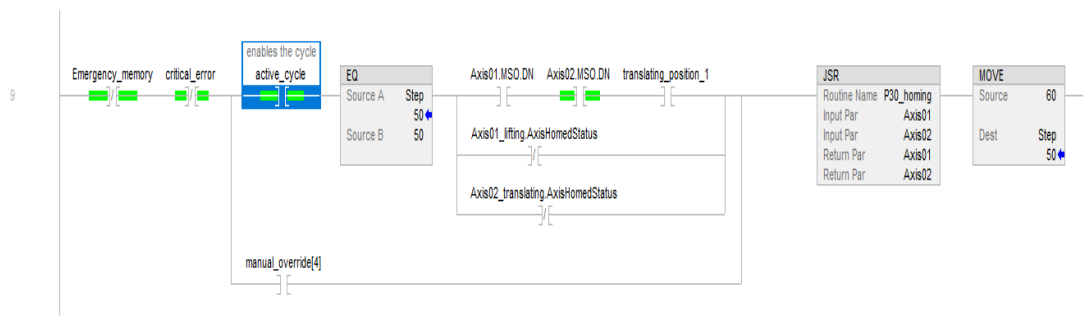


Figure 79: main routine step 50-60

P30_homing

P30_homing executes, by means of MAH commands, a return to the assigned home position of the axis. As a first step, on rung 1, a reset of MAH related bits is performed for both axes, using a FLL instruction with an empty vector. Subsequently, MAH instructions are executed according to the expected sequence: first the lifting is reversed by homing Axis01, then the machine returns at steady state position with the MAH instruction performed on Axis02 (rung 2). In case an error occurs during MAH execution, the respective .MAH.ER bit becomes true, increasing the counter at rung

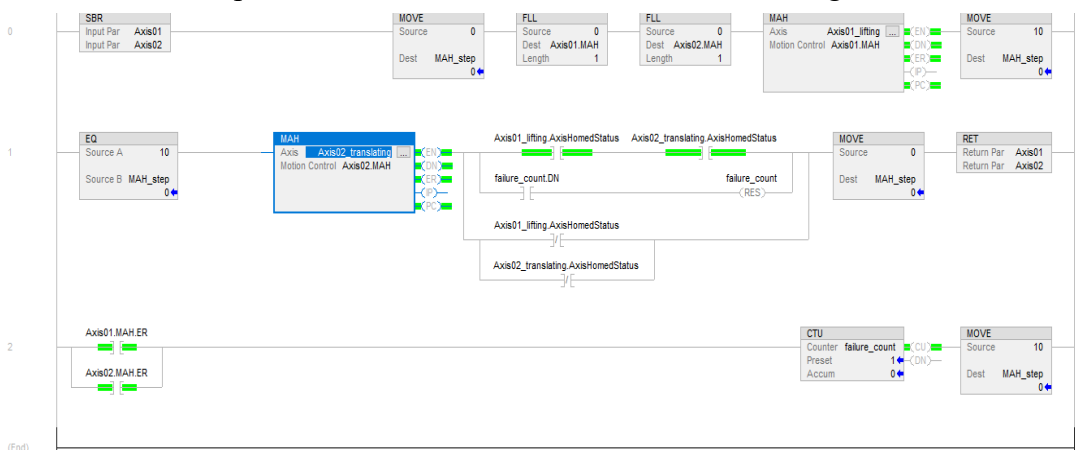


Figure 80: P30_homing

3, which forces a new attempt. The counter will be reset at the end of the new iteration in rung 2.

Main routine (step 60-0)

In rung 10, by satisfying the requirements on steady state position detection and successful completion of homing instructions, the P90_servo_off is launched.

P90 servo off

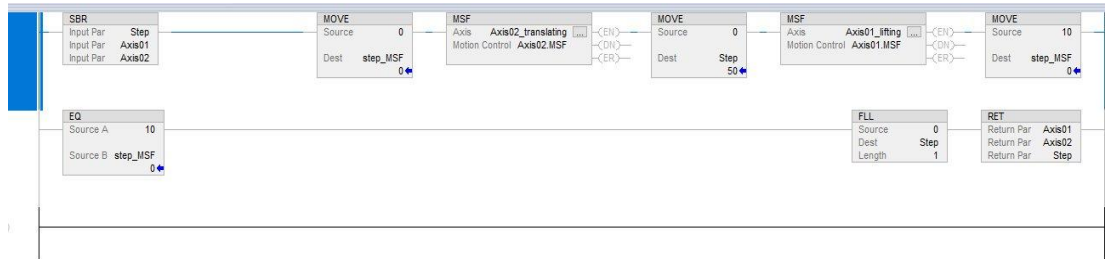


Figure 81: P90_servo_off

P90_servo_off turns off the servo motors of motion axes through the command MSF;

3.12 Results

By compiling and downloading the program on the PLC controller, it was possible, first of all, to verify that no coding or form errors were present in the program structure; then, it was checked that the variables assumed and maintained the correct values during multiple cycle iterations.

At last, the trapezoidal velocity profiles related to the two axes were extracted via software, confirming that the main goal of the PLC coding section was reached.



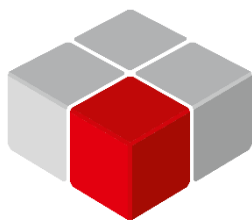
Figure 82: resulting velocity profiles from studio 5000 simulation (lifting in red and translation in green)

Chapter 4 Codesys translation and Factory I/O simulation

Being the project destined to a North American customer, it had a series of constraint related to the different norms, conventions and approaches that apply in that region. These constraints could consist, for instance, in the nominal operating frequency (60 Hz), nominal voltages and currents admissible and, for instance, adoption of typical solutions of that part of the world, such as the use of Rockwell automation hardware and software, not much diffused in Europe.

For that reason, an attempt of translation of the code explored in chapter 3 was performed, trying to maintain and use as much as possible, structure and purpose of the original code but using a German PLC software called Codesys, that was extensively used during the Master degree. Moreover, as an additional task, it was attempted to test the code on a virtual environment similar to the one of the walking beam, using Factory I/O, a simulation software that provides relatively simple industrial scenarios that could be commanded by PLC.

4.1 Codesys



CODESYS

Figure 83: Codesys logo

CODESYS (Controller Development System) is a complete software suite with an integrated developing environment (IDE) for configuring and interacting with embedded systems and PLC networks, especially in industrial fields such as manufacturing, robotics, process control.

It supports communication and compatibility with many hardware platforms, either PC-based and embedded controllers or Fieldbuses (Profibus, Modbus, CANopen); from a programming point of view, it features all the languages included in the IEC 61131-3 standard: Structured Text (ST), Ladder Diagram (LD), Function Block Diagram (GBD), Sequential Flow Chart (SFC) and many more.

The IDE integrates a complete debugging and diagnostics system, allowing: variable monitoring, online and offline debugging, breakpoint and single step execution, tracing functions to obtain a detailed overview of the general processes and timing.

In addition, thanks to the presence of visualization libraries, the user could create personalized Human Machine Interface (HMI) and Graphic User Interface (GUI) configurations for their programs.

4.2 Factory I/O

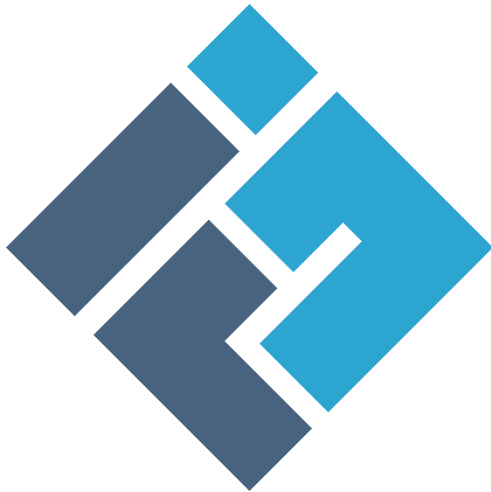


Figure 84: Factory I/O logo

Factory I/O is an automation simulation software useful for replicate, study and visualize realistic industrial systems, thanks to the wide range of components included in its libraries: roller and belt conveyors, industrial robotic arms, sensors to detect interactions and positions, actuators and buttons. All these components could be configured and integrated into PLC architectures via many communications protocols and standard, like Ethernet/IP, Modbus IP, Direct I/O.

From a graphical point of view, it provides a 3D visualization environment with realistic representation of a factory layout and it allows to accurately represent and control real life equipment and machinery without having access to it or to a real PLC network. It provides to the PLC programs feedback sensors inputs while simulating the actuators outputs in the designed operational scenarios, ensuring real time representation of the PLC script execution.

4.3 The chosen scenario

Given the knowledge acquired on the walking machine during the mechanical analysis, it was quite intuitive to notice that the machine operativity is limited to the XY plane of the chosen reference system, so it was sufficient to choose an alternative solution that would be able to grant motion along two directions, following the same pattern of the walking beam: two pseudo-vertical translations (lifting) and two horizontal translations.

The system of choice was a pick and place XYZ scenario, which includes two conveying lines with orthogonal directions and a robotic arm with 3 prismatic joints, one for each reference axis.

With regards to the lines, the main or input one consists in two adjacent and independently motorized roller conveyors, on which the pallets flow at constant velocity. A proximity sensor is located to ensure a precise count of items flowing on the main line.

The secondary one is a belt conveyor and perpendicular to the main one. It features a proximity sensor to provide feedback once the box is successfully positioned on the conveyor itself.

For what concerns the reference system of the scene, the Y axis has been chosen as parallel to the main conveyor direction, the X axis to the secondary conveyor, while the Z axis to the vertical to the floor.

The robotic arm is positioned on a four pedestals tubular structure above the conveyors, so that it can hover above them without interfering with the transported objects. It is able to move along the X, Y, Z directions, hence parallelly to both conveyors directions but also perpendicularly, along the vertical to the floor. It has a position range of 1.25 m along Y axis, 2.125m along the X axis and 0.5m along the Z axis

It is provided with a grabbing end effector, able to rotate its angular position during the transport of objects with fixed angular speed of 4.6 rad/s, and a detection feedback system, provided by a proximity sensor.

The area is controlled by means of an HMI panel including:

- Start push button: it starts the automatic cycle;
- Stop push button: it immediately stops the cycle in the current state but with the possibility to resume it;
- Reset push button (emergency): it stops the cycle and resets any variable/memory in the logic, restarting the cycle from the beginning;

- Digital display: shows the counter value from the sensor on the main conveyor;



Figure 85: The setup in Factory I/O

In an attempt of replicating the working conditions of the walking beam, a similar configuration was chosen for the whole scene, maintaining the idea of both vertical and horizontal translations performed by the machine. By pressing the start button, the boxes flow starts on the main conveyors and the robotic arm translates to a steady state position above the main conveyor and along its axis. Every three boxes detected by the sensor on the main line, the conveyor stops, the end effector lowers to reach the box and, when detected, grabs the box by means of a suction system. The end effector lifts the box by vertically translating enough to allow the flow to continue, conveyors motion starts again and the proximity sensors keeps counting. In the meanwhile, the robotic arm translates along the X axis, reaching the secondary belt conveyor. Here, after performing a rotation of the end effector, it deposits the box on the conveyor by vertically translating downwards and, after, by deactivating the grabbing tool. Once that the box is detected by a proximity sensor, the motion of the secondary conveyor starts, leaving space for the next box. In the meanwhile, the counter has counted up to three box again, stopping the flow of the main conveyor until the box is not picked up again and the cycle repeats automatically.

4.4 The I/O configuration

The Factory I/O model presents a series of possible input and output that could be selected and inserted in the I/O card of the simulation. Given the project need of having control of the robotic arm position to assure precise delivery of the parts, it was necessary to activate input registers from the configuration menu, as they allow the exchange of INT, REAL, WORD variables between different devices and/or softwares. With regards to the rest of the variables, they are all automatically considered as BOOL (Boolean) variables, hence they either assume logic value TRUE or FALSE.

From the configuration menu, the following choice of input (right-hand side) and output (left-hand side) variables was adopted:

Output Variable	Coil	Input Variable
Box at place	Coil 0	Input 0
Part at place	Coil 1	Input 1
Pick & Place 1 (Box Detected)	Coil 2	Input 2
Pick & Place 1 (C Limit)	Coil 3	Input 3
Start	Coil 4	Input 4
Reset	Coil 5	Input 5
Stop	Coil 6	Input 6
Emergency stop	Coil 7	Input 7
Auto	Coil 8	Input 8
		Input Reg 0
		Input Reg 1
		Input Reg 2
		Pick & Place 1 X Set Point (V)
		Pick & Place 1 Y Set Point(V)
		Pick & Place 1 Z Set Point (V)

Figure 86: I/O card in Factory I/O

From the output list:

- Box at place: output parameter of main conveyor sensor, the associated coil is energised when an object is detected on the main conveyor;
- Part at place: output parameter of the secondary conveyor sensor, the associated coil is energised when an object is detected on the secondary conveyor;
- Pick & Place 1 (box detected): output parameter of the robotic arm sensor, the associated coil is energised when the object is close enough to the end effector of the robotic arm;

- Pick & Place 1 (C limit): constraint on the maximum angular rotation of the end effector. It hasn't been used during the simulation as not relevant to the application;
- Start: output parameter, the associated coil is energised when generated by pressing the start push button on the HMI interface. It starts the cycle or continues a suspended one;
- Reset: output signal generated by pressing the reset push button on the HMI interface. It stops the system and resets all memories of the cycle, restoring the initial conditions;
- Stop: output signal generated by pressing the stop push button on the HMI interface. It suspends the cycle execution, that could be resumed by pressing the start button;
- Auto: output signal generated by pressing the auto selector on the HMI interface. Not used for the aim of the project, as it is a fully autonomous cycle already;

From the input list:

- Box conveyor: the signal actuates the motion of roller conveyor 1 of the main line.
- Part conveyor: the signal actuates the motion of the belt conveyor of the secondary line;
- Exit conveyor: the signal actuates the motion of roller conveyor 2 of the main line.
- Pick & Place 1 (C+): the signal actuates the rotation of the end effector;
- Pick & Place 1 (Grab): the signal activates the suction system that allows to grab the objects from the conveyors;
- Pick & Place 1 X Set Point (V): input numerical value for the position of the robotic arm along the X axis;
- Pick & Place 1 Y Set Point (V): input numerical value for the position of the robotic arm along the Y axis;
- Pick & Place 1 Y Set Point (V): input numerical value for the position of the robotic arm along the X axis;

Knowing the following configuration, the Modbus communication with Codesys could be set up.

4.5 Modbus protocol

Modbus is a serial communication protocol developed in 1979 by Modicon (a subsidiary of Schneider Electric), with the goal of realizing a communication protocol

for industrial environment. As a matter of fact, it has become a standard in industries and one of the most diffused protocols among electrical devices, thank to some of its main features, such as being very simple to use and install, open source and free. In particular, Modbus TCP/IP is widely adopted to setup PLC communication via Ethernet connections, as it allows the exchange of raw bits and words without many limitations, even among devices from different manufacturers. However, it also presents some limitations, as it was conceived in the 80s and there weren't particular needs in supporting big binary objects. Hence there isn't a standardized approach to registry representation or description, as all the registries are treated as 16-bit words, without the possibility to interpret or define them univocally: each device manufacturer usually provides documentation to properly declare registries.

This kind of difficulties were met also in the execution of this last part of the project.

4.6 I/O communication protocol configuration

In order to ensure proper dialogue between Codesys and Factory I/O, it was needed to setup the communication protocol on both softwares, ensuring that the same parametrization for the I/O cards was setup. In factory I/O, the following communication settings were configured, so that the Ethernet connection with Codesys could be established.

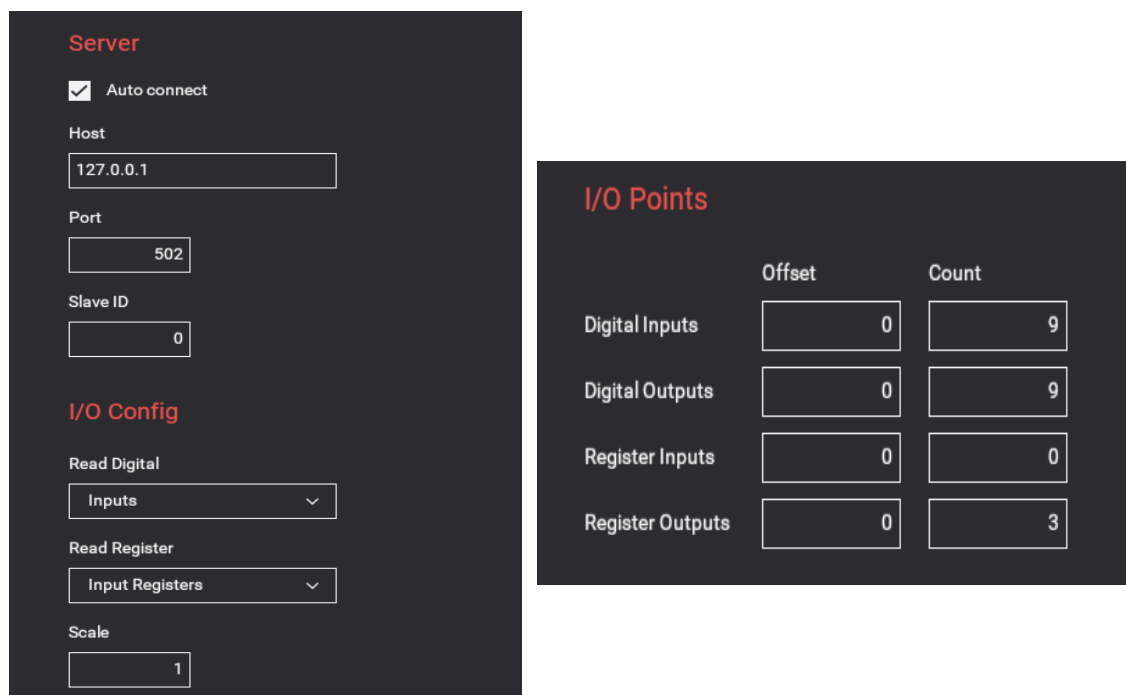


Figure 87& 88: I/O communication setup in Factory I/O

In Codesys, it was necessary to setup a communication device first: among the various communication systems available, the Ethernet/IP protocol was selected and the ModbusTCP_Slave_Device was chosen.

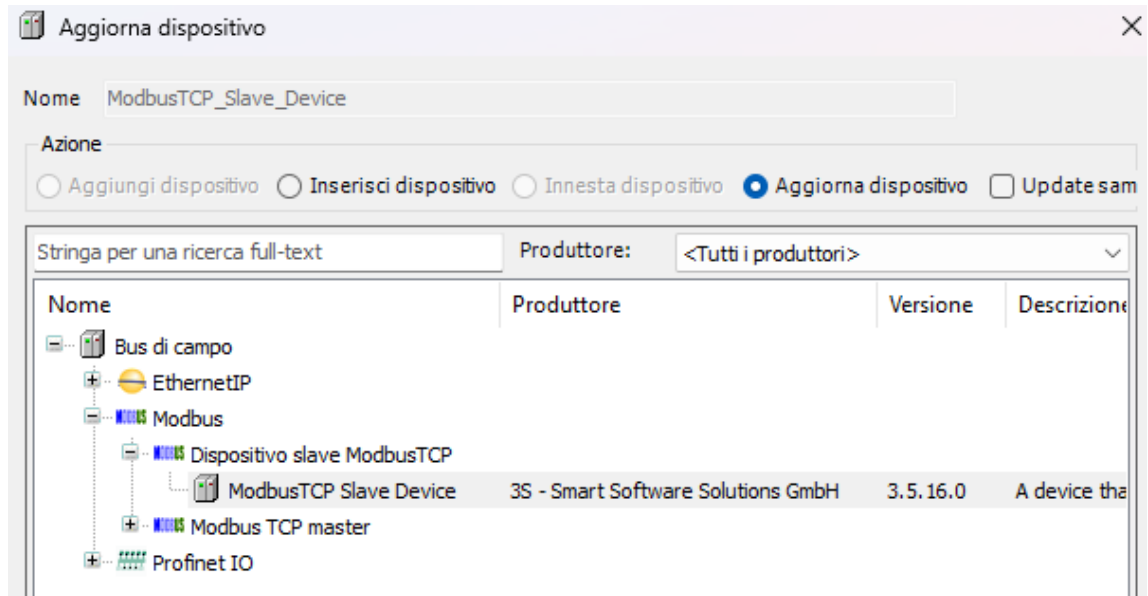


Figure 89: communication device setup in Codesys

Subsequently, the I/O module was setup, ensuring that the device had enough I/O slots and registers to correctly receive and send signals to the Factory I/O model.

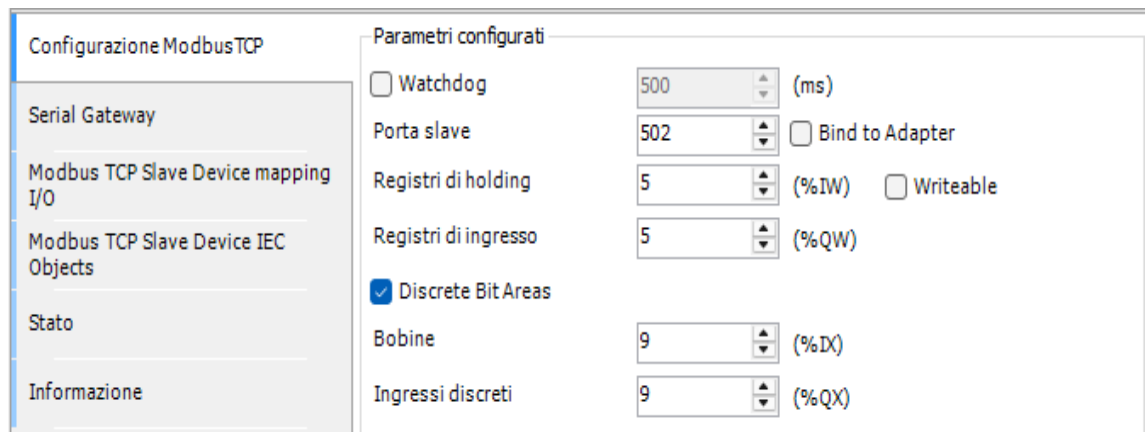


Figure 90: I/O card setup in Codesys

At last, the PLC connection is established by the “start PLC” command via Codesys Control Win V3 SysTray, a Codesys sub-application that consent to virtually replicate a physical PLC controller and allow communication in between devices. Hence, the following network is configured and enabled:

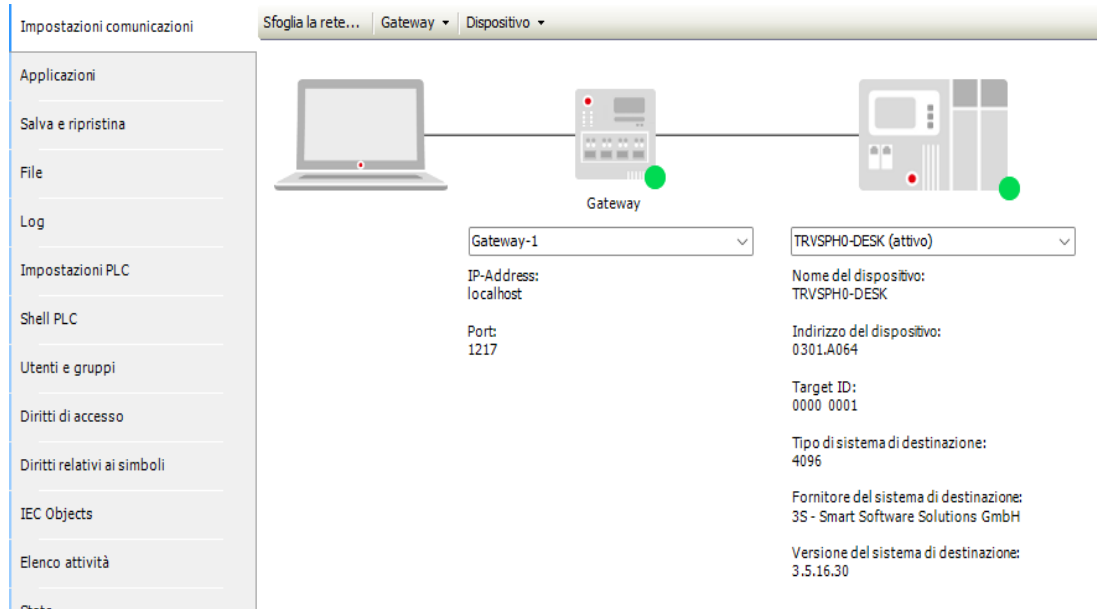


Figure 91: device communication setup in Codesys

4.7 Software development in Codesys

The next step would consist in programming the scenario in Codesys environment, translating as much as possible the routine that was developed in Studio 5000 but simplifying and adapting it to the new system.

Variabile	Canale	Indirizzo	Tipo
ModbusTCP_Slave_Device			
Registri di holding		%IW0	ARRAY [0..4] OF WORD
Registri di holding[0]		%IW0	WORD
Registri di holding[1]		%IW1	WORD
Registri di holding[2]		%IW2	WORD
Registri di holding[3]		%IW3	WORD
Registri di holding[4]		%IW4	WORD
Registri di ingresso		%QW0	ARRAY [0..4] OF WORD
Registri di ingresso[0]		%QW0	WORD
Registri di ingresso[1]		%QW1	WORD
Registri di ingresso[2]		%QW2	WORD
Registri di ingresso[3]		%QW3	WORD
Registri di ingresso[4]		%QW4	WORD
Bobine		%IB10	ARRAY [0..1] OF BYTE
Bobine[0]		%IB10	BYTE
Bobine[1]		%IB11	BYTE
Ingressi discreti		%QB10	ARRAY [0..1] OF BYTE
Ingressi discreti[0]		%QB10	BYTE
Ingressi discreti[1]		%QB11	BYTE

Figure 92: I/O parameters in Codesys

Similarly to Studio 5000, where variables could be directly created and imported by the user, in Codesys the variables that will be used in the main routine must be declared, otherwise it won't be possible for the software to recognize and use them during the program execution. In particular, it was necessary to define the variables based on their address bit location on the I/O card. Remembering the device I/O configuration that was imposed before, we recall that the symbol %IBxx identifies the input bytes, each one formed by 8 bits %IBxx.n , with n=[0,...,7]; similarly, symbol %QB identifies the output bytes, each one formed by 8 bits %QBxx.n , with n=[0,...,7], while %QWxx identifies words, each one made of 16 bits %QWxx.n, with n=[0,...,15]. To ensure the exact correspondence between variables in Factory I/O and Codesys, it is necessary to assign the bit addresses following the same order shown in Factory I/O communication card, otherwise the input and output parameter would be mixed up. The I/O variables are declared as follow in the variable declaration section of the program:

```

VAR
I0 AT %IX10.0:BOOL; // BOX AT PLACE
I1 AT %IX10.1:BOOL; // PART AT PLACE
I2 AT %IX10.2:BOOL; // DETECTED
I3 AT %IX10.3:BOOL; // C LIMIT
I4 AT %IX10.4:BOOL; // START
I5 AT %IX10.5:BOOL; // RESET
I6 AT %IX10.6:BOOL; // STOP
I7 AT %IX10.7:BOOL; // EMERGENCY
I8 AT %IX11.0:BOOL; // AUTO

Q0 AT %QX10.0:BOOL; // box CONVEYOR
Q1 AT %QX10.1:BOOL; // GLASS CONVEYOR
Q2 AT %QX10.2:BOOL; // EXIT CONVEYOR
Q3 AT %QX10.3:BOOL; // C+
Q4 AT %QX10.4:BOOL; // GRAB
Q5 AT %QX10.5:BOOL; // Exit conveyor
PVX AT %QW0:INT:=5; //pick and place 1 set point x
PVY AT %QW1:INT:=5; //pick and place 1 set point y
PVZ AT %QW2:INT:=0; //pick and place 1 set point z

```

Figure 93: I/O variables declaration in the main program

4.7.1 The batch method

As one might recall, the structure of the main routine in studio 5000 was dictated by the presence of multiple step equality checks that ensured the correct and ordered execution of required actions and subroutines.

Given the difference in libraries and functions available in the two softwares, a simpler and alternative approach to the step method could consist in the so called “batch method”.

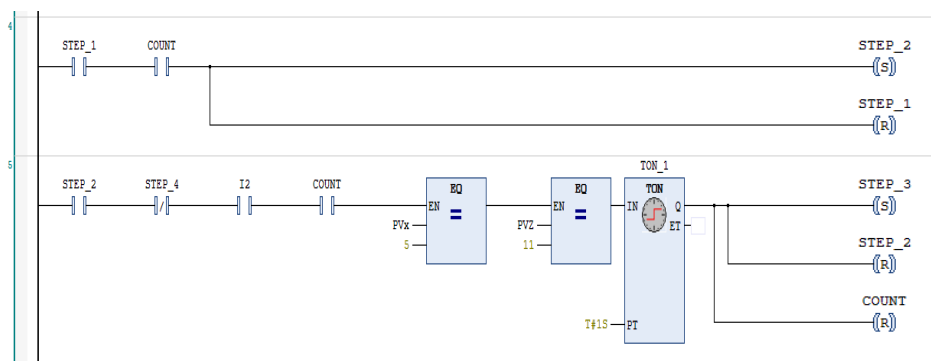


Figure 94: batch method example

The “batch method” allows the simplification and correct execution of complex cycles by means of memories, either physical or virtual ones. At first, the cycle is divided into steps, based on the satisfaction of certain requirements, usually input variables from sensors feedbacks or variables related to the execution of previous steps; to each step, a set-reset memory is associated: upon execution of a step, the associated memory is set as “TRUE”, while the memory associated to the previous step is reset as “FALSE”.

Setting a step memory as true, activates the corresponding output rung, which allows the execution of the action associated to the step itself.

4.8 The program structure

Taking into account the I/O parameters available in the environment, a 9 steps program was developed using the batch method.

Step 1

At rung 1, two parallel initial conditions were imposed so that two possible scenarios could be considered: the start of the automatic cycle and the automatic iteration of multiple cycles.

The start of the automatic cycle is simply caused by the press of the start button, which sets as "TRUE" the normally open contact I4, associated to the input bit %IX10.4.

Alternatively, if STEP_9="TRUE" and the value of parameter PVX=5, after 3 seconds set STEP_1 as true and resets STEP_9, preventing the existence of possible blocking signals.

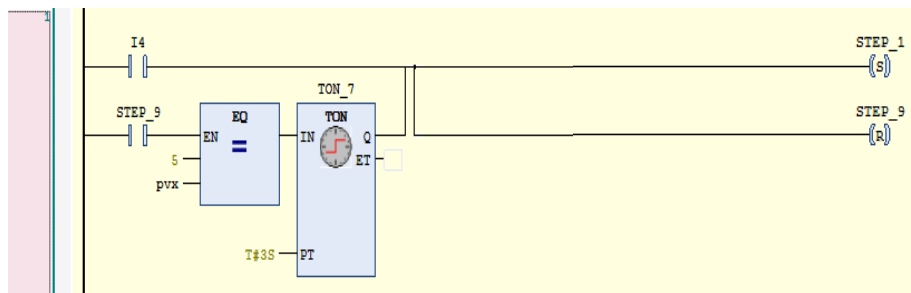


Figure 95: start of cycle or step 9 effect

In rung 2, the COUNT variable is related to the counter function CTU_0 in rung 2: every time that the series of contact Q0 (main conveyor 1 in motion) and I0 (box detected by the proximity sensor on the main line) transitions to a TRUE value, the counter value increases of 1 unit. When it reaches the value 3, the memory COUNT is energised and set to TRUE. The counter value is reset either when the reset button is pressed (I5=TRUE) or Step 4 is reached (STEP_4=TRUE) but the value of COUNT remains unaffected.

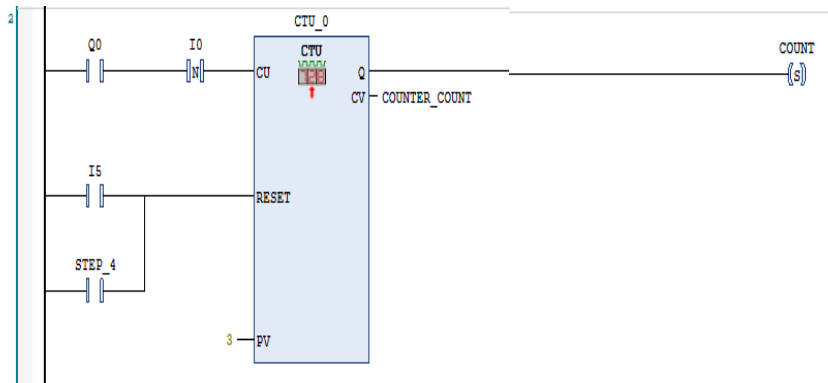


Figure 96: counter CTU_0

If COUNT=TRUE, memories Q0 ,Q1 and Q5 are reset, stopping the roller and belt conveyors; this action could be also performed by pressing the stop button (I6). (rung 12)

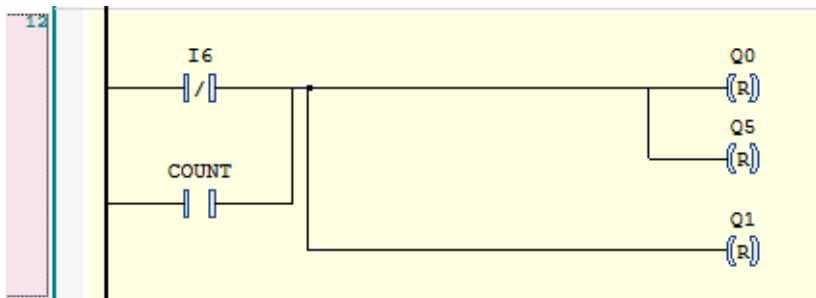


Figure 97: Counter effect

Step 2

At rung 3,the contemporary presence of STEP_1 and COUNT allow to set memory STEP_2 and reset STEP_1, moving to the execution of rung 14: upon the execution of grab by the robotic arm (Q4=FALSE) and PVZ=0, the end effector of the robotic arm is lowered along the z-axis, at set point position PVZ=11 (grabbing position);

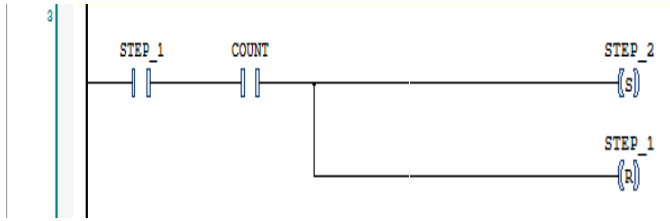


Figure 98: from step 1 to step 2

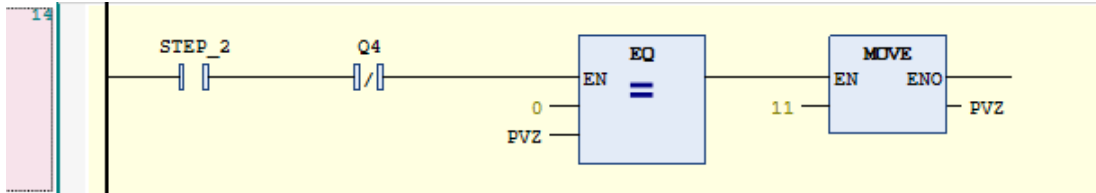


Figure 99: step 2 effect

At rung 11, if the start push button is pressed (start of a new cycle) or when step 4 is reached, the memories Q0 (conveyor 1 main line) and Q5 are set to TRUE (conveyor 2 main line), setting both conveyor in motion and resuming the flow of components.

Step 3

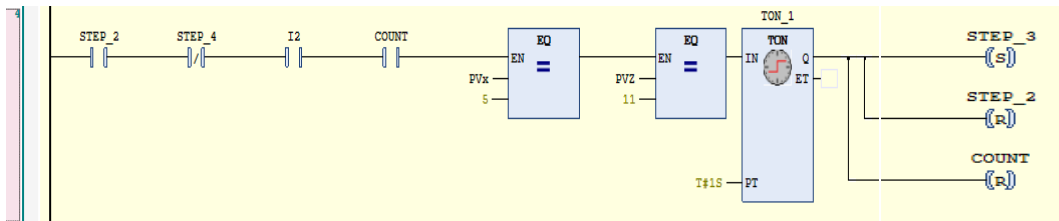


Figure 100: from step 2 to step 3

At rung 4, when step 2 is reached, the robotic arm is in position PVX=5 and the end effector is lowered to position PVZ=11, if the component is detected by the proximity sensor of the end effector itself (I2=TRUE), the delay on timer TON_1 sets STEP_3 memory and resets STEP_2 and COUNT ones after 3 seconds of delay.

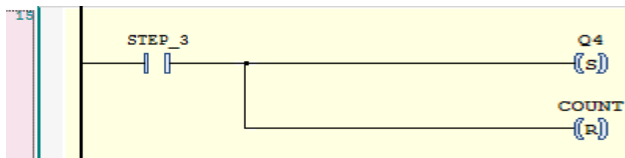


Figure 101: step 3 effect

By setting STEP_3=TRUE, via rung 15, the grabbing suction tool is enabled (Q4=TRUE) and the COUNT memory is reset;

Step 4

Once both STEP_3 and Q4 are “TRUE”, after a delay of 3 seconds, STEP_4 is set and STEP_3 is reset: at rung 16, PVZ value is changed to 3, causing the lift of the component from the main line by means of the robotic arm.

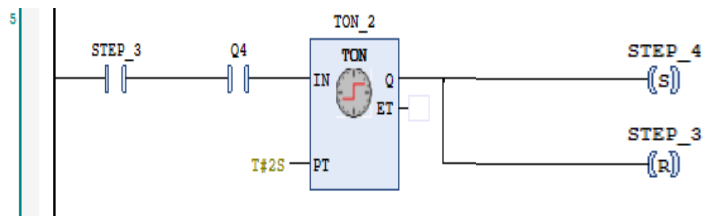


Figure 102: from step 3 to step 4

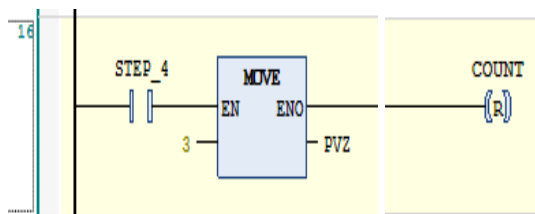


Figure 103: step 4 effect

At rung 2, the counter CTU_0 is reset to 0 while at rung 11 main conveyors 1 and 2 are set back in motion.

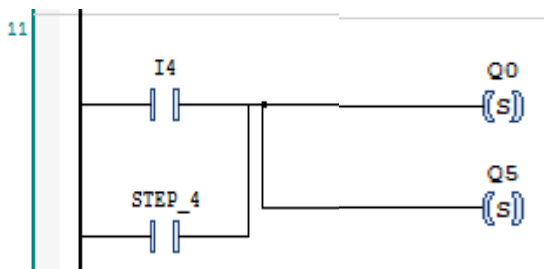


Figure 104: conveyor motion set

Step 5

Once that the position PVZ=3 is verified and STEP_4 is still TRUE, STEP_5 is set and STEP_4 is reset at rung 6;

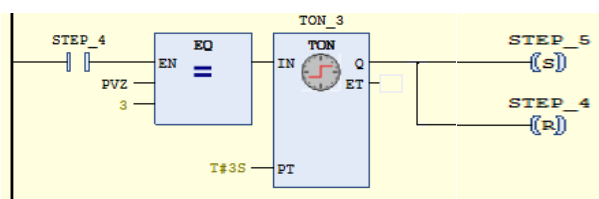


Figure 105: from step 4 to step 5

Setting STEP_5 true moves the value of PVX to 10, meaning a translation of the robotic arm to the maximum position achievable along the X axis. (Rung 17)

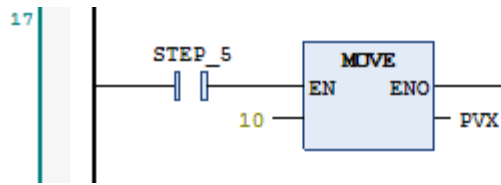


Figure 106: step 5 effect

Step 6

Once that both STEP_5 and PVX=10 are TRUE, memory STEP_6 is set and STEP_5 is reset with 3 seconds of delay (rung 7).

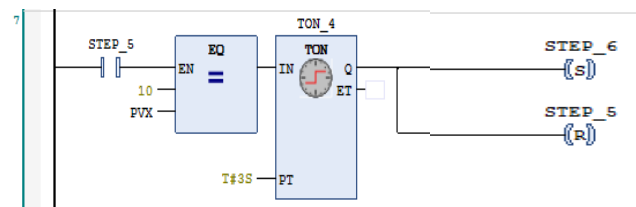


Figure 107: from step 5 to step 6

At rung 18, the rotation of the end effector is activated (Q3=TRUE).



Figure 108: step 6 effect

Step 7

Once that both STEP_6 and Q3 are TRUE, memory STEP_7 is set and STEP_6 is reset with 3 seconds of delay (rung 8).

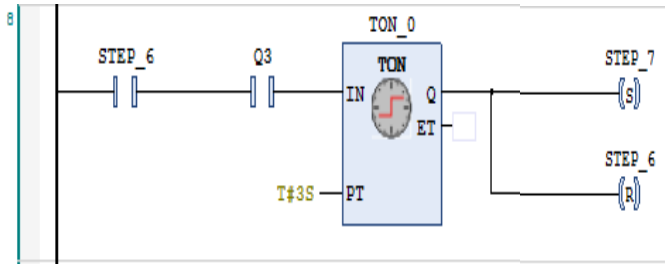


Figure 109: from step 6 to step 7

At rung 19, the grabbing system of the end effector is turned off by resetting memory Q4.

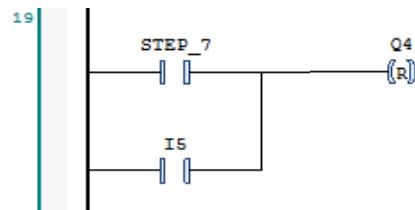


Figure 110: step 7 effect

Step 8

Once that STEP_7 is TRUE and Q4 is reset, memory STEP_8 is set and STEP_7 is reset with 3 seconds of delay (rung 9).

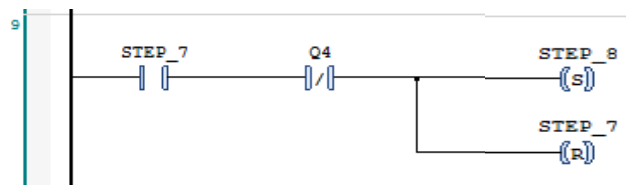


Figure 111: from step 7 to step 8

At rung 20, the vertical position PVZ of the end effector is set to zero, hence the steady state positioning along z-axis, while COUNT is reset and the secondary conveyor is set in motion (Q1 set).

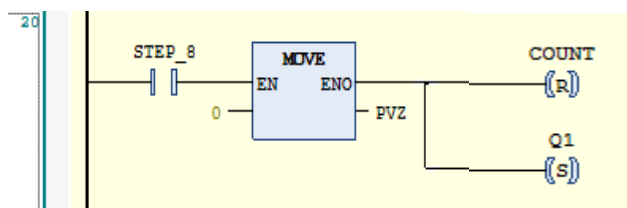


Figure 112: step 8 effect

Step 9

Once that STEP_8 is TRUE and PVZ=0 is verified, memory STEP_9 is set and STEP_8 is reset with 3 seconds of delay (rung 9).

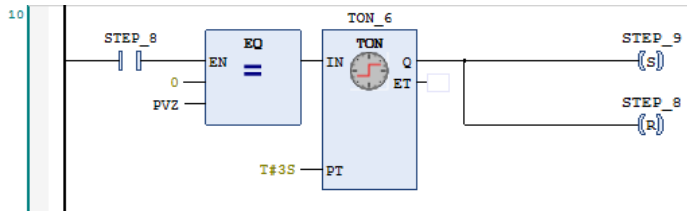


Figure 113: from step 8 to step 9

At rung 21, PVX is set to 5, which is the steady state positioning for the robot arm along x axis. Once that PVX=5 is verified, at rung 1 STEP_1 is set and STEP_9 is reset, allowing the automatic restart of the cycle.

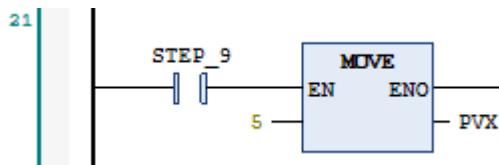


Figure 114: step 9 effect

Reset/emergency

If the reset button is pressed (I5=TRUE), all the steps, conveyors and counter memories are immediately reset, preventing the robotic arm and the conveyors to move any further and allowing a fresh start of a cycle (rung 24).

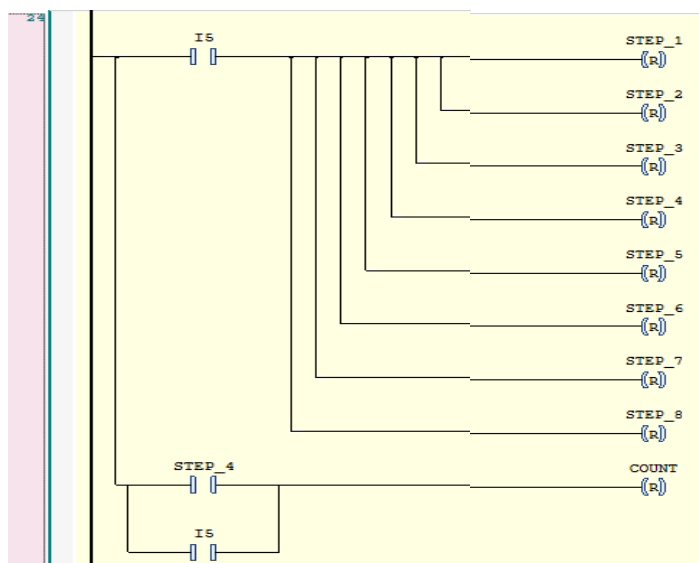


Figure 115: reset/emergency effect

Moreover, the position vectors PVX,PVY and PVZ for the end effector of the robotic arm are set on the steady state positions (rung 13).

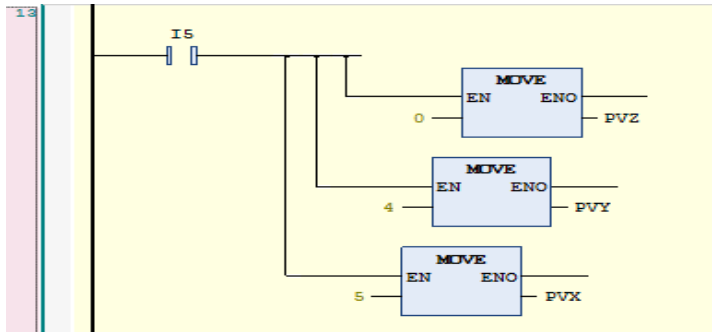


Figure 116: position reset

STOP

If the stop button is pressed, all the conveyors are stopped. (rung 12)

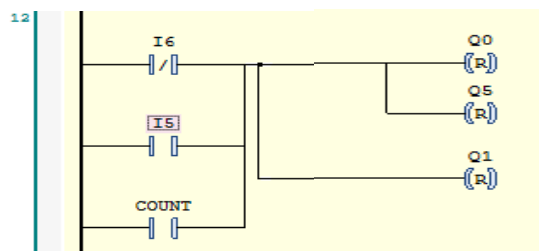


Figure 117: STOP procedure rung

4.9 Results

By running the PLC program, a perfectly functioning 3D simulation was obtained, following the original expectations. Besides obtaining a very realistic and immersive industrial model, it was verified the efficacy of the code and that the batch method represents a very good replacement for the step method employed in Studio 5000. However, the absence of specific kinematic control libraries in Codesys and of kinematic control features in Factory I/O forced to limit the simulation to a trajectory planning experiment, rather than a complete analysis as conducted on Rockwell Automation environment. Hence the use of Factory I/O might be limited to a basic industrial 3D simulator for rather simple programs with basic control problems, rather than a precise and complex plant simulator.

Conclusions

The walking beam transfer machine has proved to be an exceptional machine, able to deliver a complete cycle in less than 15 seconds, and widely satisfying all the safety requirements, without showing any critical issue from a mechanical point of view.

All the components analysed show the ability to withstand seamlessly the amount of the typical loads of a single cycle and could also be used for heavier and more demanding applications, although both motors should be updated as they are sufficiently sized for the current case.

With regards to the PLC integration, being the onboard instruments from Rockwell automation, Studio 5000 offers the best compatibility in terms of integration and implementation of features, especially in the motion control, thanks to the Kinematix Motion libraries. In fact, it allows to define precisely the velocities profiles, accelerations and have control of many other aspects related to motion and the cycle in general. The extracted cycle times and velocity profiles from simulation are respected, as expected.

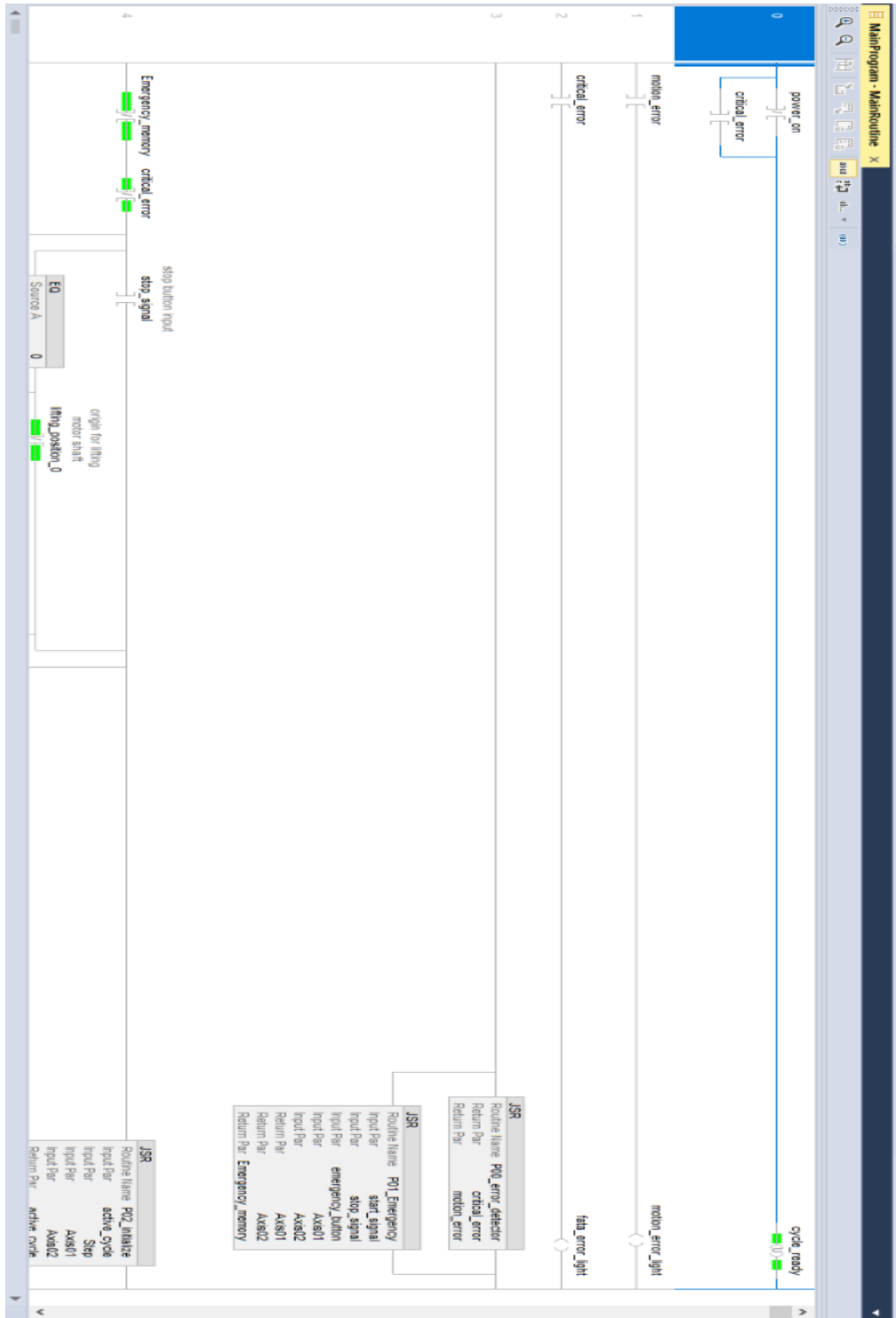
The Codesys implementation of the code was simplified as it would have required the integration of more libraries or custom solutions to integrate the motion features provided by Rockwell: this is mainly due to the absence of unification, hence different manufacturer implement their technology in different ways, that might differ slightly or, at times, completely. As expected, this experiment shows the beauty behind the challenging complexity of the PLC world, as it stimulates creativity, curiosity and pushes to a possibly never-ending learning path.

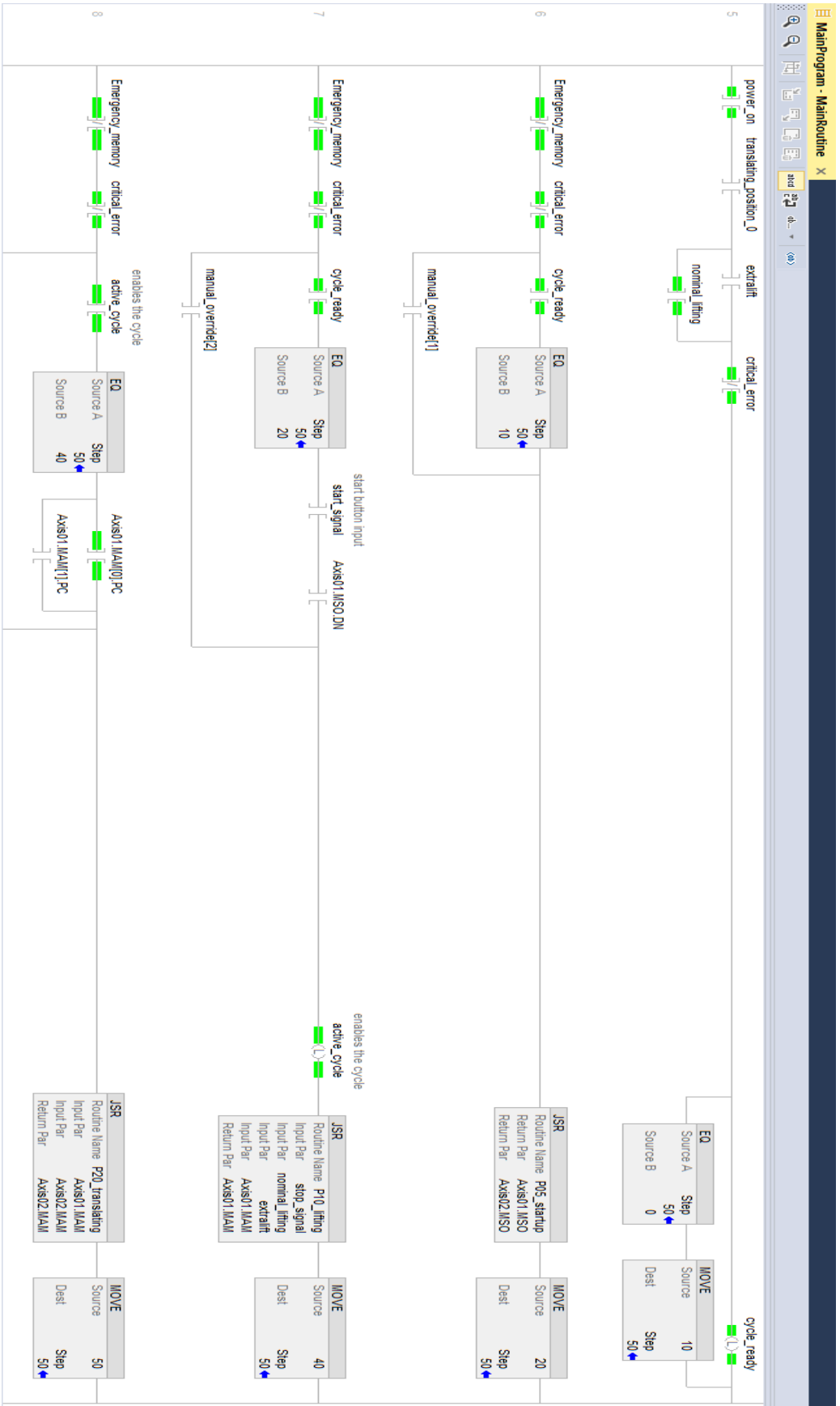
The Factory I/O simulation was very educational, as it allowed the setup of a completely virtual PLC network environment and learning how to properly use I/O cards with newly explored protocols. Moreover, since the walking beam machine had not been assembled yet at the time of the end of the project, it represented an opportunity to test and visualize the efficacy and efficiency of the PLC program in a virtual environment, even though with some limitations.

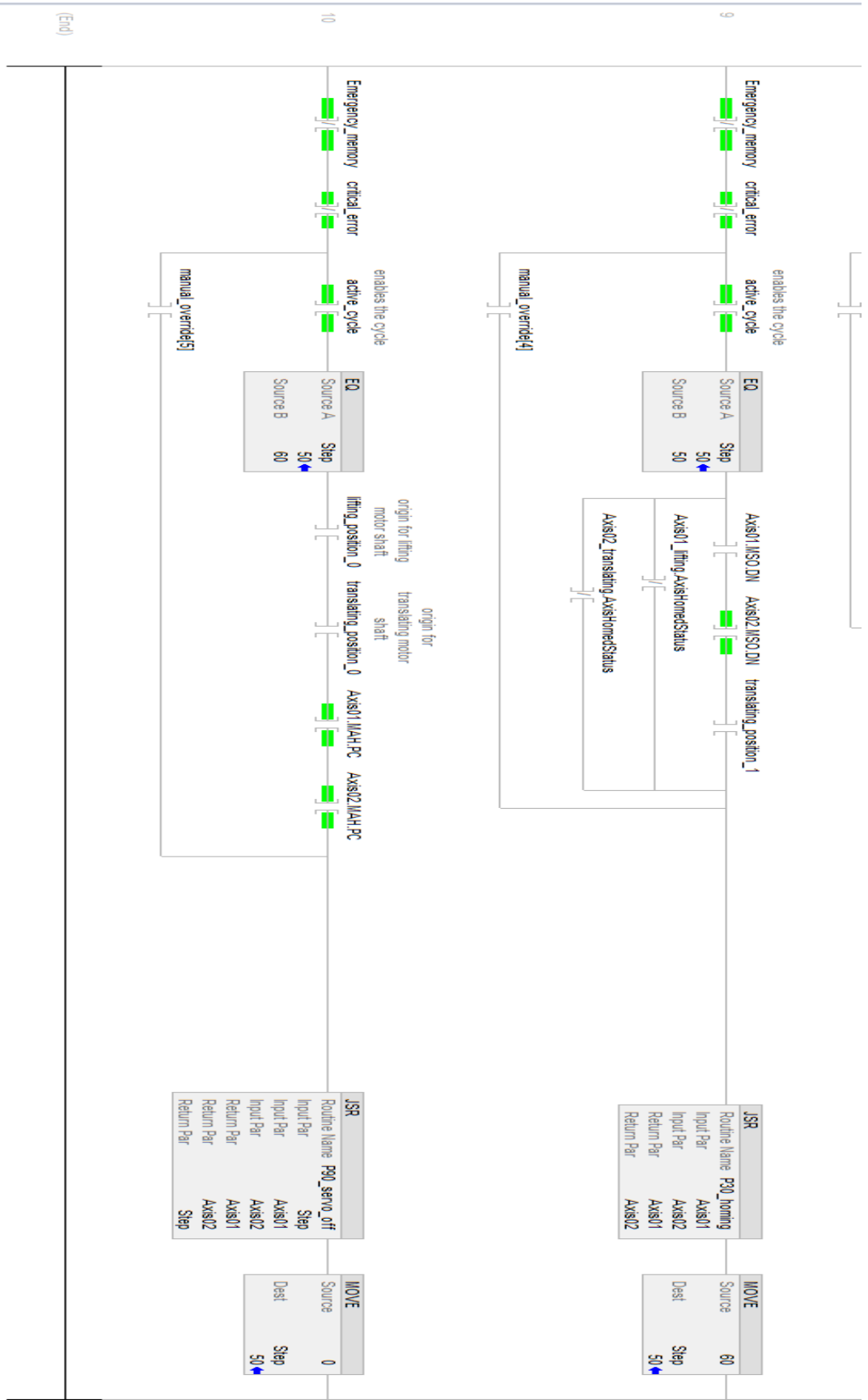
To conclude, this Master Thesis project has been a challenging and stimulating experience that allowed me to put into practice the knowledge acquired during both my Bachelor and Master degree at Politecnico di Torino and represented a personal first step in the world outside as an engineer.

Appendix A

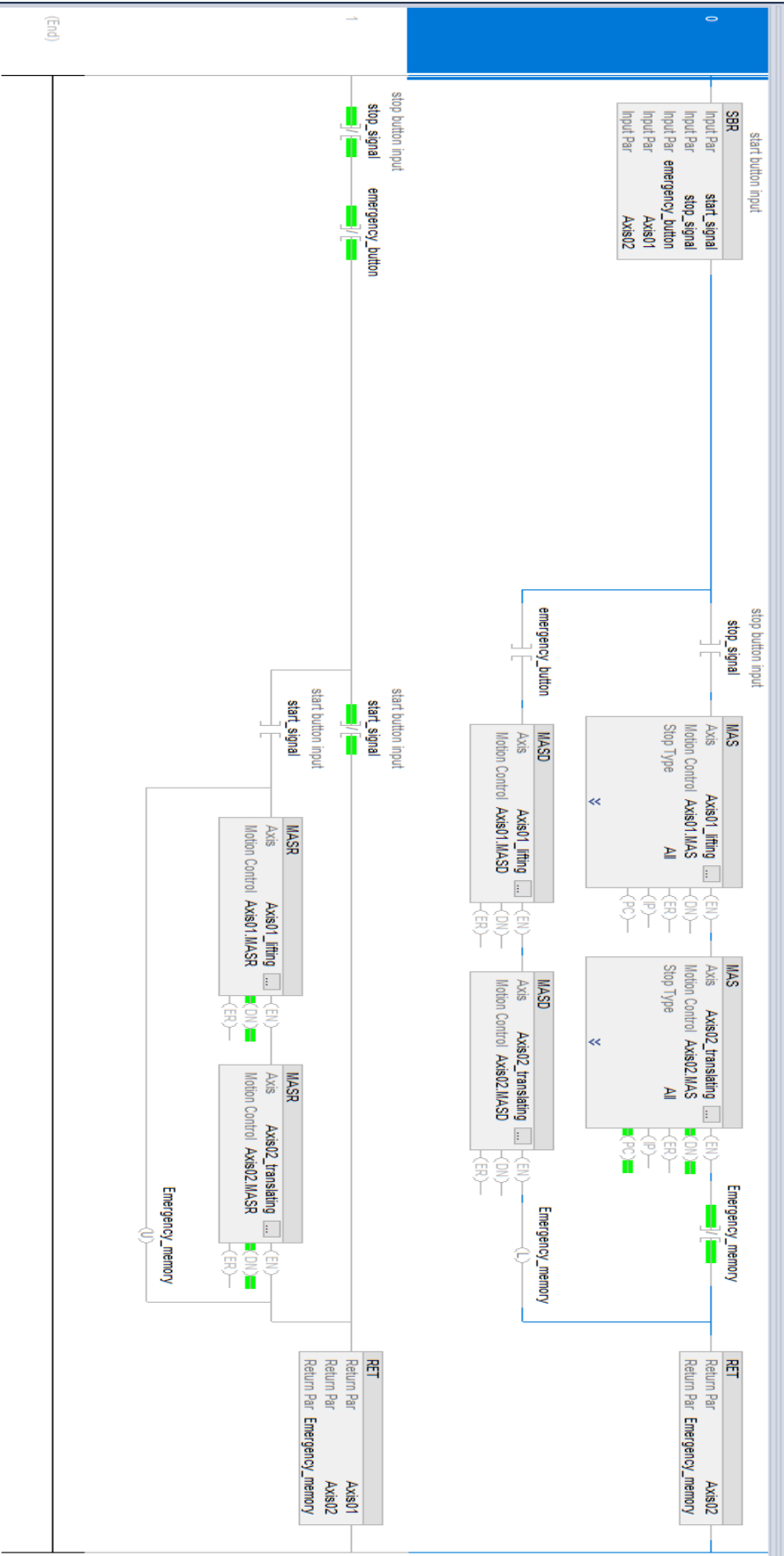
Studio 5000 code



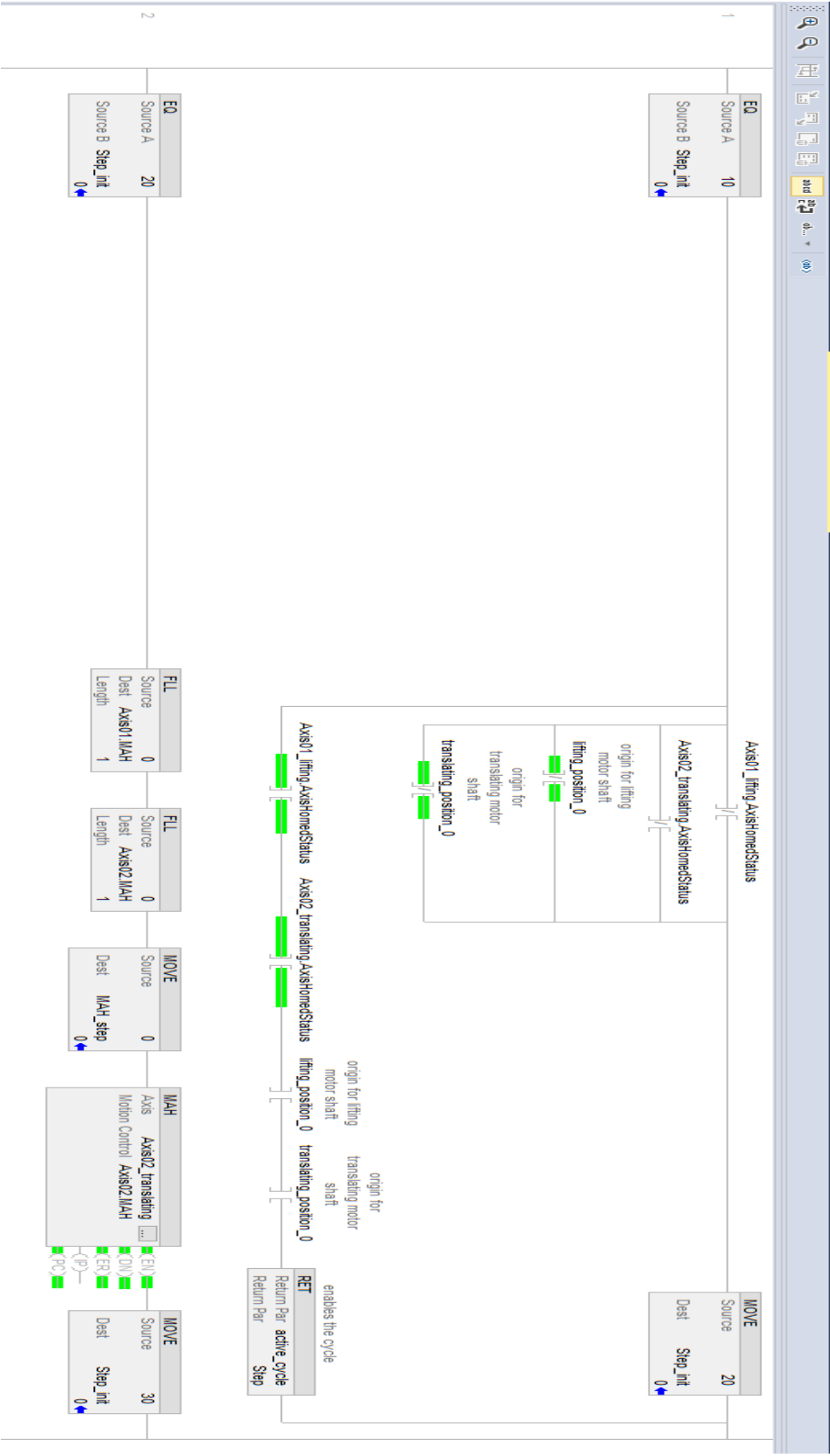


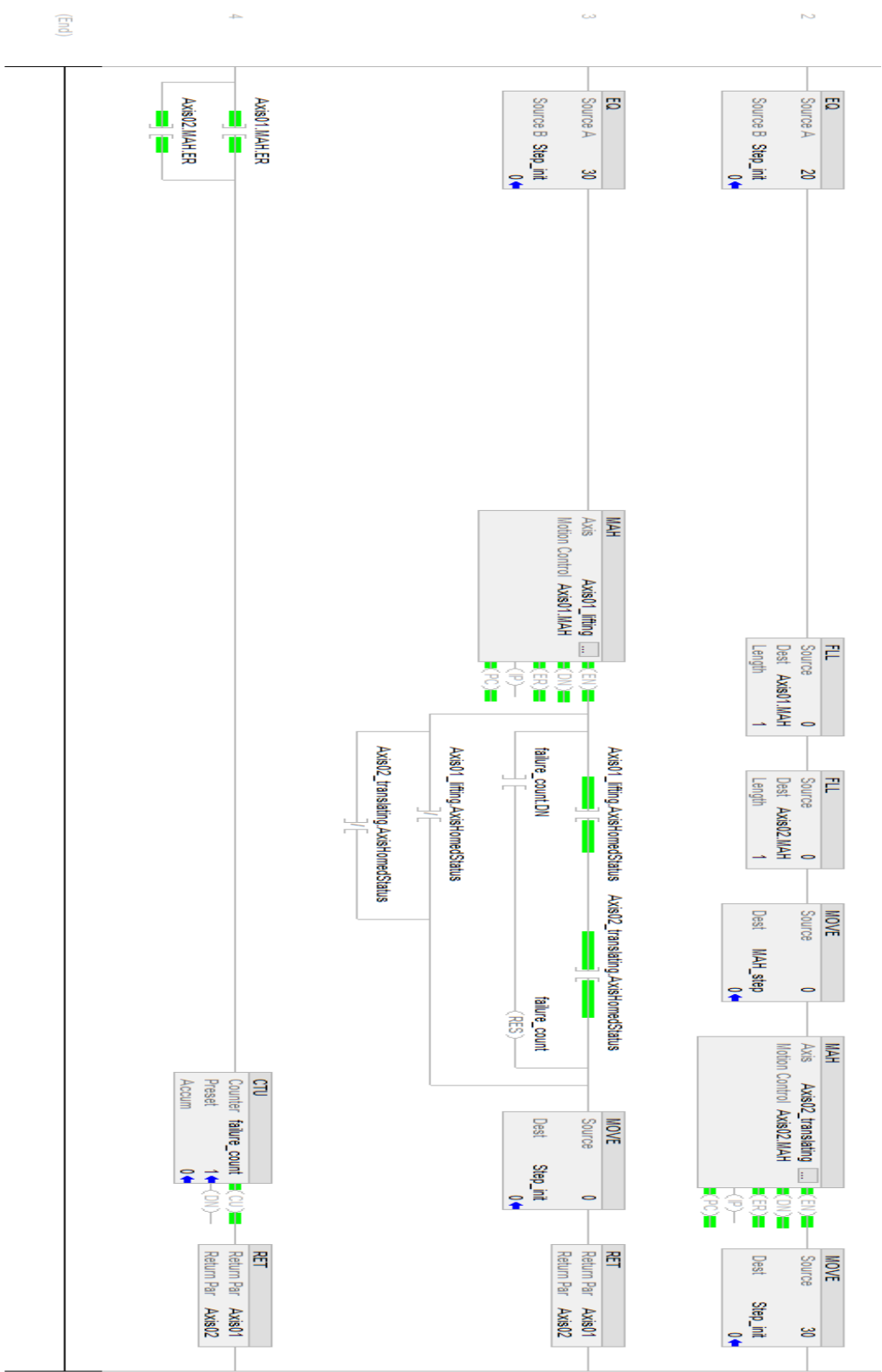


(End)

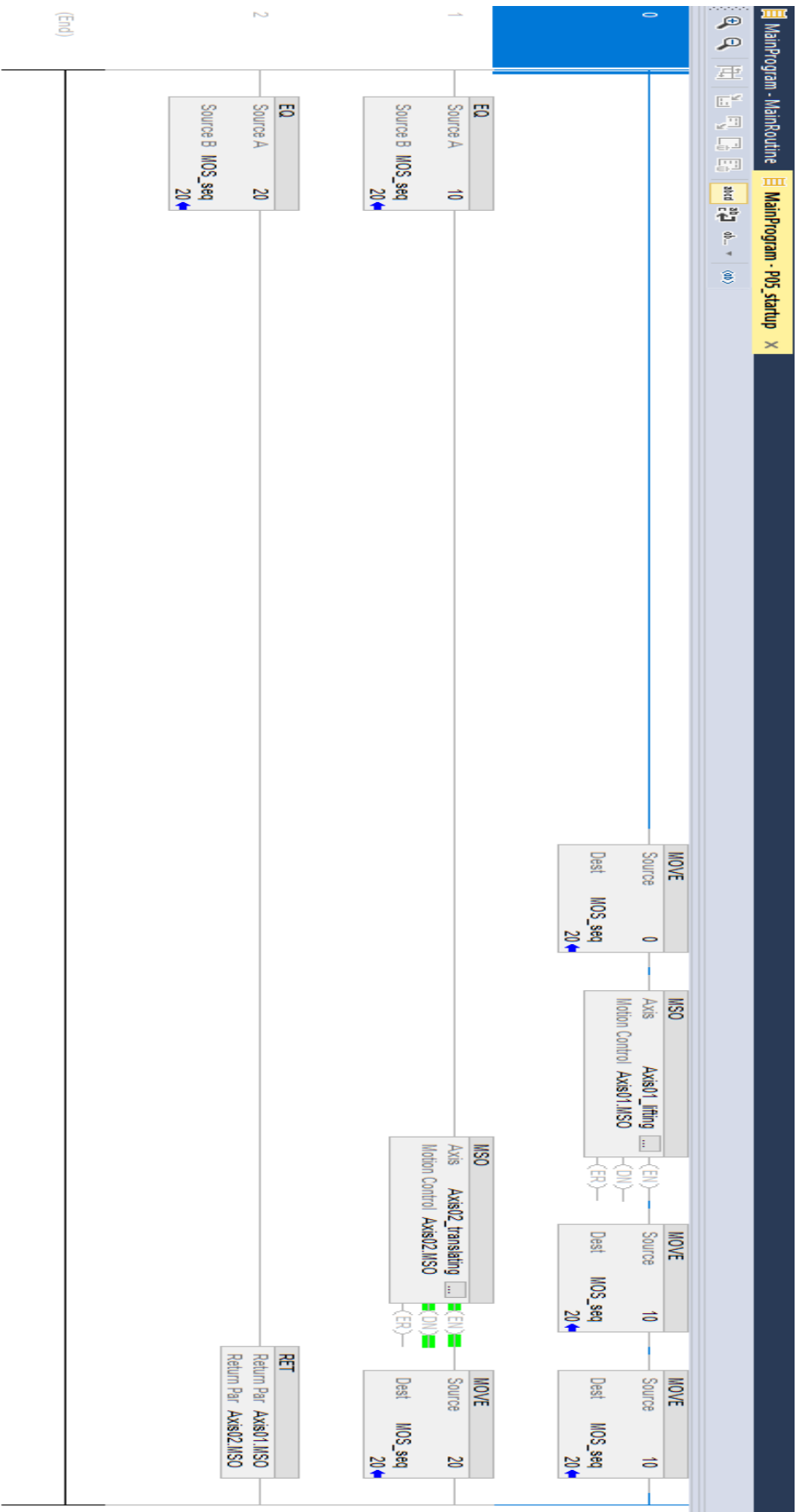


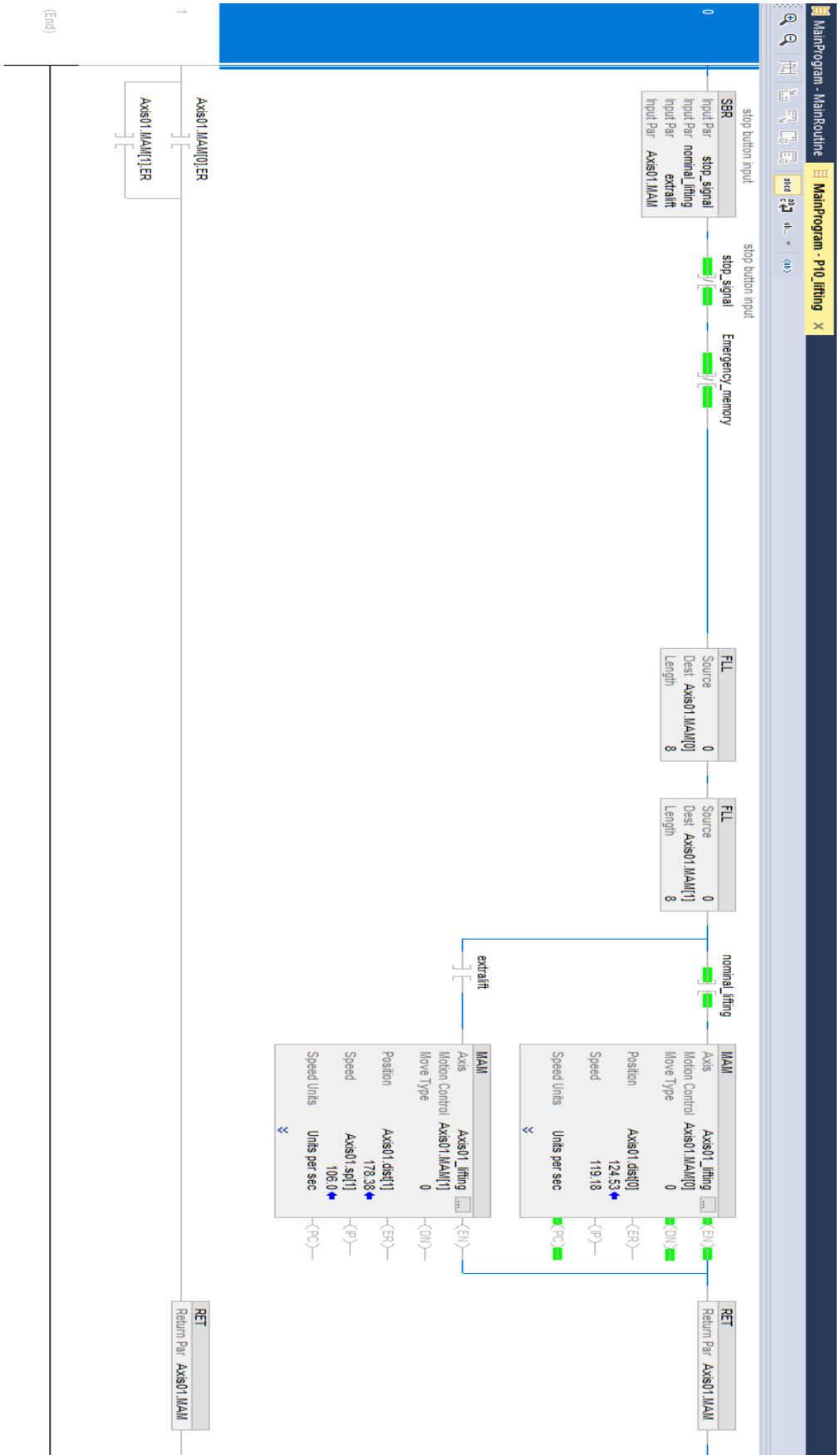
(End)

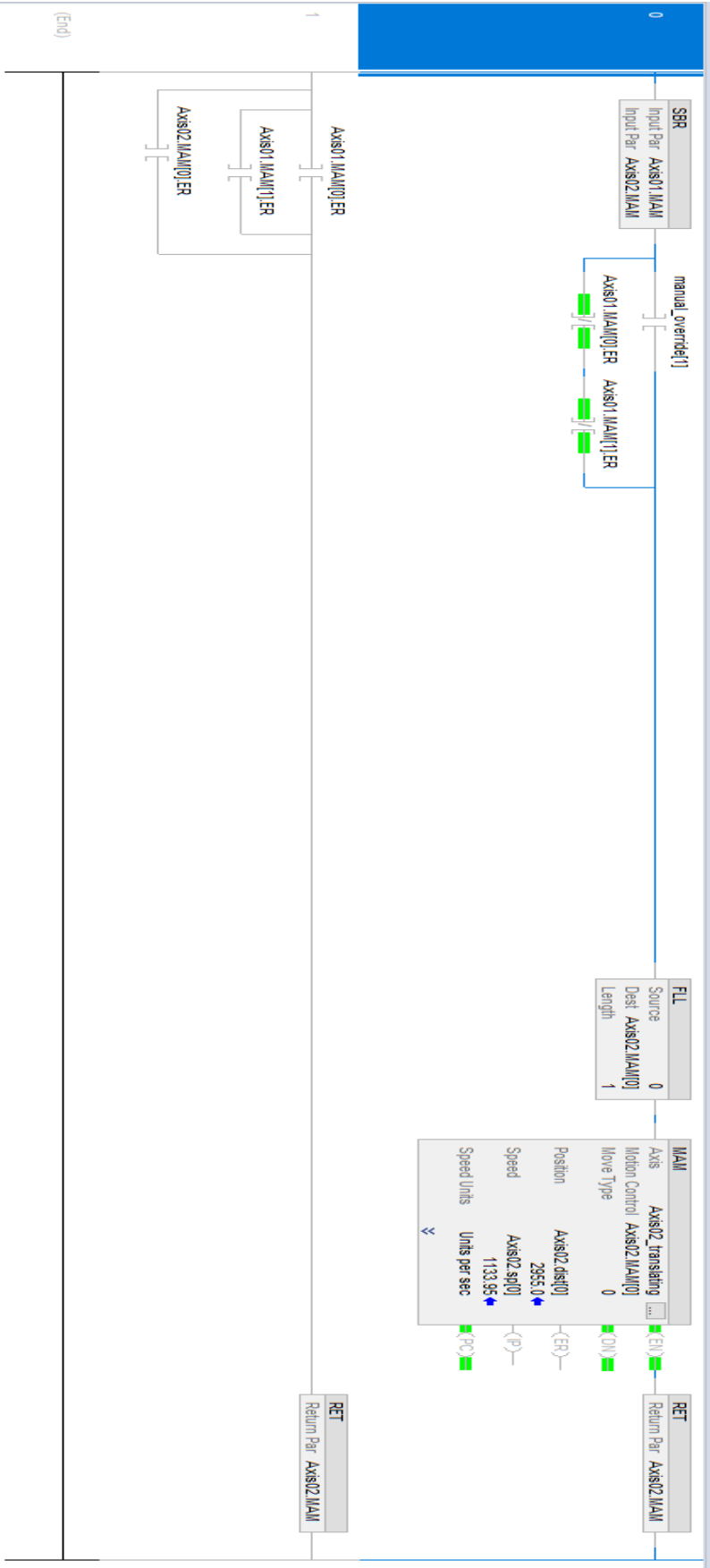


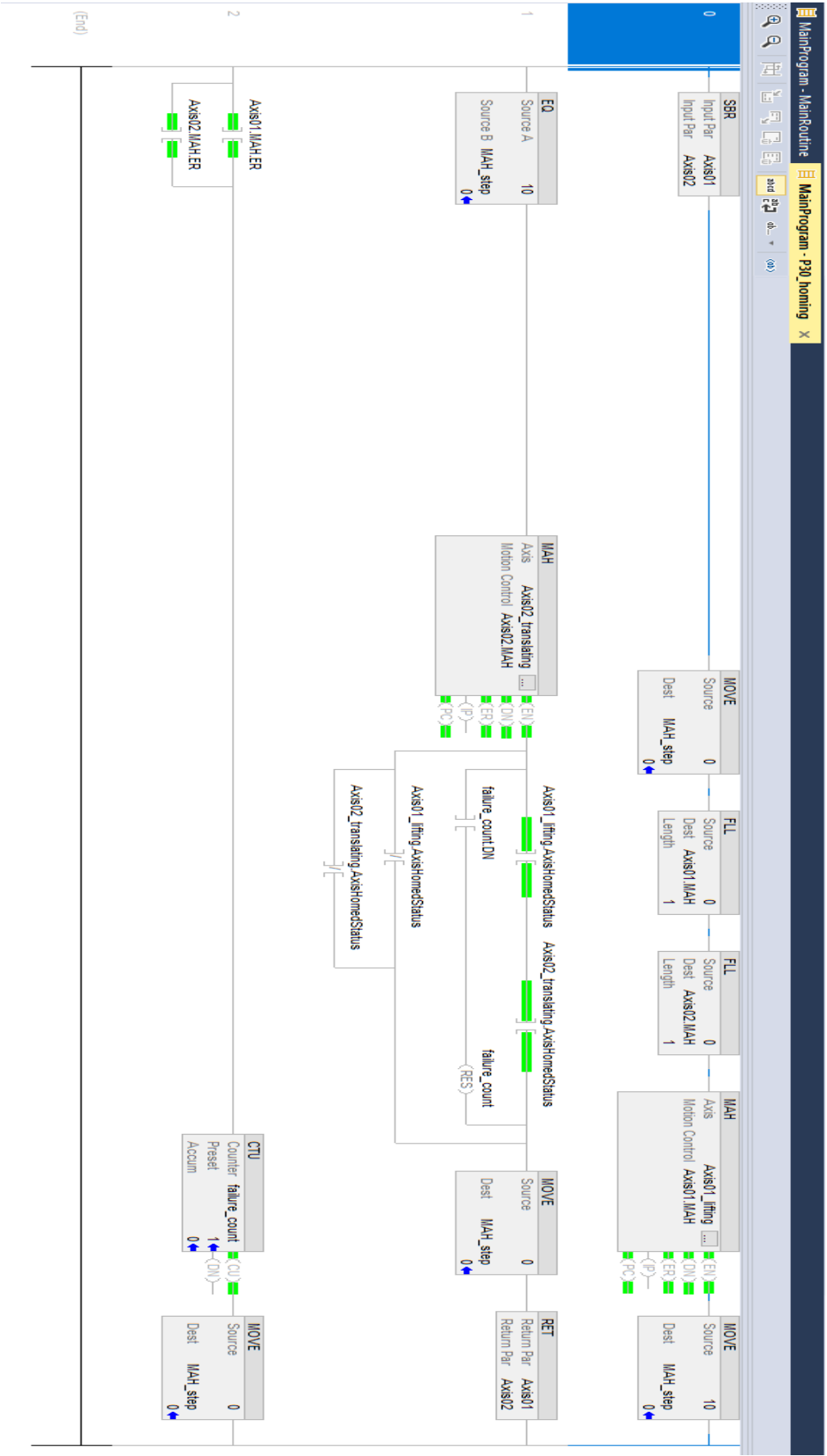


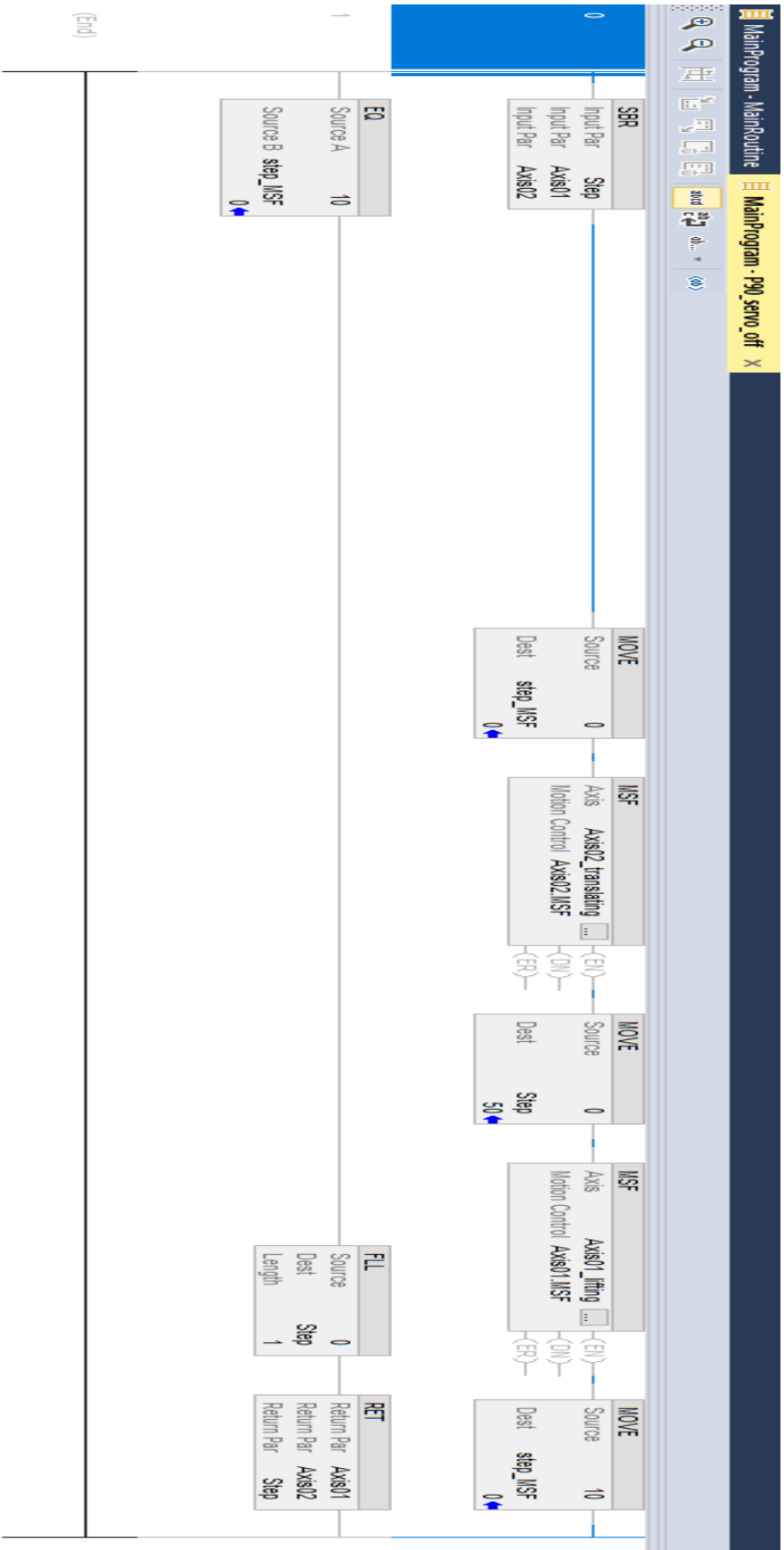
(C10)







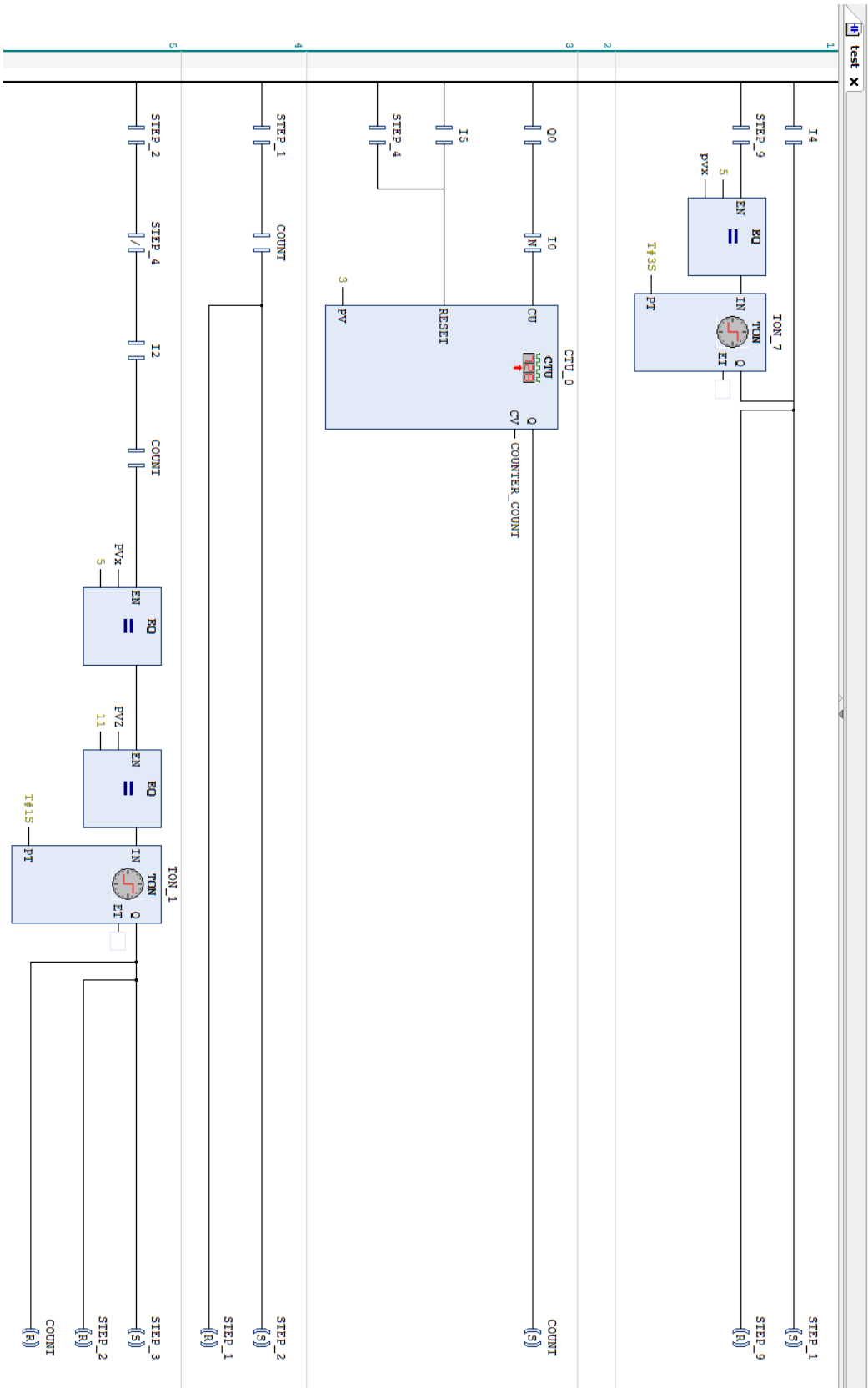


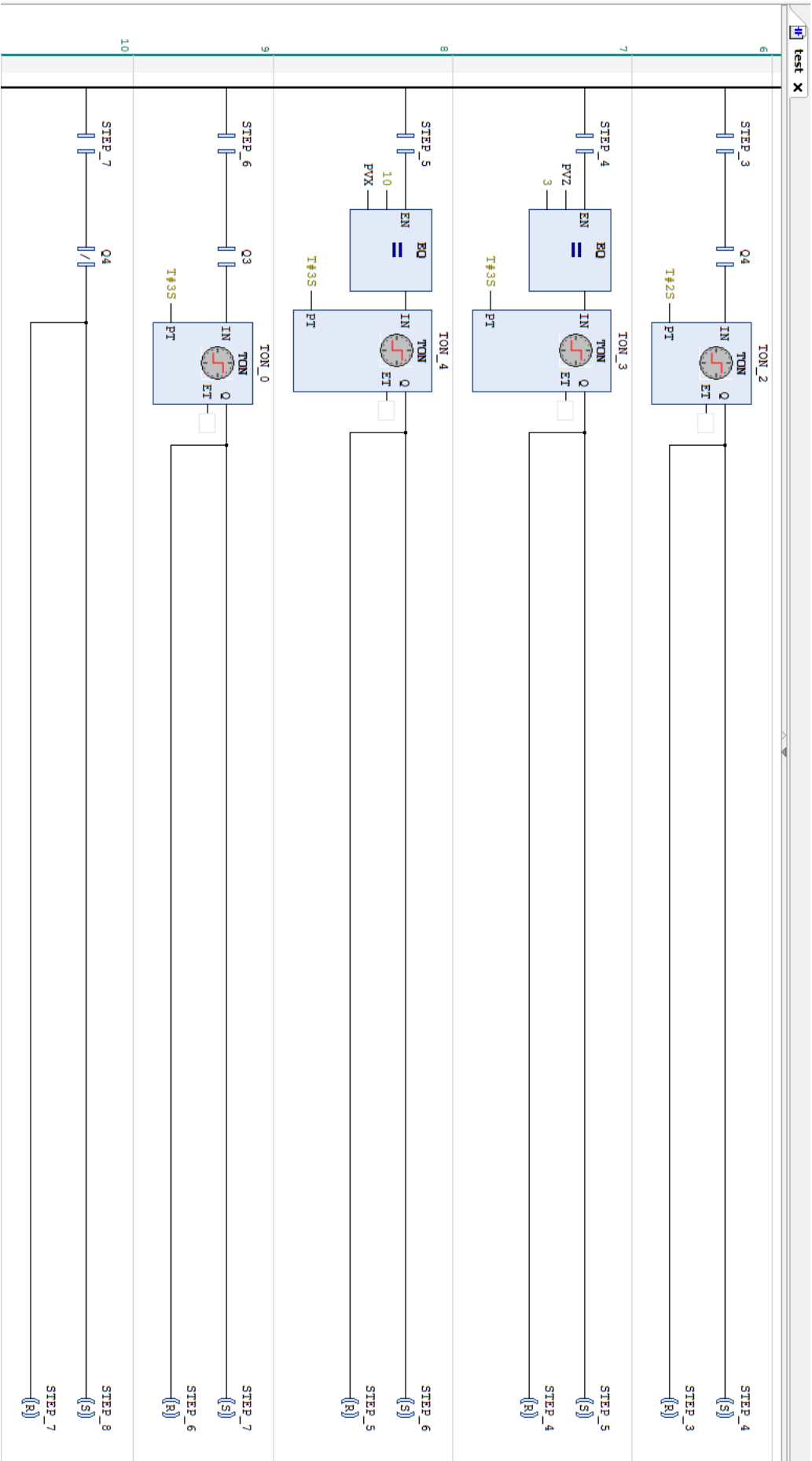


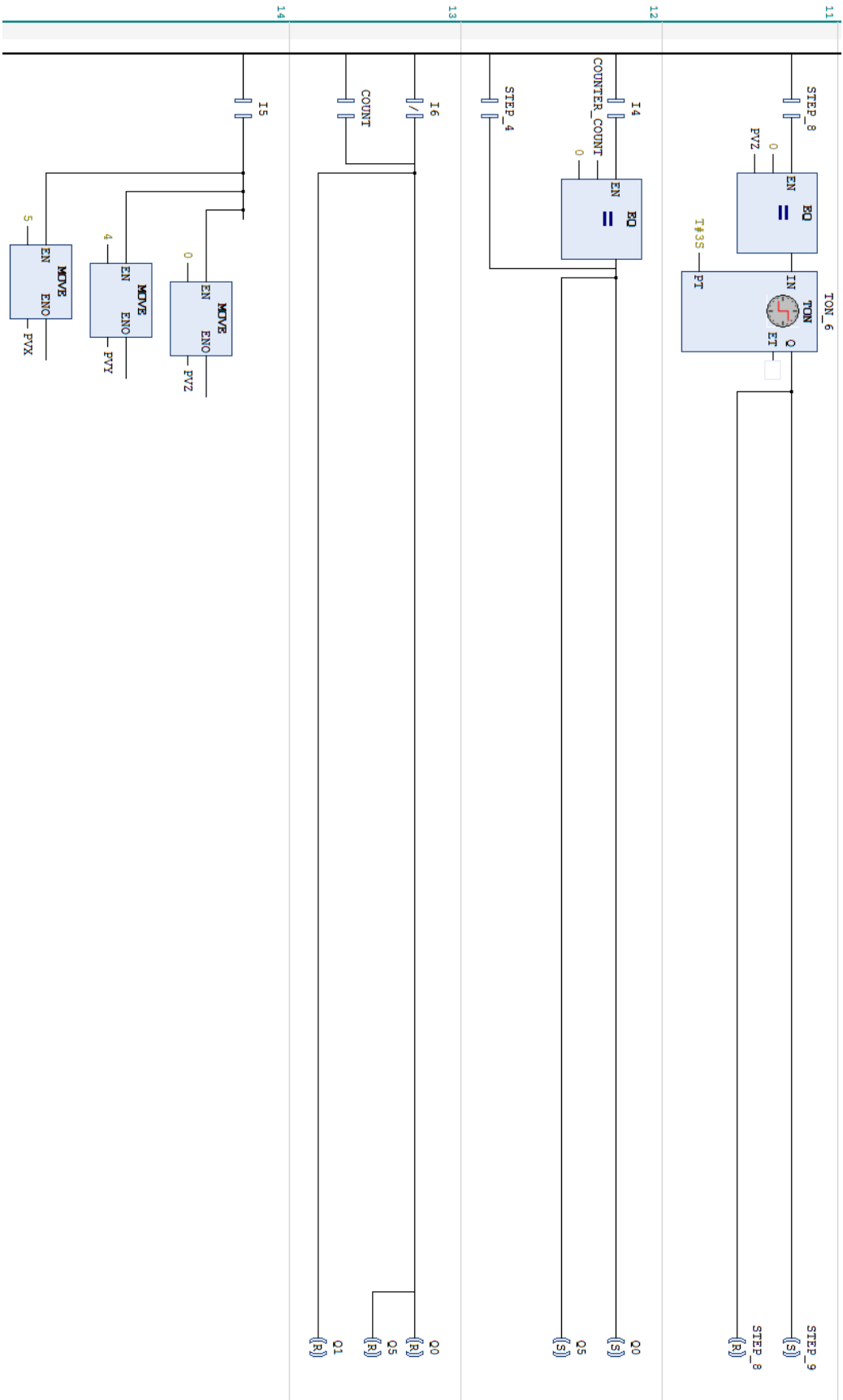
Appendix B

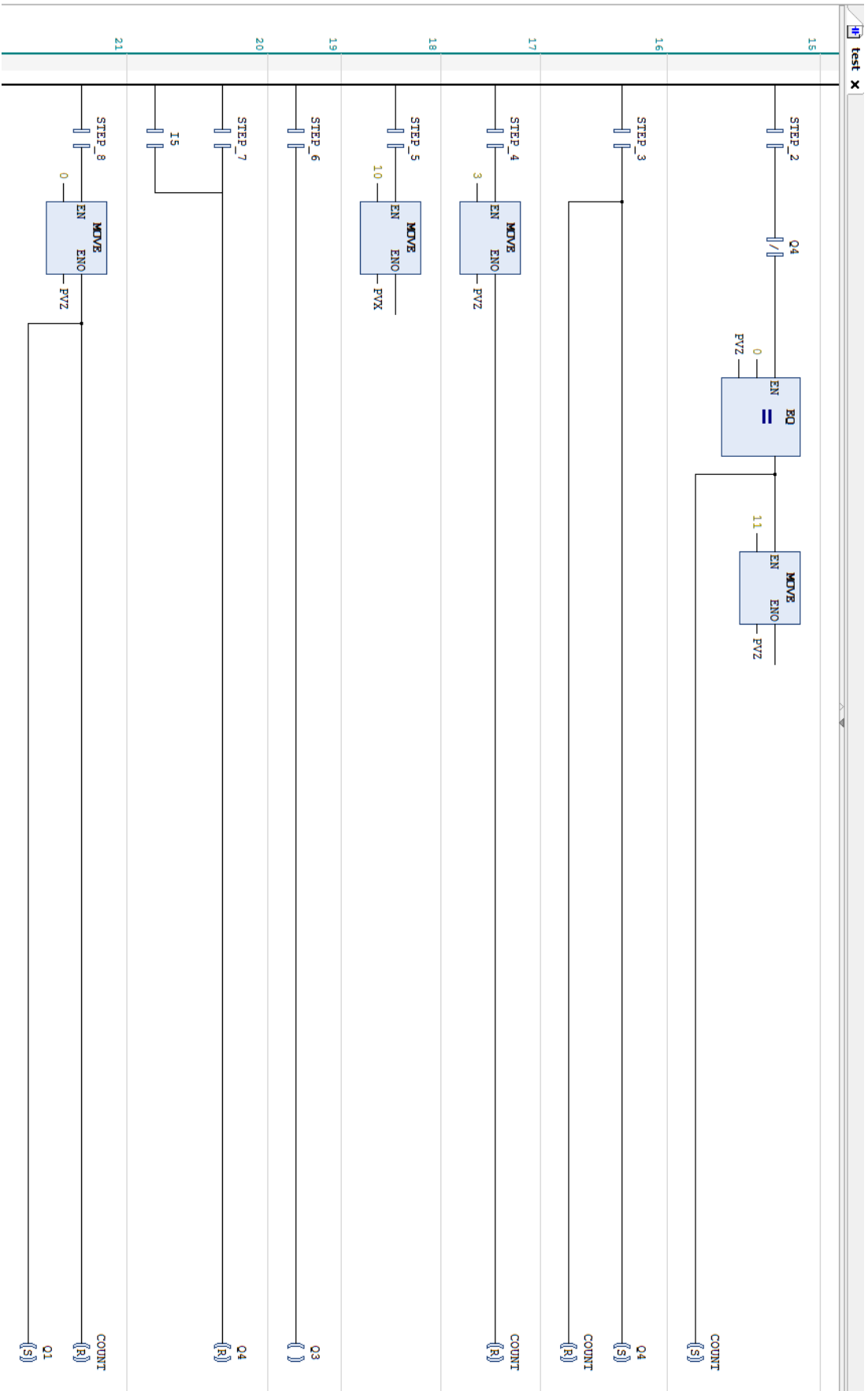
Codesys code

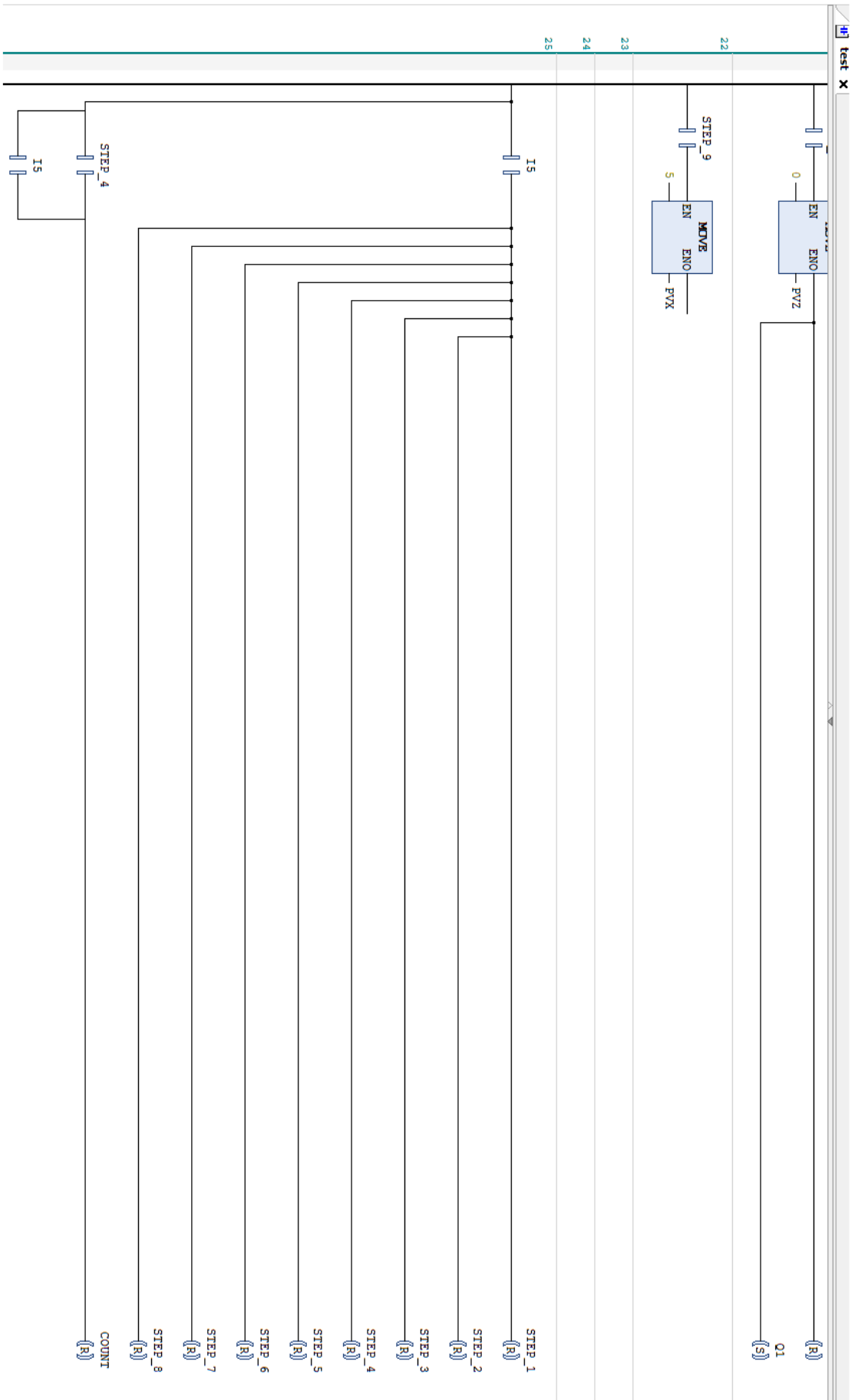
```
test x
1 PROGRAM test
2 VAR
3     I0 AT %IX10.0:BOOL; // BOX AT PLACE
4     I1 AT %IX10.1:BOOL; // PART AT PLACE
5     I2 AT %IX10.2:BOOL; // DETECTED
6     I3 AT %IX10.3:BOOL; // C LIMIT
7     I4 AT %IX10.4:BOOL; // START
8     I5 AT %IX10.5:BOOL; // RESET
9     I6 AT %IX10.6:BOOL; // STOP
10    I7 AT %IX10.7:BOOL; // EMERGENCY
11    I8 AT %IX11.0:BOOL; // AUTO
12
13    Q0 AT %QX10.0:BOOL; // box CONVEYOR
14    Q1 AT %QX10.1:BOOL; // GLASS CONVEYOR
15    Q2 AT %QX10.2:BOOL; // EXIT CONVEYOR
16    Q3 AT %QX10.3:BOOL; // C+
17    Q4 AT %QX10.4:BOOL; // GRAB
18    Q5 AT %QX10.5:BOOL; // Exit conveyor
19    Q6 AT %QX10.6:BOOL; // X-
20    Q7 AT %QX10.7:BOOL; // Y+
21    Q8 AT %QX11.0:BOOL; // Y-
22    PVX AT %QW0:INT:=5;
23    PVY AT %QW1:INT:=5;
24    PVZ AT %QW2:INT:=0;
25 CTU_0: CTU;
26     GLASS_FLOW: BOOL;
27     TON_0: TON;
28     GLASS_CONTINUE: BOOL;
29     STEP_1: BOOL;
30     STEP_2: BOOL;
31     STEP_3: BOOL;
32     STEP_X: BOOL;
33     STEP_4: BOOL;
34     STEP_5: BOOL;
35     STEP_6: BOOL;
36     STEP_7: BOOL;
37     TON_1: TON;
38     TON_2: TON;
39     TON_3: TON;
40     TON_4: TON;
41     TON_5: TON;
42     STEP_8: BOOL;
43     TON_6: TON;
44     STEP_9: BOOL;
45     TON_7: TON;
46     COUNT: BOOL;
47     COUNTER_COUNT: INT;
48 END_VAR
49
```











Bibliography

Manfred Eigen, CHAPTER 12 - OXIDE GLASSES, Editor(s): K.J. Rao, Structural Chemistry of Glasses, Elsevier Science Ltd, 2002, Pages 463-511, url: <https://www.sciencedirect.com/topics/engineering/glass-structure>;

Edgar D. Zanotto, John C. Mauro, The glassy state of matter: Its definition and ultimate fate, of Non-Crystalline Solids, Volume 471, 2017, Pages 490-495, <https://www.sciencedirect.com/science/article/abs/pii/S0022309317302685>;

Oney F., The American Ceramic Society, "New definition of glass describes non-equilibrium state of matter ending in crystallization", 20th October 2017, <https://ceramics.org/ceramic-tech-today/new-definition-of-glass-describes-non-equilibrium-state-of-matter-ending-in-crystallization/>;

IMARC Group, Flat Glass Market Size, Share, Trends and Forecast by Technology, Product Type, Raw Material, End-Use, Type, End Use Industry, and Region, 2025-2033, 2024, <https://www.imarcgroup.com/flat-glass-market>

Lorraine F. Francis, Chapter 3 - Melt Processes, Editor(s): Lorraine F. Francis, Materials Processing, Academic Press, 2016, url: <https://www.sciencedirect.com/topics/engineering/float-glass-process>;

GMI Insights, Glass Manufacturing Market – By Product, By Sector, By Region– Global Forecast, 2025 – 2034, February 2025, url: <https://www.gminsights.com/industry-analysis/glass-manufacturing-market>

"Rockwell Automation, Studio 5000 user guide" url: https://literature.rockwellautomation.com/idc/groups/literature/documents/rm/motion-rm002_-en-p.pdf;

G. Petrucci, "Lezioni di Costruzione di Macchine", 20. COLLEGAMENTI FILETTATI E CHIODATI, 2022, url: <https://sites.unipa.it/giovanni.petrucci/Disp/Bulloni.pdf>

Codesys GmbH, Codesys help guide, url: <https://www.helpme-codesys.com/>;

Real Games, Factory I/O user guide, url: <https://docs.factoryio.com/> ;